

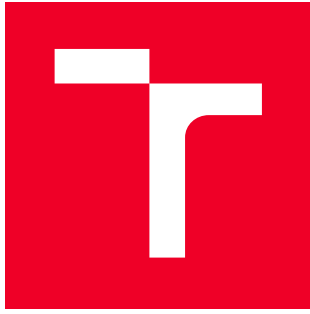
BRNO UNIVERSITY OF TECHNOLOGY

Faculty of Electrical Engineering  
and Communication

HABILITATION THESIS

Brno, 2019

Bc. et Ing. PETR MÜNSTER, Ph.D.



# BRNO UNIVERSITY OF TECHNOLOGY

VYSOKÉ UČENÍ TECHNICKÉ V BRNĚ

FACULTY OF ELECTRICAL ENGINEERING  
AND COMMUNICATION

FAKULTA ELEKTROTECHNIKY A KOMUNIKAČNÍCH TECHNOLOGIÍ

DEPARTMENT OF TELECOMMUNICATIONS

ÚSTAV TELEKOMUNIKACÍ

## SMART INFRASTRUCTURES BASED ON DISTRIBUTED FIBRE OPTIC SENSING

CHYTRÉ INFRASTRUKTURY ZALOŽENÉ NA DISTRIBUOVANÉM OPTICKÉM  
VLÁKNOVÉM SNÍMÁNÍ

HABILITATION THESIS

HABILITAČNÍ PRÁCE

AUTHOR  
AUTOR PRÁCE

Bc. et Ing. Petr Múnster, Ph.D.

BRNO 2019

## **ABSTRACT**

The habilitation thesis deals with smart infrastructures using distributed fibre optic sensors to protect critical infrastructures. The thesis focuses on the analysis of suitability of selected distributed sensing techniques for use on fibers with active data transmission. The thesis consists of three main parts. The first part contains description of techniques suitable for critical infrastructure protection and explanation of basic parameters related to the solved problems. The second part presents a comprehensive practical evaluation of simultaneous transmission of high-power sensing signal with data and non-data services, as well as a comparison of the sensitivity of a polarization interferometer with a classical two-arm interferometer. The third part presents two of the author's new proposals of methods suitable for deployment on fibers with active data transmission and at the same time a proposal of the possibilities of distributed sensing signal amplification to minimize the output power and thus minimize interactions with other signals. The first proposed system deals with the analysis of the polarization state of an optical signal when external interference is applied to the fibre. A unique detection system is presented, which is simple and economically effective compared to classical analysis using a polarimeter. The second design is based on a dual Mach-Zehnder interferometer using frequency shift signal.

## **KEYWORDS**

smart infrastructure; distributed sensing; reflectometry; interferometry; optical fibre; critical infrastructure

## **ABSTRAKT**

Habilitační práce pojednává o chytrých infrastrukturách využívajících distribuované optické vláknové senzory pro ochranu kritických infrastruktur. Práce se zaměřuje na analýzu vhodnosti vybraných technik distribuovaného snímání pro použití na vláknech s aktivním datovým přenosem. Práce se skládá ze tří hlavních částí. První část obsahuje popis technik vhodných pro ochranu kritických infrastruktur a vysvětlení základních parametrů souvisejících s řešenou problematikou. Druhá část představuje komplexní praktické zhodnocení simultánního přenosu vysoce výkonného sensorického signálu s datovými, ale nedatovými službami a rovněž srovnání citlivosti polarizačního interferometru s klasickým dvou ramenným interferometrem. Třetí část uvádí dva autorovy nové návrhy metod vhodných pro nasazení na vlákna s aktivním datovým přenosem a současně návrh možností distribuovaného zesílení sensorického signálu pro minimalizaci výstupního výkonu. První navržený systém se zabývá analýzou stavu polarizace optického signálu při působení vnějšího rušení na vlákno. Je představen unikátní detekční systém, který je oproti klasické analýze pomocí polarimetru ekonomicky výhodný. Druhý návrh je založen na duálním Machově-Zehnderově interferometru s využitím frekvenčního posunu signálu.

## **KLÍČOVÁ SLOVA**

chytrá infrastruktura; distribuované snímání; reflektometrie; interferometrie; optické vlákno; kritická infrastruktura

MÛNSTER, Petr. *Smart infrastructures based on distributed fibre optics ensing*. Brno, 2019, 93 p. Habilitation thesis. Brno University of Technology, Faculty of Electrical Engineering and Communication, Department of Telecommunications.

---

Vysázeno pomocí balíčku `thesis` verze 3.03; <http://latex.feec.vutbr.cz>

## ACKNOWLEDGEMENTS

I would first like to thank my family, especially my wife Romana and sons Vojtěch and Štěpán. I could not have done it without them and without their support. Second, I would like to thank my dear friend and colleague Tomáš Horváth for all his help and technical support.

Thanks go out to my colleagues in CESNET, especially Dr. Josef Vojtěch and also my colleagues at Brno University of Technology, especially prof. Miloslav Filka, for their assistance (academic, scientific, and otherwise) through the course of this research.

## DECLARATION

I declare that I have written the Habilitation Thesis titled “Smart Infrastructures Based on Distributed Fibre Optic Sensing” independently and using exclusively the technical references and other sources of information cited in the thesis and listed in the comprehensive bibliography at the end of the thesis.

As the author I furthermore declare that, with respect to the creation of this Habilitation Thesis, I have not infringed any copyright or violated anyone’s personal and/or ownership rights. In this context, I am fully aware of the consequences of breaking Regulation S 11 of the Copyright Act No. 121/2000 Coll. of the Czech Republic, as amended, and of any breach of rights related to intellectual property or introduced within amendments to relevant Acts such as the Intellectual Property Act or the Criminal Code, Act No. 40/2009 Coll., Section 2, Head VI, Part 4.

Brno .....

.....

author’s signature

# Contents

List of symbols, physical constants and abbreviations	11
Úvod	13
<b>1 Thesis Overview</b>	<b>15</b>
1.1 Scope and Research Motivation . . . . .	15
1.2 Thesis Objectives . . . . .	15
1.3 Relation to Author's Publications and Contribution . . . . .	16
1.4 Thesis Organization . . . . .	17
<b>2 Fibre Optic Sensors Background</b>	<b>19</b>
2.1 Background and Preliminaries . . . . .	20
2.1.1 Laser Diode Wavelength . . . . .	20
2.1.2 Optical Power . . . . .	20
2.1.3 Laser Diode Spectral Linewidth . . . . .	21
2.1.4 Coherence Length . . . . .	21
2.1.5 Polarization of the Light . . . . .	22
2.2 Distributed Fibre Optic Sensors . . . . .	24
2.2.1 Interferometric Sensors . . . . .	24
2.2.2 Reflectometry-based Sensors . . . . .	27
2.3 Data and Non-data Services . . . . .	34
2.3.1 Accurate Time . . . . .	34
2.3.2 High-speed Data . . . . .	36
<b>3 Assessment of Suitability of Fibre Optic Sensing Techniques for Use in Data Networks</b>	<b>39</b>
3.1 Photonics Services Description . . . . .	39
3.1.1 Accurate Time Transmission . . . . .	39
3.1.2 High-speed Data Systems . . . . .	42
3.1.3 Sensing System . . . . .	42
3.2 Simultaneous Transmission of the High-power $\Phi$ -OTDR, Standard Data, Accurate Time and Their Possible Interaction . . . . .	44
3.2.1 State of the Art . . . . .	45
3.2.2 Experimental Setup and Results . . . . .	47
3.2.3 Conclusions . . . . .	53
3.3 Sensitivity Comparison of an Interferometry and Polarization Methods	55
3.3.1 Experimental Setup . . . . .	55

3.3.2	Results and Discussion . . . . .	57
3.3.3	Conclusions . . . . .	63
<b>4</b>	<b>Novel Systems Based on Interferometric and Reflectometric Principles for Efficient Distributed Sensing</b>	<b>64</b>
4.1	$\Phi$ -OTDR Signal Amplification . . . . .	64
4.1.1	Pulse Signal Amplification with a Low Repetition Rate by Standard Telecommunication EDFA . . . . .	65
4.1.2	Pulse Signal Amplification by Raman Amplifier . . . . .	67
4.1.3	Remote Amplification of a Pulse Signal . . . . .	70
4.1.4	Conclusion . . . . .	73
4.2	Novel Method of Measurement of Polarization Transient Effects Caused by Mechanical Stress on Optical fibre . . . . .	74
4.2.1	Methodology . . . . .	74
4.2.2	Results and Discussion . . . . .	75
4.2.3	Conclusion . . . . .	77
4.3	Distributed Fibre Optic Sensing System Based on Dual Mach-Zehnder Interferometer Using Frequency Shift . . . . .	78
4.3.1	Scheme and Principle of the Invention . . . . .	78
<b>5</b>	<b>Conclusion</b>	<b>80</b>
	<b>Bibliography</b>	<b>82</b>

# List of Figures

2.1	Graph of component price vs. component availability over time [23]. . .	19
2.2	Intrinsic fibre optic sensors with highlighting technologies suitable for smart optical infrastructures [23]. . . . .	24
2.3	Basic configuration of the Mach-Zehnder interferometer. . . . .	26
2.4	Basic configuration of the Michelson interferometer. . . . .	27
2.5	Backscattering in single mode optical fibre. . . . .	28
2.6	Basic configuration of the $\Phi$ -OTDR. LD (Laser Diode), G (waveform generator), AOM (Acousto-Optic Modulator), EDFA (Erbium Doped Fibre Amplifier). . . . .	29
2.7	Rayleigh scattering [4]. . . . .	30
2.8	Example of B-OTDR setup. . . . .	32
3.1	Home developed time adapter . . . . .	40
3.2	Scheme of developed time adapter by CESNET. . . . .	40
3.3	Photo of the time transfer adapter developed by CESNET . . . . .	41
3.4	Photo of the FTB-1 with FTB-700G tester [25]. . . . .	42
3.5	Photo of the Coriant Groove G30 [14]. . . . .	43
3.6	Photo of the own designed and developed DAS. . . . .	43
3.7	Measurement scheme with $\Phi$ -OTDR details. . . . .	47
3.8	Wavelengths allocation for measurement scheme – time, $\Phi$ -OTDR, data, and frequency. . . . .	48
3.9	Influence of high-power pulse signal on quality (BER) of DP-QPSK data signal for G.652 fibre. . . . .	49
3.10	Influence of high-power pulse signal on quality (q-factor) of DP-QPSK data signal for G.653 fibre. . . . .	49
3.11	Influence of high-power pulse signal on quality of DP-QPSK data signal for G.652 fibre. . . . .	50
3.12	Influence of high-power pulse signal on quality of DP-QPSK data signal for G.653 fibre. . . . .	51
3.13	Measurement results for G.652D (on the left side) and G.653 fibre (on the right side). . . . .	52
3.14	Measurement results for G.655 (on the left side) and a combination of G.652D and G.653 fibres (on the right side). . . . .	53
3.15	Experimental setup for simultaneous measurement of two sensing systems. FG: Function Generator, PBS: Polarization Beam Splitter, FBG: Fibre Bragg Grating, PD: Photodetector, TIA: Transimpedance Amplifier, LD: Laser Diode. . . . .	55

3.16	Experimental setup of the Michelson interferometer is highlighted in green. . . . .	56
3.17	Experimental setup of polarization interferometer is highlighted in orange. . . . .	57
3.18	Received signals from both sensing systems (interferometer – red signal, polarization – blue signal) and their spectra (below) for 1030 Hz.	58
3.19	Detail of received signal for polarization measurement and corresponding spectra (below) for 1030 Hz. . . . .	59
3.20	Received signals from both sensing systems (interferometer – red signal, polarization – blue signal) and their spectra (below) for 530 Hz. .	59
3.21	Received signals from both sensing systems (interferometer – red signal, polarization – blue signal) and their spectra (below) for 130 Hz. .	60
3.22	Polarization system. Comparison of calculated 3D spectrogram for all measured frequencies. Top-left: 1030 Hz, top-right 530 Hz, and bottom: 130 Hz. . . . .	61
3.23	Experimental university network between BUT and MU. . . . .	61
3.24	Knocking on a wall near a rack unit close to an optical fibre. Response in time and corresponding spectra (below) measured with the interferometry system. . . . .	62
3.25	3D spectrogram. Knocking on a wall near a rack unit close to an optical fibre; measured with the interferometry system. . . . .	62
3.26	SOP change caused by mechanical vibration near the cable. L: the Poincaré sphere, R: Stokes parameters. . . . .	63
4.1	Setup for optical pulse signal amplification using holding beam. Block G: signal generator, AOM: acousto-optic modulator. . . . .	65
4.2	Pulse stability with and without using stabilization LD. . . . .	66
4.3	Optimal length of optical fibre link for different pump powers. . . . .	68
4.4	Setup for optical pulse signal amplification by distributed Raman amplification. RA: Raman Amplifier, WDM: Wavelength Division Multiplex coupler. . . . .	68
4.5	Pulse power stability for different output powers of the co-propagating and counter-propagating Raman amplification. . . . .	69
4.6	Back-scatter response from the FUT for 300 mW output power of the RA. . . . .	70
4.7	Pulse power fluctuations and its degradation due to non-linear phenomena. . . . .	70
4.8	Setup of the measurement system for remote amplification. . . . .	72
4.9	Verification of the remote amplification and its influence on the optical power stability of the optical pulse. . . . .	73

4.10	The scheme of the workplace . . . . .	75
4.11	Left: The response of the polarization fibre sensor on 1 ms pulses (a) Output signal from the balanced detector, (b) Polarization rotation rate detected with polarimeter, (c) Spectrogram of the signal from the balanced detector. Right: The response of the polarization fibre sensor on mechanical stress induced by knocking on the fibre (d) Output signal from the balanced detector, (e) Polarization rotation rate detected with polarimeter, (f) Spectrogram of the signal from the balanced detector. . . . .	76
4.12	Scheme of the dual Mach-Zehnder interferometer using frequency shift.	78

# List of symbols, physical constants and abbreviations

<b>64QAM</b>	64-level Quadrature Amplitude Modulation
<b>AOM</b>	Acousto-Optic Modulator
<b>AWG</b>	Arbitrary Waveform Generator
<b>BER</b>	Bit-Error Rate
<b>B-OTDR</b>	Brillouin Optical Time Domain Reflectometry
<b>BPD</b>	Balanced Photodetector
<b>BUT</b>	Brno University of Technology
<b>CW</b>	Continuous Wave
<b>DASs</b>	Distributed Acoustic Sensors
<b>DCF</b>	Dispersion Compensating Fibre
<b>DCM</b>	Dispersion Compensating Module
<b>DFB</b>	Distributed Feedback
<b>DP-QPSK</b>	Dual Polarisation Quadrature Phase Shift Keying
<b>DSP</b>	Digital Signal Processing
<b>DTSS</b>	Distributed Temperature and Strain Sensor
<b>DWDM</b>	Dense Wavelength Division Multiplexing
<b>EDF</b>	Erbium Doped Fibre
<b>EDFA</b>	Erbium Doped Fibre Amplifier
<b>FBG</b>	Fibre Bragg Grating
<b>FEC</b>	Forward Error Correction
<b>FG</b>	Function Generator
<b>FPGA</b>	Field Programmable Gate Array
<b>FRMs</b>	Farraday Rotator Mirrors
<b>FTTH</b>	Fibre to the Home
<b>FUT</b>	Fibre Under Test
<b>FWHM</b>	Full Width at Half-Maximum
<b>GLONAS</b>	GLObal NAVigation Satellite System
<b>GMT</b>	Greenwich Mean Time
<b>GPS</b>	Global Positioning System
<b>HDPE</b>	High Density Polyethylene
<b>IEEE</b>	Institute of Electrical and Electronics Engineers
<b>ITU</b>	International Telecommunication Union Telecommunication Standardization Sector
<b>LD</b>	Laser Diode
<b>MDPI</b>	Multidisciplinary Digital Publishing Institute

<b>MI</b>	Michelson Interferometer
<b>MU</b>	Masaryk University
<b>MZI</b>	Mach-Zehnder Interferometer
<b>NREN</b>	National Research and Educational Networks
<b>NRZ</b>	Non Return-to-Zero
<b>NTP</b>	Network Time Protocol
<b>NZDSF</b>	Non-Zero Dispersion-Shifted Fibre
<b>OOK</b>	On-Off Keying
<b>OTDR</b>	Optical Time Domain Reflectometry
<b>OXCO</b>	Oven Controlled Crystal Oscillator
<b>PBS</b>	Polarization Beam Splitter
<b>PC</b>	Personal Computer
<b>PD</b>	Photodetector
<b>Φ-OTDR</b>	Phase Sensitive Optical Time Domain Reflectometer
<b>PPS</b>	Pulse Per Second
<b>pre-FEC-BER</b>	pre-Forward Error Correction–Bit Error Rate
<b>PTP</b>	Precision Time Protocol
<b>RA</b>	Raman Amplifier
<b>RF</b>	Radio-Frequency
<b>RZ</b>	Return-to-Zero
<b>SSMF</b>	Standard Single-Mode Fibre
<b>SNR</b>	Signal-to-Noise Ratio
<b>SOP</b>	State of Polarization
<b>TAI</b>	International Atomic Time
<b>TIA</b>	Transimpedance Amplifier
<b>TIC</b>	Time Interval Counter
<b>TWSTFT</b>	Two-Way Satellite Time and Frequency Transfer
<b>UDP</b>	User Datagram Protocol
<b>USA</b>	United States of America
<b>UTC</b>	Coordinated Universal Time
<b>WDM</b>	Wavelength Division Multiplex
<b>WoS</b>	Web of Science
<b>WR</b>	White Rabbit

# Introduction

The optical fibre as we know it today is relatively young. It dates back to the 1970s and is associated with Corning company. The fibre attenuation was below 20 dB/km, which of course would not allow today's long distance transmissions. Today's fibres achieve attenuation below 0.2 dB/km and more than 4.5 billion kilometres of fibres is installed across the globe. Optical fibre is the most widespread type of medium and can be found in almost every part of the globe [93].

Optical fibres allow high-speed transmission over long distances. Thanks to multiplexing techniques, it is possible to transmit multiple signals in one fibre simultaneously and multiply the optical fibre capacity. But data is not the only application that takes advantage of fibre optic infrastructures. There is an increasing interest in new services such as accurate time and ultra stable frequency transmission or a quantum key distribution. A separate chapter is the optical fibre sensors, which offer a number of advantages in comparison to conventional techniques and are in many cases irreplaceable. Until recently, telecommunications and sensor technologies were two separate fields, both in science and research, and in the commercial sector. With the increasing demand for smart cities and smart infrastructures it is possible to use the existing optical infrastructure not only for data transmission but also for sensing, for example, temperature or acoustic vibrations in the vicinity of the fibre optic cable. So-called "Smart infrastructures" can perform a number of functions, such as critical infrastructure protection [24]. The Early Warning System can serve to protect nearby pipelines, monitor traffic on roads, fire detection or protect the fibre optic infrastructure itself. Since in some places it is not possible or it is not economically advantageous to lay new fibre optic cables for transmission of new services, it is necessary to share existing fibres with active data transmission. However, this can pose a number of problems as some sensor systems use high-power optical pulses that may interfere with other services.

The purpose of this thesis is to provide the basic overview of techniques suitable for use in critical infrastructures protection. This thesis has three main goals. The first goal is to present a theoretical background which focuses on the description of various distributed sensing schemes and principles, and description of basic parameters related to the presented field. The second goal is to provide the assessment of chosen schemes in terms of possible interaction and assessment in terms of sensitivity. This part is based on author's results published in impact factor journals and international conferences indexed in WoS. The third goal is to present author's results achieved in the field of the design of advanced signal amplification techniques. This part also contains two novel concepts whereas one concept was published in impact factor journal and at international conference and the second concept has

not yet been published as this was not possible due to patent rules.

The thesis is divided into three parts that deal with described goals. Chapter 2 focuses on the pedagogical goal and contains the theoretical background and fibre optic sensing techniques description. Chapter 3 contains practical results and a detailed assessment of simultaneous transmission of data and new services, and also sensitivity comparison of two interferometry systems. Chapter 4 is dedicated to a scientific part and presents author's scientific work. The overview of this thesis is described in the Chapter 1.

# 1 Thesis Overview

In this chapter an overview of the thesis is provided. Section 1.1 presents scope of the thesis and author motivation. Then, thesis objectives are described in Section 1.2 and relation to author's publications and contributions is in Section 1.3. Finally, thesis organization is outlined in Section 1.4.

## 1.1 Scope and Research Motivation

The scope of this work involves fibre optic sensing systems for use in already existed fibre optic data infrastructure. The thesis focuses on distributed sensing systems using standard single mode optical fibre in optical cables already buried under ground. The solutions presented utilize fibre optic interference or scattering. On one hand, simple and relatively cost-effective solutions based on fibre optic interferometry but also robust systems based on phase sensitive optical time domain reflectometry are proposed. On the other hand, interferometers do not offer localization in basic configuration and their sensitivity is very high which causes interference. Reflectometry based systems are expensive, generate large amounts of data that need to be processed and use high power pulses that can interfere with data signals when fibres with active data traffic are used. Therefore, research in the field of the suitability of individual technologies is necessary and also design of new schemes is needed. This thesis deals with the design of new schemes of distributed fibre optic sensing systems based on optical interferometry, both, two-arm interferometer and single-arm polarization interferometer. For reflectometry based sensing system as is  $\Phi$ -OTDR (Phase Sensitive Optical Time Domain Reflectometer) experimental verification of a weak signal amplification is investigated. The thesis also provides suitability assessment of parallel and simultaneous transmission of the high-power phase sensitive optical time domain reflectometry signal, 100 Gbps DP-QPSK (Dual Polarisation Quadrature Phase Shift Keying) data signal, and accurate time in a single optical fibre using a wavelength division multiplexing based on DWDM (Dense Wavelength Division Multiplexing) spectral grids.

## 1.2 Thesis Objectives

The objectives of the thesis are as follows:

- The thesis presents basic assumptions in the field of optics, such as coherence length or polarization, and also the basic theory regarding to distributed fibre optic sensing technologies and principles suitable for use in optical fibre based data infrastructure.

- The second objective of the thesis is to present the detailed assessment of the suitability of selected technologies for the protection of critical infrastructures in terms of the possible interactions of the high-power pulse signal (which is typical for reflectometric systems) with other signals, as well as the comparison of the sensitivity of interferometric systems.
- The third goal of the thesis is to propose novel designs and systems that are more efficient in comparison with related work and could be deployed in various applications and scenarios where current technologies are reaching their limits or novel setups can bring some benefits.

### 1.3 Relation to Author's Publications and Contribution

This thesis presents author's scientific work and results published since 2015. The main results and proposals presented in the thesis have been published in various international journals with impact factors (e.g. [84], [65], [35], [34], [64]) and international journals and conferences dedicated to sensors or telecommunications (e.g. [69], [62], [17], [63], [66], [78], [16], [77]). In addition, the author is also a main author or co-author of various publications related to other security topics in telecommunication networks, especially in access networks, and also topics focusing on transmission of special services over fibre infrastructure (accurate time, stable frequency and a quantum key distribution). These results are published in international journals with impact factors ([37], [36], [57], [96], [40], [86]) and various international journals and conferences ([48], [39], [31], [56], [37], [83], [2], [95], [97], [38], [59], [49], [41], [32], [101], [94], [33], [30], [102], [29], [73], [74]).

None of the results or proposed solutions presented in this thesis were published in the author's Ph.D. thesis or any past author's theses. The Ph.D. thesis focused solely on telecommunication networks, specifically parameters of access networks. In this habilitation fibre optic sensors are the main topic.

The contribution of this thesis is threefold:

- **Pedagogical contribution:** Chapter 2 describes various important parameters and prerequisites from the field of fibre optic sensors necessary to know and understand to. Further, technologies suitable for use in fibre infrastructure with an active data transmission including both, interferometry and reflectometry based sensing systems are introduced to readers. The basics of accurate time and high-speed data transmission are also presented in this chapter. Moreover, the brief overview of mathematical expression of the main parameters of each system is provided. This theoretical part of the thesis of-

fers foundation and concrete examples regarding to conventional and advanced sensing technologies with a focus on a smart fibre optic infrastructure creation.

- **Practical contribution:** Chapter 3 contains description of data and non-data services used for experimental measurements. Practical results and detailed assessment of simultaneous transmission of different type of services with a high-power pulse signal is presented. The obtained results can help with future research and the practical deployment of reflectometry based sensing systems on fibres with active data transmission. Further experimental measurements bring results in the assessment of the sensitivity comparison of polarization and interferometric systems.
- **Scientific contribution:** Chapter 4 presents author's original scientific work. Two novel proposed systems and concepts of distributed sensing systems that are described in the theoretical part are presented. Main goal of both proposals described in Sections 4.2 and 4.3 is to provide efficient and practical solutions for creating of a smart fibre infrastructure. The research of a signal amplification described in Section 4.1 have been presented at international conference dedicated to telecommunications/sensing [62]. The proposal described in Section 4.2 have been presented at international conferences dedicated to telecommunications/sensing [88], [6], and one more is under preparation and will be submitted to international journal with an impact factor MDPI (Multidisciplinary Digital Publishing Institute) Sensors. The proposal described in Section 4.3 has not yet been published as it was necessary to wait for the patent application to be filed.

## 1.4 Thesis Organization

This thesis contains 4 chapters and is organized as follows:

- Chapter 1 presents the scope of the thesis in Section 1.1, the thesis objectives in Section 1.2, the contribution of the thesis with relation to author's publications in Section 1.3, and thesis organization in Section 1.4.
- Chapter 2 contains the theoretical background and presents common sensing schemes. The chapter introduces prerequisites necessary for further text understanding in Section 2.1, conventional distributed fibre optic sensor schemes in Section 2.2 and a description of data and non-data services in Section 2.3.
- Chapter 3 contains assessment of simultaneous transmission of different type of services and also sensitivity comparison of two different interferometry systems. Section 3.1 briefly introduces the photonic services which are rather common especially in research networks. Further, the chapter discusses the practical results and the detailed assessment of simultaneous transmission of

different type of services with a high-power pulse signal in Section 3.2 and the sensitivity comparison of polarization and interferometric systems in Section 3.3.

- Chapter 4 introduces author's novel proposals in the field of distributed sensing. The Chapter presents two proposals and also new techniques of a signal amplification like remote pumping or holding beam. Section 4.1 presents an amplification of a weak backscatter signal for a maximum distance extension. Section 4.2 presents a novel method based on polarization beam splitter and balanced photodetector for state of polarization analysis. Section 4.3 introduces a novel concept of the Mach-Zehnder interferometer using a frequency shift of an optical signal for creating second interferometer in the same fibres resulting in localization of the event.
- Chapter 5 concludes this thesis.

## 2 Fibre Optic Sensors Background

Nowadays, optical fibre is considered to be the most widespread medium. The main reasons include – high transmission capacity, low susceptibility to electromagnetic and radiofrequency interference, and transmission in the optical domain. In order to understand the principle of transmission, it is important to realize that light is electromagnetic wave and optical fibre propagation is based on the principle of total reflection at the interface of two refractive index environments. The refractive index therefore characterizes the environment and is a key parameter in most distributed fibre optic sensing systems.

History of deploying the first fibre-optic distributed systems dates back to the 1980s. A major limitation was the availability and cost of key components such as laser diodes, integrated optical modulators, as well as the optical fibre itself. With the advancement of new technologies, the price of components is decreasing, and the availability of these components increases rapidly, as shown in the graph in Fig. 2.1 [23].

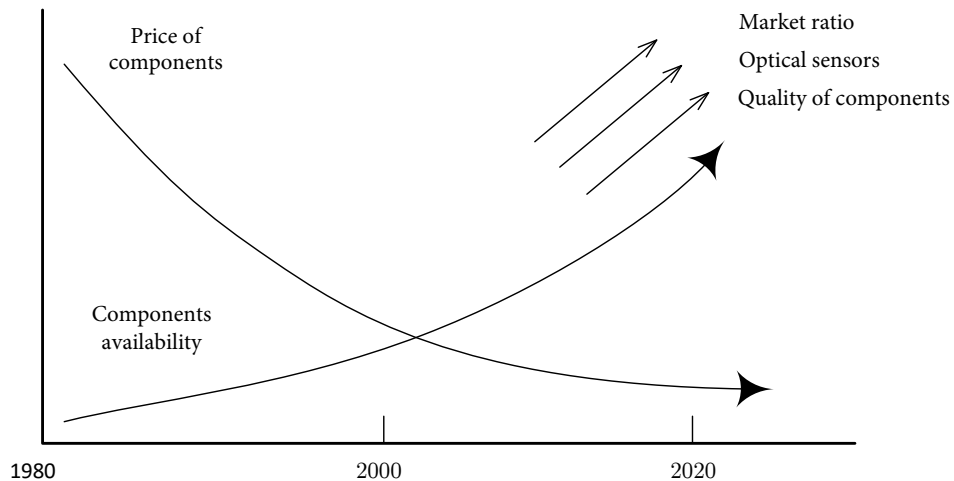


Fig. 2.1: Graph of component price vs. component availability over time [23].

## 2.1 Background and Preliminaries

The basic parameters necessary for understanding of the text below are explained in brief.

### 2.1.1 Laser Diode Wavelength

It is the expression of the frequency of laser source and expresses the length of one wave period in the given environment. Wavelength is expressed by [71]:

$$\lambda = \frac{c}{n \cdot f}, \quad (2.1)$$

where  $\lambda$  is the wavelength,  $c$  is the speed of light in vacuum,  $n$  refractive index, and  $f$  is the frequency of the laser source. Obviously, a higher frequency corresponds to a shorter wavelength. In fibre optic transmissions frequencies are in the order of hundreds of terahertz or wavelengths in the order of units of micrometers.

Usually, windows based on attenuation characteristics of standard optical fibres are used according to ITU (International Telecommunication Union Telecommunication Standardization Sector) [71]:

- **O** (Original), 1260–1360 nm,
- **E** (Extended), 1360–1460 nm,
- **S** (Short wavelength), 1460–1530 nm,
- **C** (Conventional), 1530–1565 nm,
- **L** (Long wavelength), 1565–1625 nm,
- **LU** (Ultra), over 1625 nm.

### 2.1.2 Optical Power

It characterizes the power of the laser source and thus intensity of the light radiation emitting from the source. Optical power can be in Watts or logarithmically in decibels above the milliwatt (dBm). Conversion from W to dBm can be expressed as [91]:

$$P_{dBm} = 10 \cdot \log_{10} \frac{P_{watt}}{1mW}, \quad (2.2)$$

where  $P_{Watt}$  is the power of the laser source in Watts. The power of laser sources varies according to the target application. For optical communications, sources with a transmit power of about 1 mW, i.e. 0 dBm, are used. Continuous-wave fibre optic lasers have power outputs of up to 40 mW, or 16 dBm. For special applications it is possible to get optical sources with higher power [91].

It is also important to realize the difference between peak power and average power. Based on definition of peak energy,

$$P_{peak} = \frac{E}{\Delta t}, \quad (2.3)$$

we can calculate total pulse energy from which average power is given by equation [91]:

$$P_{avg} = \frac{E}{T} = Ef. \quad (2.4)$$

Although the average power of some distributed sensor systems based on the reflectometry principle is relatively small, peak power can reach power of up to units/tens of Watts and thus affect data transmission in other channels due to non-linear phenomena.

### 2.1.3 Laser Diode Spectral Linewidth

Spectral linewidth describes mono-chromaticity of the laser source and is mostly given in Hz (usually GHz, MHz or kHz). It is measured at either a signal amplitude drop of 50% or 90% and is referred to as FWHM<sub>3dB</sub> (Full Width at Half-Maximum) or FWHM<sub>10dB</sub>. The width of the spectral line is directly influenced by the modulation of the carrier signal and is, for simple modulations, extended by twice the modulation symbol rate. Thus, the expression of the spectral linewidth makes sense, especially for continuous-wave laser sources, where current coherent transmissions already require a linewidth below 100 kHz. Spectral linewidth required for sensor applications is then determined from the required coherence length, which is discussed below.

### 2.1.4 Coherence Length

It describes the distance over which radiation loses its initial coherence (cohesion) by its propagation in the environment. Thus, the coherence length can be expressed from the knowledge of FWHM as [13]:

$$L_{coh} = \frac{c}{\pi \cdot \Delta\nu}. \quad (2.5)$$

Where  $\Delta\nu$  is the full width at half-maximum linewidth. The coherent length increases with the narrower spectral linewidth of the laser source and would be infinite for ideal monochromatic light. Selected values for the 1550 nm region are shown in Tab. 2.1

Tab. 2.1: Selected coherence lengths for the 1550 nm region

Spectral linewidth	Coherent length
200 MHz	477 mm
50 MHz	1.91 m
1 MHz	95.4 m
200 kHz	477 m
50 kHz	1.91 km
4.77 kHz	20 km
1.91 kHz	50 km
0.95 kHz	100 km

Obviously, for purely coherent short reach applications is sufficient to have a spectral linewidth in units of MHz, while for long reach applications very narrow linewidth sources in units of kHz are required.

### 2.1.5 Polarization of the Light

Light is an electromagnetic wave, which means that it is an oscillation of the electric field intensity vector  $E$  and perpendicular to it the magnetic field induction vector  $B$ . Electric and magnetic fields change in time and these changes propagate at a finite speed – solution is an electromagnetic wave. The description of the light wave is based on the solution of Maxwell’s equations. Electromagnetic waves have two planes of polarization – along the x-axis and along the y-axis. The general equation of propagation of a polarized light wave in the direction  $z$  of propagation can be described by two linearly polarized components in the x and y axes [82]:

$$E_x(z, t) = E_{0x} \cos(\tau_\omega + \phi_x), \quad (2.6)$$

$$E_y(z, t) = E_{0y} \cos(\tau_\omega + \phi_y), \quad (2.7)$$

where  $x, y$  are the components in x, y directions,  $E_x(z, t)$  and  $E_y(z, t)$  are maximum amplitudes of electric field,  $\tau_\omega$  is called propagator, and  $\phi_x, \phi_y$  describe the phases. In isotropic medium the polarization ellipse is almost same in every part and wave is elliptically polarized. State of polarization describes orientation and ellipticity of the ellipse. Ellipticity in a medium can become to be straight or circle. In that case wave is linearly polarized or circularly polarized, respectively [82].

Types of polarization in optical fibre:

- **Elliptically polarized light** – the direction of the vector  $E$  changes over time and describes the ellipse.
- **Linearly polarized light** – the direction of the vector  $E$  is constant in a particular plane.
- **Circularly polarized light** – the vector  $E$  describes the circle.

In most communication systems as well as in most sensory systems, polarization is an undesirable effect causing distortion and additional noise. On the other hand, current high-speed data transmission systems utilize polarization for increasing capacity using polarization multiplexing.

## 2.2 Distributed Fibre Optic Sensors

In general, optical sensors can be divided into extrinsic and intrinsic sensors. For extrinsic or hybrid sensors is typical that measurement itself is outside the optical fibre and optical fibre serves only for light/information transmission. In the case of intrinsic sensors, the fibre itself serves as a sensor. The basic distribution of intrinsic sensors is shown in Fig. 2.2, with highlighted technologies suitable for creating smart optical infrastructures to protect critical infrastructures.

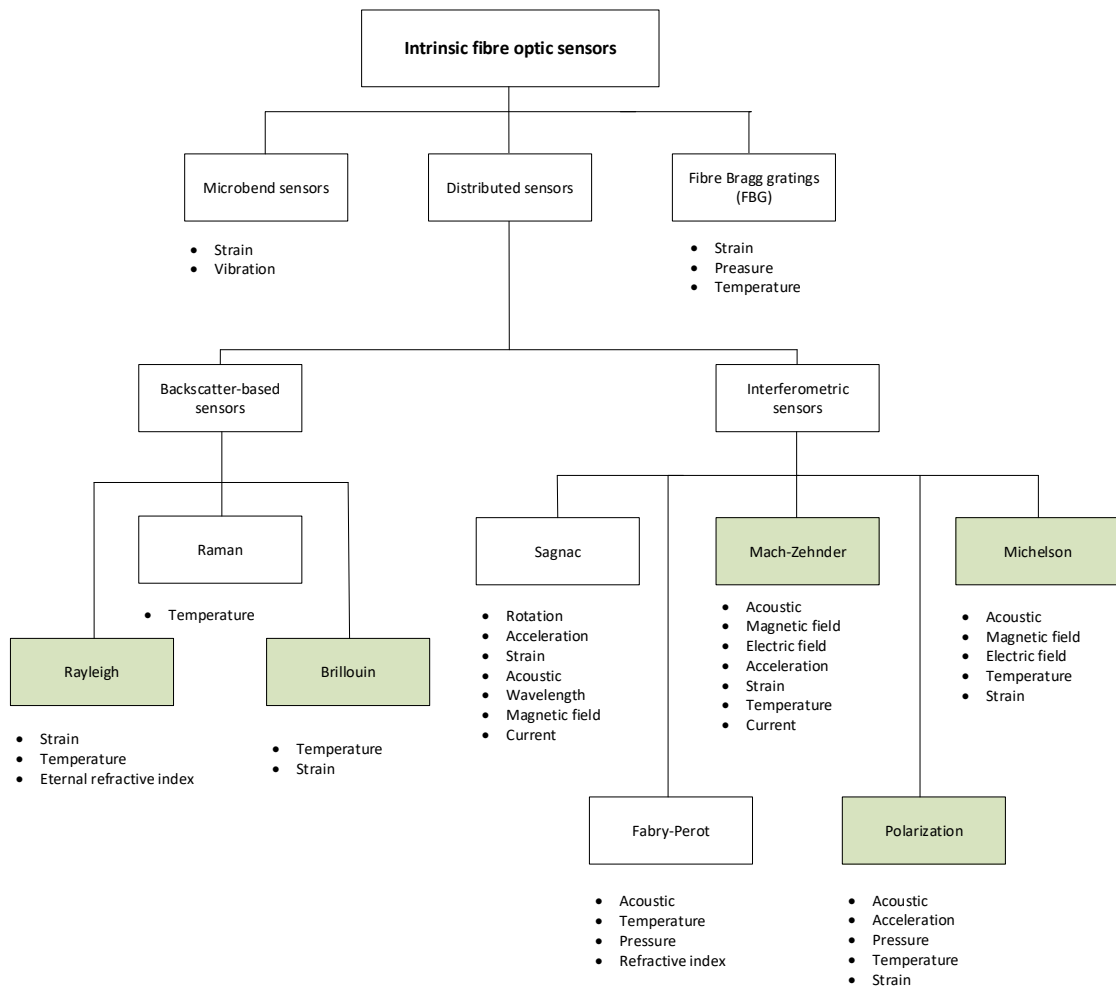


Fig. 2.2: Intrinsic fibre optic sensors with highlighting technologies suitable for smart optical infrastructures [23].

### 2.2.1 Interferometric Sensors

This section focuses on the first order interference known also as field interference which is based on spatial or temporal coherences between two light beams [79]. The

phase of the light can change due to external perturbations acting on the fibre, therefore the changes of the light phase can be used for the detection of physical quantities such as acoustic vibrations or strain. The relationship between phase change and optical path difference can be described as follows [23]:

$$\Phi(r, t) = nkL = \frac{2\pi}{\lambda}L(L, r), \quad (2.8)$$

where  $n$  is the refractive index,  $\lambda$  is the wavelength and  $L(r, t)$  describes the optical path length which is described as  $nL$ . Two beam interferometry enables the measurement of extremely small phase changes. Low frequencies below 50 kHz are measured thanks other materials as a coating are connected to the fibre by adhesives, to produce dominantly  $\Delta L$  change. In addition,  $\Delta n$  occurs due to fibre strain coefficient [23].

Stability of fibre interferometers is given not only by fibre surrounding environment but also by laser diode frequency stability. Change of laser diode frequency  $dv$  will cause change of phase  $\Delta\Phi$ . In case of laser diode frequency instability  $dv_n$ , the output can be described as [23]:

$$d\Phi_n = \frac{2\pi n \Delta L dv_n}{c}. \quad (2.9)$$

### **Mach-Zehnder Interferometer**

The use of the MZI (Mach-Zehnder Interferometer) for acoustic vibration measurement has found enormous application due to its simple configuration. MZI is considered to be a cost effective solution for a distributed fibre optical sensing. Fig. 2.3 shows the basic configuration of the Mach-Zehnder interferometer. Signal from a light source (a highly coherent laser diode) is divided in  $2 \times 2$  optical coupler into two arms. In general, external vibrations should be applied to the sensing arm while the reference arm should be isolated from external vibrations. Thus, optical path difference causes phase modulation between the sensing arm and the reference arm. Subsequently, phase modulations are converted to intensity modulation by another coupler  $2 \times 2$  and converted to an electrical signal by a photodetector [79].

In the basic configuration, only events can be detected. In order to locate the place of origin of the event, it is necessary to combine the MZI with another method (for example, dual MZI configuration is common) [79].

**Dual MZI** – signal from laser is equally divided into two paths – clockwise and counterclockwise. The clockwise signal is coupled directly and the counterclockwise signal is coupled from the opposite site. As soon as external vibration is applied to the sensing arm, a phase change between the two arms occurs at the corresponding point. At both ends, signals from the photodetectors are received. Due to the fact

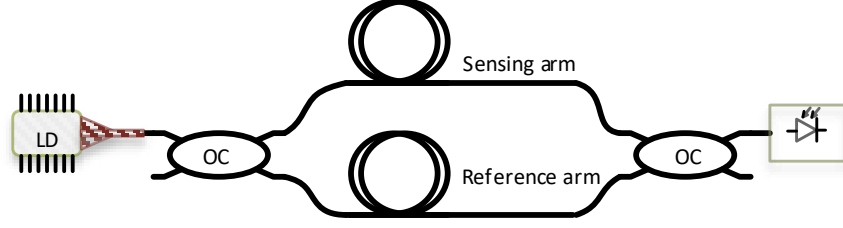


Fig. 2.3: Basic configuration of the Mach-Zehnder interferometer.

that both interferometers use the same fibres but spreading in opposite directions, an information where the external vibrations occurs can be calculated according to the formula [79]:

$$x = L_2 - c\Delta t/(2n), \quad (2.10)$$

where  $x$  is the distance from the event location to the second coupler,  $L_2$  is the length of the interference area, and  $\Delta t$  is the time delay that can be obtained by the correlation operation. Since the clockwise and counterclockwise signals are emitted from the same laser and are affected by the same vibration, the two interfering signals detected by the photodetectors have a strong correlation. Therefore, the time delay  $\Delta t$  can be calculated by locating the peak positions of the mutual correlation function between the two detected signals. This ensures localization of the event using a dual MZI [79].

### Michelson Interferometer

Like the Mach-Zehnder interferometer, the MI (Michelson Interferometer) is a widely used technique. A typical MI configuration for acoustic vibration sensing is shown in Fig. 2.4. Signal from a highly coherent laser source is divided by an optical coupler into two paths and launched into two fibres (reference and sensing). At the end of the fibres FRMs (Farraday Rotator Mirrors) are placed which cause that signals are reflected back and then recombined in the same optical coupler. It is important to keep the basic condition – the optical path difference between two beams is less than the laser coherent length. The basic MI configuration resulted in a number of modified configurations to improve a measurement capability [79].

Compare to Mach-Zehnder interferometer Michelson interferometer requires only one coupler. Because the optical signal propagates twice through the fibre the optical phase shift per unit length of fibre is doubled.

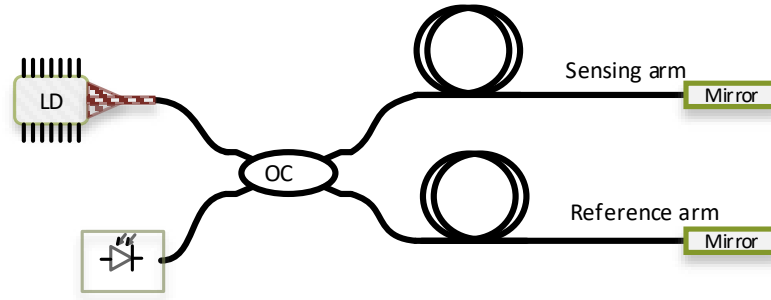


Fig. 2.4: Basic configuration of the Michelson interferometer.

### Polarization Interferometer

Polarization is a property of waves that can propagate in multiple planes. Standard single mode optical fibre is a low birefringent medium. As a result it typically exhibits changes owing to random fluctuations in the SOP (State of Polarization). The refractive index of the fibre may vary depending on strain or vibration applied on the fibre. This phenomenon is called the photoelastic phenomenon. In addition, in some cases the strain or pressure in different directions is different. The light spreading in the fibre is in general elliptically polarized and for different polarization modes  $n_1 \neq n_2$  due to fibre birefringence. Therefore, there is a phase difference between the different polarization directions, and external vibrations can be sensed by detecting a change in the polarization state [23].

### 2.2.2 Reflectometry-based Sensors

This type of fibre optic sensors are based on the use of backscattering while the forward signal propagate through the optical fibre. Scattering is a general physical process that results from the deviation of particles, toward space, from a straight trajectory. As light passes through the optical fibre, some of the radiation is not only absorbed but also scattered. Radiation scattering can occur as a result of a collision between light radiation and small solid particles of matter, possibly on molecules. Backscattering used for distributed sensing are depicted in Fig. 2.5.

There are two kinds of scatterings [23]:

- **Elastic** – in the case of elastic scattering, the energy of the reflected photon (even for a molecule) does not change and the wavelength is not changed. Elastic scattering includes Rayleigh scattering.
- **Inelastic** – in inelastic scattering, part of the photon energy is transferred to the molecule, or part of the energy is also received. The resulting radiation has

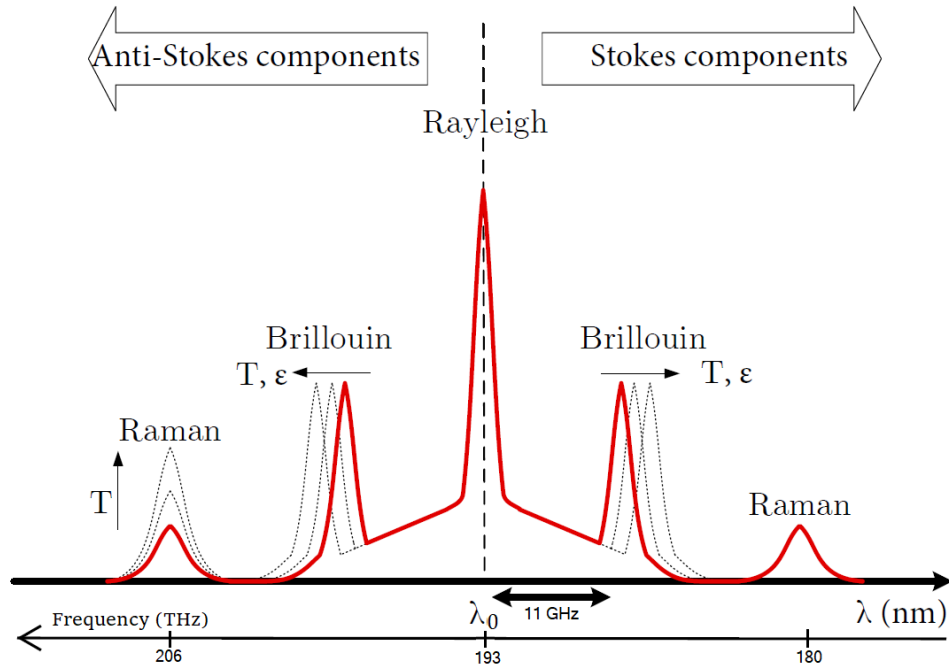


Fig. 2.5: Backscattering in single mode optical fibre.

a different frequency than the original frequency. Inelastic scattering includes e.g. Raman scattering.

### Phase Sensitive Optical Time Domain Reflectometry, $\Phi$ -OTDR

The first information about OTDR was reported more than 30 years ago [15], [7]. From that time this technique is widely used in telecommunications for detection of disturbances in fibre optical links. In basic configuration a modulated laser source, fibre optic circulator and photodetector are used for the Rayleigh backscatter detection. Since the laser source spectral width is relatively broad (from GHz to THz range), the back-scatter signal is insensitive to all events caused by temperature or acoustic vibrations. Using the narrow linewidth laser source system becomes sensitive to temperature and acoustics. Basic configuration of the  $\Phi$ -OTDR is depicted in Fig. 2.6.  $\Phi$ -OTDR systems are often referred to as DASs (Distributed Acoustic Sensors).

The backscatter method evaluates the dependence of the backscattered optical power during the propagation of the optical pulse through the measured fibre. In 1899, the English physicist John William Strutt, later also called Lord Rayleigh, described of this phenomenon. It was based on the assumption that light molecules are scattered directly by the air molecules and mathematically justified that the energy

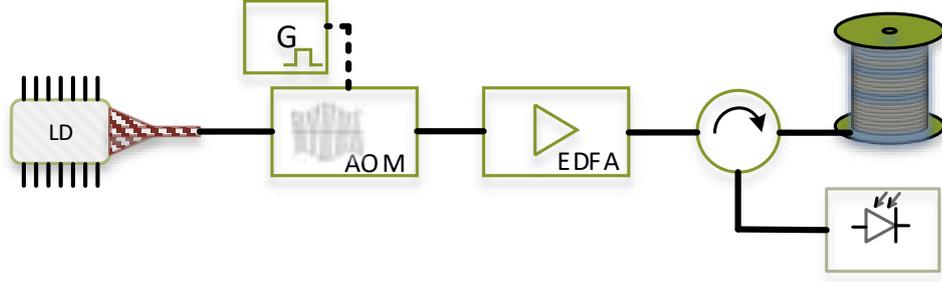


Fig. 2.6: Basic configuration of the  $\Phi$ -OTDR. LD (Laser Diode), G (waveform generator), AOM (Acousto-Optic Modulator), EDFA (Erbium Doped Fibre Amplifier).

of scattered radiation strongly depends on the wavelength, inversely proportional to its fourth power and directly proportional to the eighth power of the refractive index of the environment. This means that light with a larger wavelength (eg. red) diffuses less than light with a shorter wavelength (eg. blue) [28]. The Rayleigh scattering (see Fig. 2.7) is based on the elastic collision of photons of the incoming light with the molecule of the measured physical quantity. In this elastic collision, the energy  $E$  of the reflected photon does not change, which means that the newly formed scattered light radiation does not change the wavelength [4]. When a photon collides with a molecule, the molecule momentarily reaches an excited (higher) vibration energy level, but almost immediately returns to its initial energy level. Since there is no absorption, but also no emission of energy, the photon after the collision has the same energy as before the collision and therefore the same wavelength [4].

Rayleigh scattering can be described by Rayleigh scattering coefficient [18]

$$\gamma_R = \frac{8 \cdot \pi^3}{3 \cdot \lambda^4} \cdot n^8 \cdot p^2 \cdot \beta_T \cdot k \cdot T \quad (m^{-1}), \quad (2.11)$$

where  $\lambda$  denotes the wavelength,  $n$  is the refractive index,  $p$  is the photoelectric constant,  $\beta_T$  denotes the isothermal compressibility of the material,  $k$  is the Boltzmann constant, and  $T$  indicates the absolute temperature.

The backscatter power may be described as [18]:

$$P_R(t) = \frac{P_i \cdot S \cdot \gamma_R \cdot W_0 \cdot v_g \cdot \exp^{-\gamma \cdot v_g \cdot t}}{2} = P_R(0) \cdot \exp^{-\gamma \cdot v_g \cdot t}. \quad (2.12)$$

The  $\gamma$  is the attenuation coefficient and is equal to  $1/20^{th}$  of the gradient of a plot of Rayleigh back-scatter attenuation in dB. The  $P_i$  is the input power,  $\gamma_R$  is the Rayleigh scattering coefficient and  $S$  is the fraction of captured optical power and is defined for step index fibres as [18]:

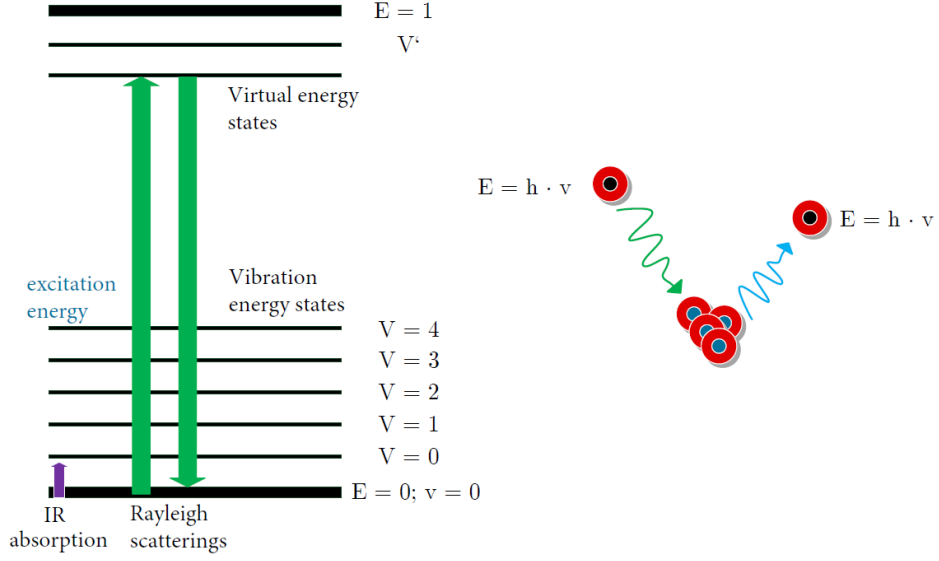


Fig. 2.7: Rayleigh scattering [4].

$$S = \frac{NA^2}{4n^2}, \quad (2.13)$$

where  $NA$  is the numerical aperture and  $n$  is the fibre refractive index. Using values  $NA = 0.12$ ,  $n = 1.46$  and  $\gamma_R = 4.6 \cdot 10^{-5}$  the Eq. (2.12) can be simplified as [18]:

$$P_R(t) = 7.8 \cdot E_p \cdot \exp^{-\gamma \cdot v_g \cdot t} = 7.8 \cdot E_p \cdot \exp^{-2\gamma \cdot x}. \quad (2.14)$$

In the Eq. (2.14)  $E_p = P_i \cdot W_0$  represents the pulse energy in Joules. For average power 150 mW and pulse duration 200 ns the  $P_R(0)$  is 230 nW [18].

The pulse repetition rate is dependent on the maximal length of the optical fibre, as described in Eq. (2.15).

$$\tau = \frac{2 \cdot L}{v_g} = \frac{2 \cdot L}{c/n} \quad (s). \quad (2.15)$$

For fibre optical link with total length of 40 km necessary time for one pulse spreading from the beginning to the end and back is defined as:

$$\tau = \frac{2 \cdot L}{c/n} = \frac{2 \cdot 40 \cdot 10^3}{3 \cdot 10^8 / 1.46} = 3.89 \cdot 10^{-4} \quad (s), \quad (2.16)$$

and repetition rate is then:

$$f = \frac{1}{\tau} = \frac{1}{3.89 \cdot 10^{-4}} = 2.57 \quad (kHz). \quad (2.17)$$

Spatial resolution for a pulse with the time duration of 500 ns is:

$$\Delta z = \frac{c \cdot T_p}{2} = \frac{2 \cdot 10^8 \cdot 5 \cdot 10^{-7}}{2} = 50 \quad (m). \quad (2.18)$$

More information about other parameters of the sensor system such as spatial resolution or about required technical parameters of the equipments of the system can be found in reference [85].

### **Brillouin Optical Time Domain Reflectometry – B-OTDR (Brillouin Optical Time Domain Reflectometry)**

In principle, the Brillouin OTDR is also based on conventional OTDR. B-OTDR systems are often referred to as DTSS (Distributed Temperature and Strain Sensor). The method utilizes stimulated Brillouin scattering at a supercritical value of the optical power input. The side bands close to the carrier wavelength, the so-called Brillouin Stokes and anti-Stokes, are used for the evaluation. These systems are capable of sensing temperature in addition to vibrations (strain) [70].

The interaction between the propagating optical wave and the acoustic oscillating particles of the optical fibre (phonons) generates Brillouin scattering, which propagates in the opposite direction. Since the phonon are exponentially distributed, the Brillouin scattering spectrum has the character of a Lorenz distribution. The frequency of the backscattered signal is shifted from the frequency of original signal by  $\nu_B \approx 11$  GHz for a wavelength of 1 550 nm. This frequency shift is referred to as the Brillouin shift  $\nu_B$ . If the fibre is stressed longitudinally by the pressure of  $\epsilon$ , the Brillouin frequency shift  $\nu_B$  will be proportional to this pressure. This can be expressed as [70]:

$$\nu_B(\epsilon) = \nu_B(0) + \frac{d\nu_B(\epsilon)}{d\epsilon} \cdot \epsilon, \quad (2.19)$$

where  $\nu_B(0)$  is the initial Brillouin shift,  $\nu_B(\epsilon)$  the Brillouin shift caused by strain  $\epsilon$  and coefficient  $d\nu_B/d\epsilon$  is given by [70]:

$$\frac{d\nu_B}{d\epsilon} = 0.5 \quad (GHz / \% \text{ strain}). \quad (2.20)$$

The Brillouin shift can also be expressed generally based on a change in refractive index [58]:

$$\nu_B = 2 \cdot \frac{nV_A}{\lambda_0} \quad (Hz), \quad (2.21)$$

where  $n$  is the fibre core refraction index,  $\lambda_0$  is the wavelength and the constant  $V_A$  expresses the rate of acoustic signal propagation in a given environment. It can be expressed by relation [58]:

$$V_A = \sqrt{\frac{K}{\rho}} \quad (m/s), \quad (2.22)$$

where the parameter  $K$  expresses the modulus of compression and  $\rho$  indicates the density of the material by which the acoustic wave propagates. For standard single mode optical fibres this value is 5 775 m/s [58].

The distance from the beginning of the measured fibre to the point of origin of the Brillouin scattering shift can be expressed by the time of propagation of the optical pulse from its transmission to the receipt of the backscattered signal  $T$  [70]:

$$Z = \frac{cT}{2n}, \quad (2.23)$$

where  $c$  is the speed of light in vacuum and  $n$  is the refractive index of the optical fibre core. Based on the power of the frequency shifted signal, it is possible to calculate the corresponding strain applied on the fibre at a specific distance by means of the Lorenz curve.

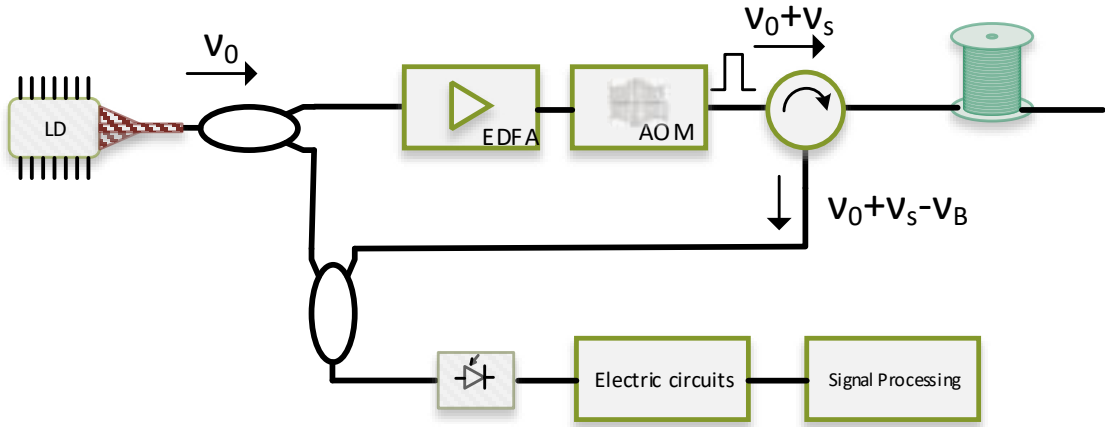


Fig. 2.8: Example of B-OTDR setup.

An example of a B-OTDR configuration scheme is shown in Fig. 2.8. The signal emitted by the DFB (Distributed Feedback) laser at  $\nu_0$  passes through an EDFA and a pulse modulator which also make a frequency conversion with a frequency shift  $\nu_S$  approximately corresponding to a Brillouin shift  $\nu_B \approx 11$  GHz at a wavelength of 1 550 nm. This signal is then launched to the fibre under test. The power of the Stokes component (shift  $\nu_B$  towards lower frequencies) of the backscattered signal is generally higher than that of the anti-Stokes component (shift  $\nu_B$  towards higher frequencies). Therefore, only the Stokes component, which is very close to the original frequency  $\nu_0$  can be used for measurement and then [70]:

$$\nu_0 + \nu_S - \nu_B \approx \nu_0. \quad (2.24)$$

In this way, it is possible to create a coherent heterodyne signal. Gradual change of the modulated frequency  $\nu_S$  eg. in steps of 10 MHz and by repeated measurements

gives a spectrum of Brillouin scattering at each point of the measured fibre. By further signal processing it is possible to convert the measured signal into a strain distribution along the optical fibre. The spatial resolution is given by the equation 2.18 as in the common OTDR. How much dB is Brillouin backscattered signal attenuated is given by [3]:

$$R_B = 10 \log \left[ \alpha_B \cdot S \frac{c \cdot T_p}{2} \right] \quad (dB), \quad (2.25)$$

where  $\alpha_B$  is the Brillouin attenuation coefficient ( $\approx 1.32 \cdot 10^{-6} \text{ m}^{-1}$ ),  $S$  is the ratio of the Brillouin backscattered signal to the total scattered signal,  $c$  is the speed of light propagation in the fibre and  $T_p$  is the pulse width. For pulse width  $1 \mu\text{s}$  and corresponding spatial resolution  $100 \text{ m}$  it is  $\approx -67.5 \text{ dB}$ .

The filtering of the Brillouin backscattered signal from the Rayleigh takes place in the electrical region by means of a bandpass filter with a bandwidth  $B$ , thereby attenuating it. This is defined as the ratio between the filtered signal component and the total Brillouin scattering. This attenuation can be calculated by the equation[3]:

$$T_S = 10 \log \left[ \frac{2 \cdot B}{\pi \Delta \nu_B} \right] \quad (dB), \quad (2.26)$$

where  $\Delta \nu_B$  is the Brillouin shift (explained above). For a bandwidth of  $1 \text{ MHz}$  corresponding to a spatial resolution of  $100 \text{ m}$  and a Brillouin shift of  $\Delta \nu_B = 30 \text{ MHz}$ , the signal is attenuated by an additional  $16.5 \text{ dB}$  by electrical filtration.

For the above settings, the Brillouin backscattered signal would be  $\approx 84 \text{ dB}$  lower than the forward signal, which is more than 3 orders of magnitude compared to the Rayleigh backscatter component. For this reason, it is necessary for the B-OTDR to use a coherent heterodyne detection, by which the signal can be amplified by up to  $20 \text{ dB}$  [3].

The critical power value at which the stimulated Brillouin scattering ( $P_{SBS}$ ) becomes apparent can be expressed as the signal power at which the backscatter is [58]:

$$P_{SBS} = 4,4 \cdot 10^{-3} d^2 \lambda^2 \alpha B \quad (W), \quad (2.27)$$

where  $d$  is the core diameter with the attenuation  $\alpha$ , the wavelength  $\lambda$ , and spectrum width  $B$ . Stimulated Brillouin scattering arises from  $5 \text{ mW}$  of power coupled to the optical fibre.

DTSS systems are mainly used in geotechnics and construction, the fibre length is usually several kilometres or tens of kilometres and the resolution of the unit of meters. For use in a current fibre data infrastructure as a more suitable seems to be modified configuration B-OTDA (Brillouin Optical Time Domain Analysis) which

allows using of lower optical power thanks to optical amplification based on OPLL (Optical Phase Lock Loop).

## 2.3 Data and Non-data Services

### 2.3.1 Accurate Time

The need to measure and know the current time is essential in all areas of human activities. Such need has accompanied the human civilization since its very beginning, although in the past, people mostly depended on utilization of a calendar. Time, as known today, was derived from the apparent movement of the Sun in the sky (more precisely, from the Earth's movement within the Solar System). However, this came with an issue: as soon as the necessity of knowing and measuring also smaller units of time such as hours, minutes, etc., problems did arise. Traditional solutions of course exist since ancient times, but as the time progressed, new types of time measurements such as so-called water clocks, or purely mechanical constructions which do not depend on Sun's movement have been discovered [34].

The clock is nowadays being understood as a device that contains a source of frequency produced by periodically repeated event and a device dedicated to counting such events. This principle applies to every clock, from pendulum, electronically controlled clock, crystals clock, to atomic clock (where a period source and the associated counter are always present). All types of clocks, even if being very precise, they slightly differ from each other. This leads to a question about how to compare the precision of a large variety of different types of clocks? The first step in order to do that is to select a reference time scale. In the past, GMT (Greenwich Mean Time) quantifying the mean solar time at the meridian passing through the Greenwich Observatory, was chosen for this purpose. At the same time, this observatory ensured the distribution of time both by shooting from a cannon at noon, and later also optically, using a falling balloon. This method was provided a good-enough precision for ships moored to the Thames in the vicinity of Greenwich. Other observatories could have implemented the GMT scale in a similar way, enough to know their longitude, i.e. the time shift from the prime meridian [34].

With the emergence of accurate time and frequency standards, an irregularity of the average solar time was detected, leading to an average solar time scale being no longer appropriate. As a result, the definition of the second as a  $1/86400$  of an average solar day had to be updated. After the construction of atomic clocks, which is based on utilization of small changes of electron energy in the atoms with a single valence electron, a unit of second was redefined in 1967: "The second is the duration of 9 192 631 770 periods of the radiation corresponding to the transition

between the two hyperfine levels of the ground state of the cesium 133 atom". This so-called atomic second also introduced two new time scales: TAI (International Atomic Time) and UTC (Coordinated Universal Time). TAI is a time scale that uses the combined output of some 400 highly accurate atomic clocks. It is mainly used in physics. UTC is the basis for civil time today. It is based on the same atomic second clock provided by atomic clocks, but respects Earth's rotation by including a leap second when the the solar time scale UT1 differs from UTC for more than 0.9 seconds. UTC is therefore a discontinuous time scale and gradually deviates from the TAI. At present, the difference is 37 s [34].

The previously mentioned description of UTC and TAI time scales in fact introduces a major technical problem: how to accurately compare time scales represented by the atomic clocks from different locations? Since the 1970's when the TAI scale has been defined, many different methods have been developed. These methods include the simplest ones such as transferring of running atomic clocks between laboratories, as well as more sophisticated ones that are used nowadays at a distance of several thousand kilometres, such as the simultaneous receiving signal from the same GNSS satellite at two different locations. The time uncertainties reached using this particular method are in the order of nanoseconds. Significantly more accurate, but very costly, is the TWSTFT (Two-Way Satellite Time and Frequency Transfer) method, using a reserved channel on a geostationary communication satellite. This method is mainly used between laboratories in Europe and the USA (United States of America) achieving uncertainty below 1 ns. Over the last decade, optical fibres have begun to succeed in such field. Various methods of transmitting precise time and stable frequency over a distance of hundreds to thousands of kilometres have been developed. Optical fibres have been used practically for almost 10 years and represent the only realistic possibility of comparing the output of the most stable current sources of frequency, the so-called optical clocks whose frequency output is in the optical range of the electromagnetic spectrum, unlike the classical atomic clocks generating the frequency in the range GHz. After the planned redefinition of second, based on optical clocks, the importance of optical fibre transmission is going to be even more significant [34].

The optical path requirements used for the transmission of time and/or frequency depend primarily on the choice of the utilized method [34]:

1. Network packet transfer – classical network technologies i.e. NTP (Network Time Protocol) and PTP (Precision Time Protocol), resp. IEEE-1588 (Institute of Electrical and Electronics Engineers) protocol do not impose on the optical path any specific requirements: Layer 2 (Ethernet) or Layer 4 UDP (User Datagram Protocol) is used. The actual transmission takes place in the same way as in the case of a metallic cables, and it is not important whether

the optical transmission is bi-directional (a single fibre is used) or uses a pair of unidirectional optical fibres.

2. WR (White Rabbit) technology – uses a synchronous Ethernet over the optical fibre. It is based on the assumption of the same length of the optical path in both directions. It also assumes a presence of bidirectional transmission in single fibre and uses standard optical transceivers.
3. Technology based on amplitude modulation by RF (Radio-Frequency) signal – for this purpose, various methods have been developed. The characteristic feature of these methods is the RF modulation signal for encoding transmitted time labels. These methods assume a symmetrical transfer path in both directions, i.e. bi-directional transmission using a single fibre, and possibly suitable methods for compensating delay variations due to external influences, especially temperature. In terms of the required bandwidth, a single DWDM channel for each direction is sufficient. Standard transceivers or fibre lasers are used as the source of the optical signal.
4. Transmission of unmodulated optical signal – subject of transmission is the unmodulated carrier signal from stabilized laser, which is controlled by a source of stable optical signal (e.g. an optical clock). Therefore, such method is used only for the frequency transmission, and not utilize for the time transmission. The standard uncompensated transmission path provides stability in the order of  $1 \cdot e^{-14}$  to  $1 \cdot e^{-15}$ . To increase the stability to the order of  $1 \cdot e^{-19}$ , it is required to stabilize optical fibre noise, i.e. to eliminate low-frequency interference caused mainly by vibration and shaking of the optical fibre. This method has low optical channel width requirements, a 50 GHz DWDM channel is sufficient enough.

### 2.3.2 High-speed Data

High-speed data networks are ubiquitous today almost everywhere and the only medium capable to satisfy constantly growing needs for more capacity is fibre. Some current data transmissions are based on OOK (On-Off Keying), but new systems are based on coherent detection principles and use multilevel phase modulations like DP-QPSK for 100 Gbps transmission speeds and 64QAM (64-level Quadrature Amplitude Modulation) is used for 400 Gbps transmission for commercially available equipment [34].

#### OOK (On-Off Keying)

The simplest technique uses optical pulses. If an electrical signal is transmitted in a certain time window (slot), it corresponds to a logical value of “1”, if the electrical

signal is not transmitted it corresponds to a logical value of “0”. Based on the logic state “1” or “0”, the optical signal is ON or OFF. This technique is a special kind of amplitude digital modulation and is called OOK modulation.

OOK modulation can be distinguished into two basic formats, RZ (Return-to-Zero) and NRZ (Non Return-to-Zero). The simplest modulation format is NRZ. The optical pulse of the NRZ format is generated over the entire duration of one bit. In the RZ format, the time of each optical pulse is shorter than the bit slot time, half that of the NRZ format, the amplitude of the optical pulse returns to zero before the bit duration ends. The advantage of the NRZ format is the relatively small bandwidth which allows a simple transmitter and receiver design. Optical pulses have a narrow optical spectrum. This reduced spectral width improves dispersion resistance and is also advantageous for implementation in DWDM systems [72]. The reduced spectral width also brings disadvantages resulting in an increase of inter-symbol interference between individual pulses. In addition, long sequences of the same bit values may cause loss of signal synchronization. The NRZ format is not suitable for high-speed and long-distance transmission systems, especially current 100 Gbps and higher transmissions [72].

For the RZ format is typical that the amplitude of the optical pulse returns to neutral level (zero voltage) at half the bit duration. These returns to neutral levels are used for signal synchronization. Furthermore, the RZ format allows increased resistance to non-linear phenomena, suppressing the effect of inter-symbol interference, suppressing the effects of polarizing mode dispersion, and increasing receiver sensitivity. The disadvantage is the larger spectral width of the RZ format than the NRZ format. The large spectral width reduces dispersion resistance, while decreasing the spectral efficiency. The RZ format is suitable for high-speed and long-distance transmission systems, but for 100 Gbps and higher transmissions high-order modulation formats must be used [72].

### **DP-QPSK (Dual-Polarization Quadrature Phase Shift Keying)**

The current trend is to use multiplexing at the level of symbols from data streams. Multiplexing in this case is not mean to multiply the bit rate using multiple wavelengths but to multiply the symbol rate by using a polarization multiplex. The modulation (symbol) rate indicates the number of signal elements (symbols) transmitted per second.

Quadrature Phase Shift Keying is a digital modulation technique used in optical fibre communication. It uses two orthogonal polarization planes of the laser beam, using QPSK modulation for each polarization plane [44]. QPSK modulation can transfer a pair of data bits (dibit) to a signal element, a symbol, DP-QPSK doubles

this value, and can transfer four bits of data to one symbol. DP-QPSK uses the polarization switching of two different QPSK signals to double spectral efficiency. DP-QPSK is a modulation mainly used in polarization multiplex systems with transmissions over 100 Gbps in combination with coherent detection and self-correcting codes [54].

# 3 Assessment of Suitability of Fibre Optic Sensing Techniques for Use in Data Networks

The goal of the Chapter is to evaluate possible interactions of fibre optic sensor signals with other signals (data signals and accurate time transmission) in a single optical fibre. Discussed are different standards of optical fibres and also various spectral grids. The chapter also presents sensitivity comparison of two different sensing systems. This Chapter contains various results from selected author's publications such as [63], [66], [65], [61], [60], [35], [34], and [64] that are focused on simultaneous transmission of sensing signals with another data/non-data signals and also on comparison of polarization and interferometry sensing systems. The structure of the Chapter is as follows: In the first Section, data and especially non-data services are defined in terms of measurement. The second Section describes experimental measurement results of simultaneous transmission of selected services with high-power sensing signal over different types of fibres. Presented sensing system is own developed system that was awarded at the Photonics Europe – Innovation Village in 2018 [92]. The results have been published in the journals with impact factor [35], [34] and at international conferences indexed in WoS (Web of Science) [61], [60]. The last Section focuses on sensitivity comparison of an interferometry and polarization methods for use in fibre infrastructure protection. Presented results have been published in the journal with impact factor [65] and at international conferences indexed in WoS [63], [66].

## 3.1 Photonics Services Description

### 3.1.1 Accurate Time Transmission

Systems for highly accurate time scales comparison utilize a method based on a bi-directional transmission with symmetrical transport delay in both directions [19, 90]. The principle can be seen in Fig. 3.1.

The two adapters are connected by a two-way optical line. Each of the adapters is provided with the 1 PPS (Pulse Per Second) timing signal and 10 MHz frequency from local clock at its input, two electrical signals are internally generated, specifically:  $T_{Ri}$  ( $i = A, B$ ), representing the received and decoded 1PPS signal from the remote adapter, and  $T_{Si}$  representing the moment when the encoded 1PPS signal is sent to the optical line. The  $T_{Si}$  and  $T_{Ri}$  signals are fed into two TIC (Time Interval Counter), that are started by the  $T_i$  signal – the 1PPS input signal. The first

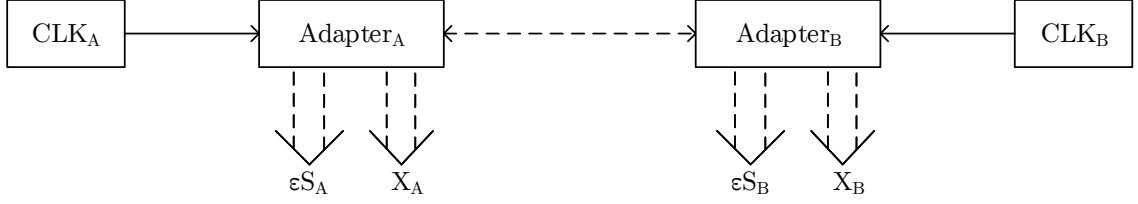


Fig. 3.1: Home developed time adapter

TIC is used to measure the interval  $x_i$  between  $T_i$  and  $T_{Ri}$  (the difference between a local and a remote 1PPS). The second TIC is used to measure the delay in the  $\varepsilon_{S_i}$  adapter, i.e. the time between the  $T_i$  and  $T_{S_i}$  signals. Internal structure of the adapter is shown in Fig. 3.2, photo of a real device is in Fig. 3.3 [34].

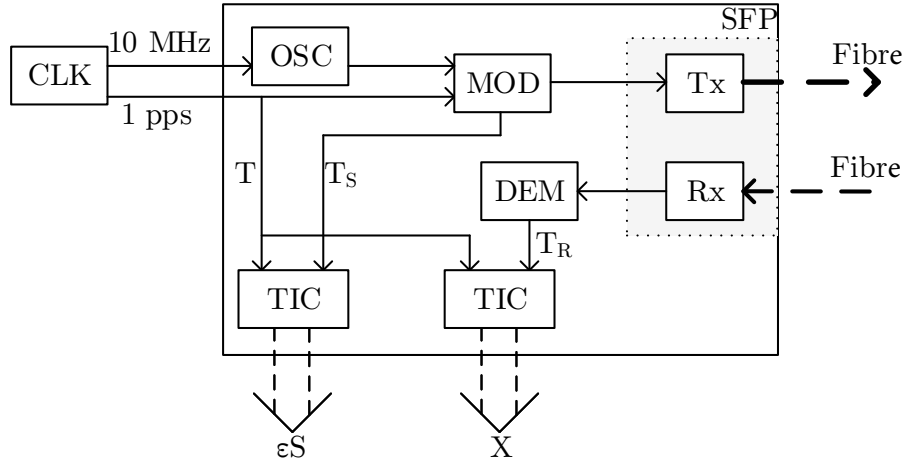


Fig. 3.2: Scheme of developed time adapter by CESNET.

The 1PPS pulse from the local clock arrives at the adapter A at time  $t_A$ . It is then sent to the optical line at time  $t_{SA}$  and received by the adapter B at time  $t_{RB}$ . By analogy, 1PPS from the remote clock arriving at the adapter B at time  $t_B$ , is sent at  $t_{SB}$  and received by the adapter A at time  $t_{RA}$ . Thus,  $\Theta_{AB} = t_B - t_A$  is the offset of both clocks,  $\varepsilon_{S_i} = t_{S_i} - t_i; i = \mathbf{A}, \mathbf{B}$  is the delay within the adapter  $i$ , and  $\delta_{AB} = t_{RB} - t_{SA}$  (can also be defined as  $\delta_{BA} = t_{RA} - t_{SB}$ ) is the line delay from A to B (B to A) [34].

By using TICs outputs (two in each location), it is possible to measure the internal delay of the  $\varepsilon_{S_i}$  adapter and the following time intervals [34]:

$$x_A = t_{RA} - t_A = \Theta_{AB} + \varepsilon_{SB} + \delta_{BA}, \quad (3.1)$$

$$x_B = t_{RB} - t_B = -\Theta_{AB} + \varepsilon_{SA} + \delta_{AB}. \quad (3.2)$$

In the case of a symmetric line, the delay  $\delta$  in both directions will be the same, specifically:  $\delta = \delta_{AB} = \delta_{BA}$ . In a real optical path, we can either transmit the signal unidirectional with the same wavelength in a pair of optical fibres or bi-directionally in a single optical fibre at different wavelengths. In the first case, there will struggle with an asymmetry of the physical length of the fibres, in the latter case the optical propagation velocity will slightly differ, as is given by the coefficient of chromatic dispersion, which generally depends on the wavelength. In both cases, there will be an asymmetry of delay  $\Delta$  [34]:

$$\Delta = \delta_{BA} - \delta_{AB}, \quad (3.3)$$

which needs to be computed in the case of a bidirectional transmission in a single fibre or evaluated during the phase of the calibration of the transmission route. With that said, the time offset of the clock is given by [34]:

$$\Theta_{AB} = \frac{((x_A - x_B) + (\varepsilon_{SA} - \varepsilon_{SB}) - \Delta)}{2}. \quad (3.4)$$

As mentioned above, wavelength and polarization sensitivity of refractive index needs to be taken into account. For example,  $L = 95$  km,  $d = 17.5$  ps/nm/km,  $\Delta\lambda = 0.8$  nm and  $D = 200$  ps/nm results in the propagation time difference of 1.49 ns. Otherwise, in case of time transfer in a pair of unidirectional fibre, there is no possibility to calculate the delay asymmetry, as we cannot guarantee the same physical length of both fibres – the delay asymmetry must be evaluated during the phase of the calibration of the transmission route [34]. With that said, the time offset of the clock is given by:

$$\Theta_{AB} = \frac{((x_A - x_B) + (\varepsilon_{SA} - \varepsilon_{SB}) - \Delta)}{2}. \quad (3.5)$$



Fig. 3.3: Photo of the time transfer adapter developed by CESNET

### 3.1.2 High-speed Data Systems

The used transmission systems are based on OOK modulation in the case of 1/10 Gbps bit-rate, and DP-QPSK modulation in the case of 100 Gbps bit-rate.

#### High-speed OOK data system

For 1/10 Gbps measurements, the EXFO FTB-700G service tester in the FTB-1 platform was used. The device allows to evaluate the BER (Bit-Error Rate) of the transmitted data signal. The Fig. 3.4 shows photo of the measurement device used for testing [25].



Fig. 3.4: Photo of the FTB-1 with FTB-700G tester [25].

#### High-speed coherent data system

The Coriant Groove™ platform for data transfer was used. This platform is dedicated for high-speed networks (up to Tbps) and supports programmable DWDM line interface bandwidth and performs optimization of a high-capacity transmission from 100G to 200G per port. Coherent line interfaces provide flexible rates for each transmission speed 100G (DP-QPSK), 150G (DP-8QAM), and 200G (DP-16QAM) etc. [14]. The Fig. 3.5 shows a photo of the measurement device used for testing.

### 3.1.3 Sensing System

We used our own back-scatter based fibre-optic sensor system based on the Rayleigh scattering. Basic block scheme of CESNET's  $\Phi$ -OTDR system is shown in the bottom part in Fig. 3.7. The ultra-narrow linewidth laser from a commercial vendor generates a CW (Continuous Wave) signal at 1550.92 nm which is first divided by coupler 50:50 into two arms. One part of the signal was used as a local oscillator for a back-scatter signal amplification, the other one was amplified in a high-power



Fig. 3.5: Photo of the Coriant Groove G30 [14].

EDFA to output optical power up to 27 dBm (0.5 W). Amplified output signal from high-power EDFA was then modulated by AOM to high-power pulse signal with a maximum value of 23 dBm due to insertion losses of AOM and patch cables. On both circulators, there are FBGs (Fibre Bragg Gratings) which serve as precise mirror with a central wavelength corresponding to wavelength 1550.92 nm of used laser. In our case, two circulators with FBGs also enable launching of other signals (data, time, and frequency) into fibre. The Fig.3.6 shows a photo of the measurement device used for testing.



Fig. 3.6: Photo of the own designed and developed DAS.

## 3.2 Simultaneous Transmission of the High-power $\Phi$ -OTDR, Standard Data, Accurate Time and Their Possible Interaction

Since optical fibre is a standard medium for all current and newly build networks these networks offer possibility for connecting new type of applications over long distances almost to anywhere. However, with increasing number of applications, number of dedicated fibres growing up. This constitution is quite unpractical and uneconomical especially if wavelength division multiplexing technology enables transmission of multiple different signals over one fibre. It is more than suitable to use this technology for cost reduction and network efficiency increase. Wavelength division multiplexing technology is a common technology in data networks where parameters of all signals are optimized (especially maximum optical power) for simultaneous transmission. In case of non-data applications the situation is more difficult because each application is represented by different type of signal and has its own requirements for transmission parameters. Hence it is necessary to evaluate possible interactions before field deployment. We dealt with possible interaction of a coherent 100 Gbps DP-QPSK data signal with new applications like accurate time transmission and high-power pulse signal used for distributed sensing. In laboratory setup we performed a measurement with a standard G.652D single mode optical fibre, G.655 fibre which can also be found in some networks and also with G.653 which may cause more non-linear interactions. All signals were transmitted in a grid with 100GHz spacing according to ITU standard [26].

Fibre networks are the only way how to satisfy the ever growing needs for more bandwidth and this trend will continue in following years because no successional technology is expected to replace optical fibre soon. Commercial optical transmission systems can transmit data at speed 400 Gbps per one lambda [21], with one terabit just round the corner, and the total number of lambdas is up to one hundred or even more. This is tremendous amount of data but there are also other areas of fibre optic networks, which are not focused only on enormous number of bits transmitted.

New applications like accurate time transfer or ultra-stable frequency transfer have been rather common, especially in NREN (National Research and Educational Networks). High speeds cannot satisfy requirements of such applications because minimal and stable delays are necessary. Other area which has been developed rapidly in recent years is fibre-optic sensing. Fibre-optic sensors are used in many areas of industry and it is clear that such interest in these sensors increases every year.

High speed data transmission, new applications like time and frequency and fibre-

optic sensors must share the common fibre optic infrastructure because it would not be economically feasible to build separate fibre networks, especially on bigger geographical scales like pan-European long distance networks. For this reason, parallel and simultaneous transmission of standard data, time/frequency, and sensing signals is rather new and unexplored area of research.

With rise of coherent optical transmission systems we can see some new trends when building optical networks. Few years ago it was necessary to deploy compensators of chromatic dispersion to allow 10 Gbps signals using OOK to achieve more than 80 km. Coherent systems were able to transmit 100 Gbps signals to distances up to a few thousands of kilometres without any need to compensate for chromatic or polarization mode dispersion and today 200 Gbps signals can travel up to one thousand kilometres over standard single mode fibre G.652. Because of such big distances, vendors do recommend to remove all compensators of chromatic dispersion and promote so called DCM (Dispersion Compensating Module) free networks because it is well known fact that DCFs (Dispersion Compensating Fibres) will decrease all optical reach of coherent systems because of stronger nonlinear effects (DCF has smaller core diameter hence higher power density and stronger nonlinear effects). DSP (Digital Signal Processing) can compensate for linear (chromatic dispersion) and stochastic (polarization mode dispersion) phenomena but DSPs cannot compensate for noise coming from optical amplifiers or nonlinear effects. There are papers describing these facts and practical aspects are described in the deliverable of pan-European project and R&E network GÉANT [1].

Unfortunately, accurate time signals are slow and OOK modulated, therefore may experience the degrading effects of chromatic dispersion (effects of polarization mode dispersion are less distinctive). Ultra-stable frequency signals are not modulated at all, information transmitted is the frequency of photons and such signals are CW. Fibre sensing signals can be somewhere in between these limits and it is evident that fibre optic networks optimized for coherent high speed signals and systems are not optimal for new time/frequency/sensing applications.

### **3.2.1 State of the Art**

The accurate time or stable frequency are traditionally important in the fields of metrology, navigation, fundamental physics, and legal time keeping. Nowadays, they are also important for significantly broader range of fields, e.g., sensing, Earth sciences, geodesy, astronomy and seismology. Advances in atomic, optical and quantum science have led to significant improvement in the accuracy of atomic clocks. Research in the field of atomic clock/s helped to push the boundaries of basic and applied research. The concept of atomic optical time is presented in [55]. Moreover,

authors of [8] presented research focused on increasing the accuracy of atomic clock up to  $6.4 \cdot 10^{-18}$ . This resulted in the improvement of the International System of Units' (SI) [10], the search for time variation of fundamental constants [80], the clock-based geodesy [42], as well as other accuracy tests of the fundamental laws of nature [8]. Traditional radiofrequency methods of precise time and transmission and dissemination use satellite methods. More accurate Two Way Satellite Time and Frequency Transfer (TWSTFT) method [45] achieves sub nanosecond stability however it requires pair of dedicated channels on geostationary satellite, so it tends to be very expensive. Much affordable is so called Common View method using one or more Global Navigation Satellite Systems as GPS (Global Positioning System) , GALILEO, GLONAS (GLObal NAvigation Satellite System) , etc [104]. However optical methods are able to deliver significant improvements in terms of stability mainly to utilisation of optical carrier with frequency of hundreds of THz (typically 200–600 THz). They can be used to satellite communication [76] or deployed on the ground, However the performance of the ground methods is compromised by limited reach and stability due to weather induced attenuation or turbulences respectively, [27]. Methods using optical fibres benefits from significantly shorter path compared with satellite based methods) and the possibility of active transmission stabilization. Optical time transfer methods deliver accuracy in the order of picoseconds (or even better) which is significantly better when compared to standard network methods, i.e., according to the IEEE Std. 1588. Another advantage over satellite transfer is elimination of possible jamming and spoofing attacks and also elimination of the antennas and the necessity of having a clear sky view, which might be challenging-to-achieve in underground facilities or very large buildings. Recently, there has been increased number of theoretical studies, laboratory trials and even field implementations of time and frequency transfer, e.g., [20, 81, 68, 98, 96, 100, 89, 53, 12]. Many works [107, 99, 51, 103] deal with simultaneous transmissions of accurate time and stable frequency. By transferring exact time and stable frequency, simultaneous transmission of two photonic services is realized. Next, [52] presents a simultaneous transmission, where the timestamps transmission is implemented by phase modulation with a spread spectrum pseudorandom modulation at 20 Mchip/s. A significant part of works report overcoming large distances using fibres shared with data transmissions [20, 53, 98, 96, 100]. At present, there are only a limited number of publications dealing parallel involvement of further photonic services e.g. optical fibre sensing. Works [61, 35, 60] describe the idea of involvement and realization of parallel optical fibre sensing, however in a little limited manner for different types of optical fibre and sensing system pulse duration only.

### 3.2.2 Experimental Setup and Results

During the measurement, emphasis on different fibres was placed. Initial testing was conducted using a photonic service (accurate time), sensing system, and data transfer. Each of the services was defined by its own wavelength. Measurement of BER was performed automatically using Coriant Groove™ G30 in 1 minute period. We aimed at demonstrating the possibilities of data flow being influenced by the pulse generated by our sensing system. It can be assumed that low-power signal will result in the availability of a service throughout the testing, whereas gradual increase in pulse duration will eventually affect the data signal. The data signal was not the only service being monitored. The accurate time transmission allows evaluation of delay in the fibre. Optical fibres are defined by their type and refractive index. After each of the optical fibres was measured, a combination of different types of fibres was created. Measured values of pre-FEC-BER (pre-Forward Error Correction–Bit Error Rate) indicate error rate prior applying any correction algorithm.

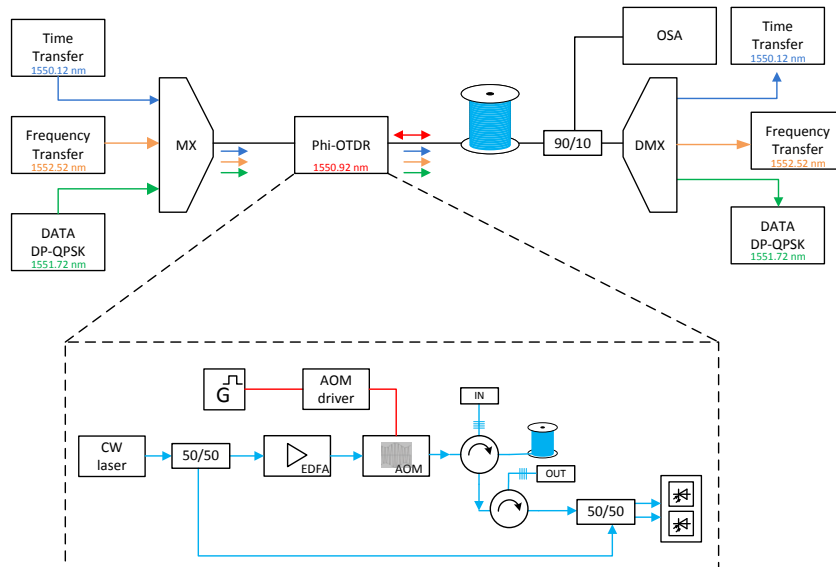


Fig. 3.7: Measurement scheme with  $\Phi$ -OTDR details.

The scheme depicted in Fig. 3.7 contains: accurate time, stable frequency, data signal, and high-power sensing system. First, time with frequency and data (DP-QPSK) were multiplexed together with 100GHz channel spacing. Sensing signal was added later (sensor signal uses high-power pulses which could damage multiplexer input port) and was transferred with other services through one fibre. The lengths of used fibres were 7 km in case of G.652D and G.653, and 10 km in case of G.655 fibre.

### Combination: Time, Sensor, Data and Frequency, G.652D and G.655 fibres

Fig. 3.8 shows allocated wavelengths of all services. More precisely, the following wavelengths were used: time transfer at 1550.12 nm (channel 34), frequency transfer at 1552.52 nm (channel 31), data transfer at 1551.72 nm (channel 32), and  $\Phi$ -OTDR at 1550.92 nm (channel 33).

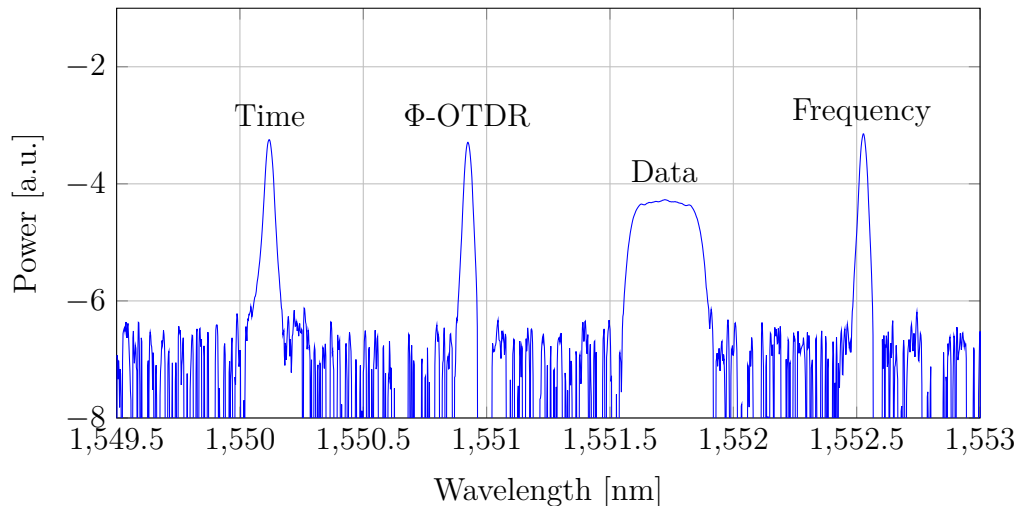


Fig. 3.8: Wavelengths allocation for measurement scheme – time,  $\Phi$ -OTDR, data, and frequency.

### Results and Discussion

The first measurement was with a spool of standard telecommunication fibre G.652D with a 10 kHz repetition rate and with different pulse durations (200, 500, and 1000 ns). The attenuation of such fibre is less than 0.2 dB/km at 1550 nm and  $\approx 0.31$  dB/km at 1310 nm, respectively. Second measurement was realized with the same pulse durations and repetition rate but a different spool of fibre was used. Fibre G.655 has higher attenuation values in comparison with G.652D:  $\approx 0.21$  dB/km at 1550 nm and  $\approx 0.35$  dB/km at 1310 nm. The quality of data signal measures commercial system itself. Graphs in Fig. 3.9 show comparison of pre-BER-FEC of 100G DP-QPSK data transfer for both fibres. From Fig. 3.9 on the left is obvious that BER values are approximately constant till the launched power reaches value of 24 dBm. Then the BER value is decreasing rapidly. For G.655 fibre were obtained approximately the same results as for G.652D but the threshold was 22 dBm. After another increasing of EDFA output power the data transmission had more errors, see Fig. 3.9 right.

Graphs in Fig. 3.10 provide a comparison of q-factor of 100G DP-QPSK data transfer for both fibres. For all measured pulse durations, dependence of a q-factor on EDFA output power is approximately same as in case of BER measurement.

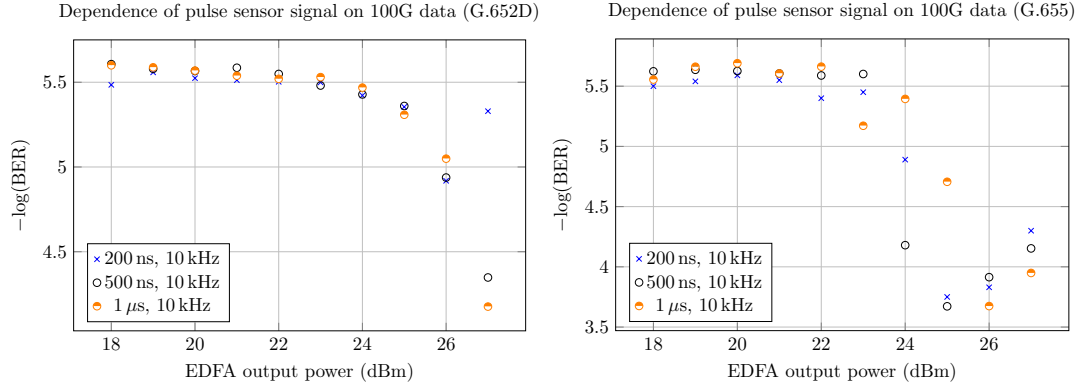


Fig. 3.9: Influence of high-power pulse signal on quality (BER) of DP-QPSK data signal for G.652 fibre.

Increasing of EDFA output power over some threshold and increase of pulse duration value lead to decrease of q-factor values. All results show decreasing pre-BER-FEC and q-factor values for higher EDFA powers but time and frequency transmissions remained stable all the time.

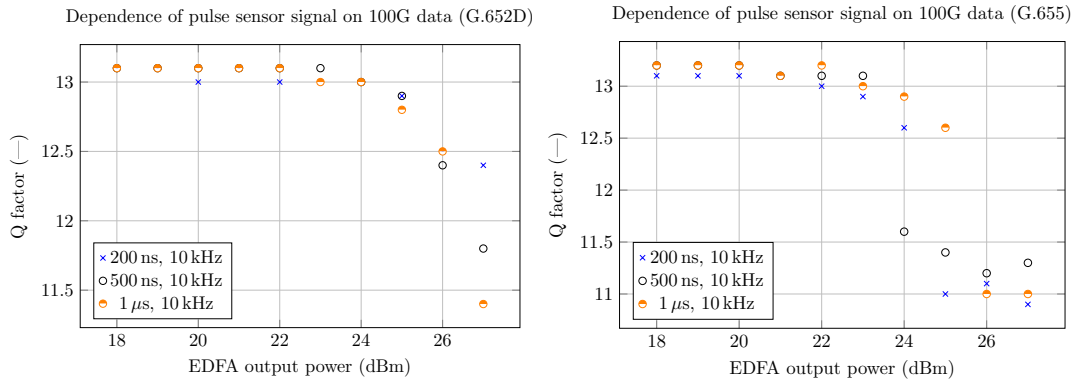


Fig. 3.10: Influence of high-power pulse signal on quality (q-factor) of DP-QPSK data signal for G.653 fibre.

### Combination: Data, Sensor, Time and Frequency, G.652D and G.653 Fibres

From Fig.3.8 is evident used channel spacing which is 100 GHz. Corresponding wavelengths of systems were: 1 550.12 nm (channel #34) for data transfer, 1 550.92 nm (channel #33) for sensor system, 1 551.72 nm (channel #32) for accurate time transfer, and 1 552.52 nm (channel #31) for stable frequency transfer. In this case not only pulse duration and EDFA output power were changed but also different repetition rates were evaluated.

## Results and Discussion

The first measurement was with a spool of optical fibre G.652D. It is standard telecommunication fibre with zero dispersion wavelength about 1300 nm and attenuation less than 0.2 dB/km at 1550 nm. Since the spacing between high-power sensor signal and frequency transfer was 200 GHz the frequency was relatively stable for all the measurement. The remaining two systems (time transfer and data) were set only 100 GHz next to sensor system and hence they were affected more. In case of accurate time transfer the system worked only in two modes: for EDFA output optical power up to 25 dBm system worked well with propagation delay 35471 ns. For power over 25 dBm system completely stopped working. The quality of data signal evaluates commercial system itself. Graphs in Fig. 3.11 show Q-factor and pre-BER-FEC of 100G DP-QPSK data transfer. One can see decreasing values of Q-factor when EDFA output optical power exceeds 25 dBm. The same situation appears for pre-BER-FEC. With increasing optical power of a pulse signal the number of errors increase. Thanks to FEC (Forward Error Correction) system is able to correct all corrupted/missed data but at the cost of reducing the maximum transmission rate.

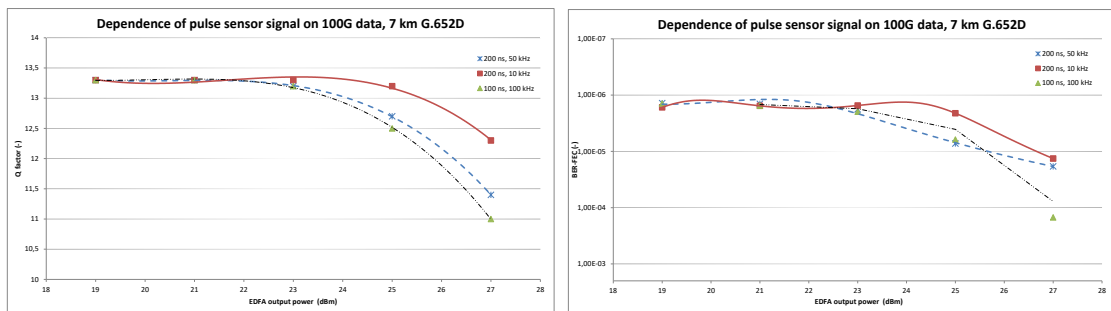


Fig. 3.11: Influence of high-power pulse signal on quality of DP-QPSK data signal for G.652 fibre.

The same measurement has been performed using DSF fibre which has zero dispersion wavelength about 1550 nm. As was described earlier we expected much more nonlinear effects and hence higher signal degradation. Measurement results are depicted in graphs (Fig. 3.12) showing Q-factor and pre-BER-FEC of 100G DP-QPSK data transfer.

Compare to G.652 fibre decreasing of Q-factor values started for lower EDFA output optical power in case of G.653. The same situation appears for pre-BER-FEC. For power over 23 dBm number of bit errors grew up. The FEC system was not able to correct all corrupted/missed data in this case. Time transmission was affected when power exceeded 23 dBm.

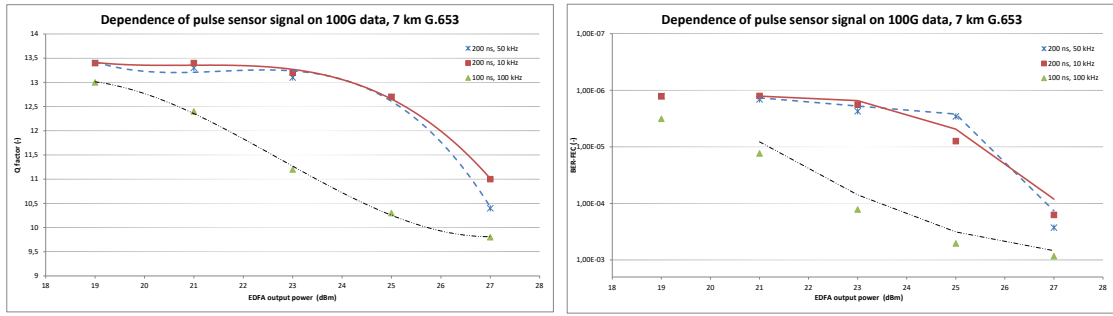


Fig. 3.12: Influence of high-power pulse signal on quality of DP-QPSK data signal for G.653 fibre.

### Combination: Time, Sensor, Data, G.652D, G.653, G.655 Fibres and Combination of G.652D and G.653 Fibres

The following wavelengths were used: time transfer at 1550.12 nm (channel 34), data transfer at 1551.72 nm (channel 32), and  $\Phi$ -OTDR at 1550,92 nm (channel 33). As in the first measurement the repetition rate was 10 kHz and dependence of various pulse durations on EDFA output power was evaluated.

### Results and Discussion

Fig. 3.13 shows the results for G.652D and G.653 fibres, respectively. As can be seen, the associated pre-FEC-BER values are independent and show a certain scattering pattern. However, linear dependence cannot be assumed at this point. The scattering could theoretically be eliminated by using a longer measuring period. For our measurement, the period of one minute was chosen. Coriant Groove™ G30 supports measuring ranges of 1, 15, or 60 minutes. As more emphasis is put on proving an influence among the services, use of longer period was not necessary. The pre-FEC-BER values are indicative of the measurements. However, as can be seen in Fig. 3.13, the values of pre-FEC-BER gradually decreasing as the increasing power of the sensor system affects the data transmission. It should be pointed out that for the G.652D fibre, i.e. the standard telecommunication fibre, the accurate time transmission was stable for all tested pulse durations and all output power levels of the EDFA. The average time delay was  $\approx 35328.415$  ns. On the right side of Fig. 3.13, measurements of a single G.653 fibre are visualized. With the increasing sensor system's power, values of the pre-FEC-BER got worse by an order in comparison to G.652D fibre. The accurate time transmission dropped out immediately after increasing the sensing system's power from 25 dBm to 26 dBm, even for the shortest pulse with a pulse duration of 20 ns. After increasing the pulse duration from 20 to 500 ns, the accurate time transmission was corrupted if the sensory system's power level reached 23 dBm. Another increase of pulse duration up to 800 ns did not affect

the accurate time transmission. The transmission failure occurred again after the sensory system's power increased from 22 to 23 dBm. Next, the pulse duration was raised to  $1 \mu\text{s}$  and the accurate time transmission showed frequent errors (no delay value displayed) from the power of 22 dBm. This trend is reflected by decreasing the pre-BER-FEC values on Coriant Groove™ G30, as can be seen in Fig. 3.13 (on the right side). As a result, G.653 fibre was found to be the least appropriate to conduct simultaneous transmission of photonic services. The average accurate transmission time delay was  $\approx 34968,292 \text{ ns}$ .

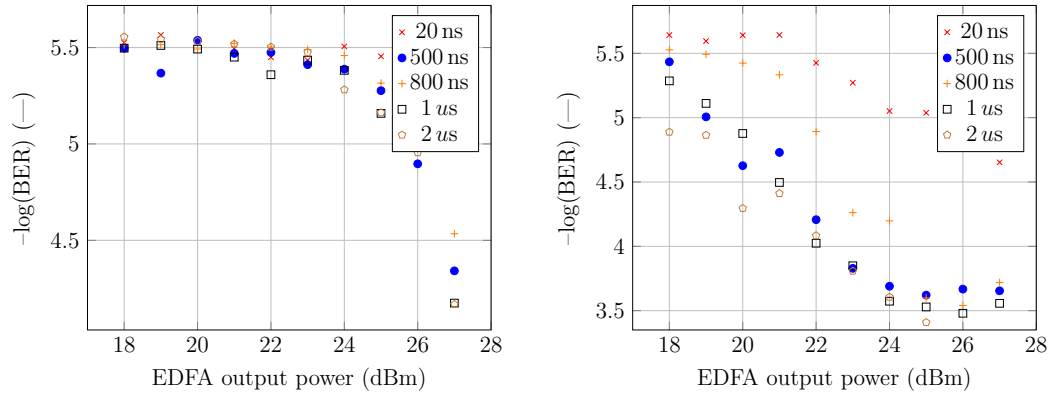


Fig. 3.13: Measurement results for G.652D (on the left side) and G.653 fibre (on the right side).

The previous two fibres had the same length of 7 km. In comparison to that, G.655 fibre has the length of 10 km. The results for G.655 fibre measurement are very similar to those for G.652D. Fig. 3.14 (on the left side) shows the measured pre-FEC-BER values for the G.655 fibre. In comparison with the previous examples, biggest scattering is to be found using this particular fibre. As mentioned above, these errors are caused by the measurement methodology, when a very short period was chosen to measure the data sequence during the evaluation. None of the tested pulse duration disturbed the accurate time transfer during the measurement, and there were no errors such those found for the G.653 fibre. With the maximum power of the sensor system and pulse durations 500, 800, 1000 and 2000 ns, comparable pre-FEC-BER values were achieved. The last measured optical route was made by combining G.652D and G.653 fibres. From the results (see Fig. 3.13) it is clear that the sensor system could not affect any of the services in the G.652D fibre. In comparison with the G.653 fibre, disturbing the accurate time transmission appeared even when the shortest pulse of the sensor system was used. For this reason, a combination of both fibres was created as the current optical-paths can be made up of individual sections where the use of different types of fibre is not excluded. Keeping the parameters stable across the optical path is essential for the operation

of photonic services. With the shortest pulse being used, there were no failures of the accurate time transmission. By increasing the pulse duration to 500 ns, occasional errors did occur, however. With a further increase of the power to 28 dBm, such errors occurred more and more frequently. The average accurate time delay was  $\approx 70234,602$  ns.

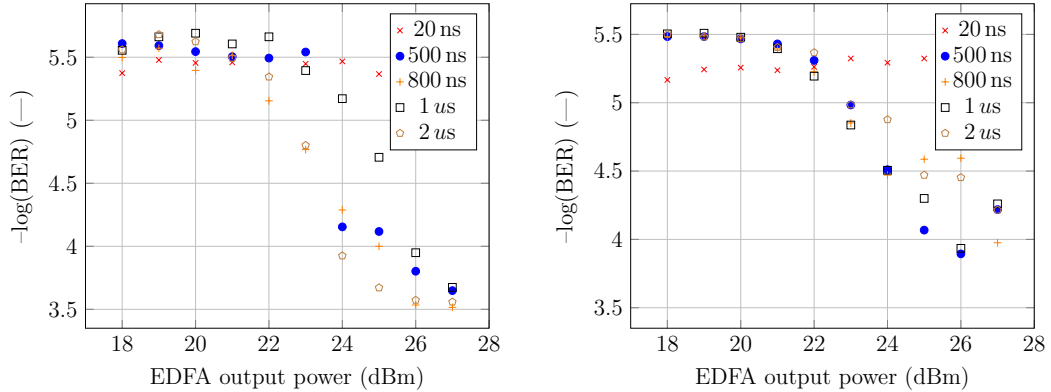


Fig. 3.14: Measurement results for G.655 (on the left side) and a combination of G.652D and G.653 fibres (on the right side).

### 3.2.3 Conclusions

In order to use the photonic services, it is crucial to keep their parameters stable with the reserved bandwidth across the spectrum throughout the optical-path. Transmission of accurate time and stable frequency is often described and implemented separately, although these are special applications that have very specific requirements to be fulfilled. Next, we also presented our own sensor system based on the principle of  $\Phi$ -OTDR as well as a system for accurate time transmission. Both of these systems were used during the measurements. As the WDM principle has been known for several decades, we can expect an increase in the use of measuring the simultaneous transmission of photonic services in a single fibre. However, it is not only about the transmission of data signals or special applications anymore. In the future, it will be necessary to take into account the deployment of sensor systems for critical infrastructure protection. Infrastructure protection is currently being a high demanded topic in the Czech Republic as well as in the world, and with the falling prices of optical fibre sensors, this trend is likely to keep going.

Although the ITU grid defines the 100 GHz spacing between services as sufficient, our measurements showed the exact opposite. The spacing between services without a sensor system is quite sufficient, however, with the use of high-power sensor systems, service interaction may occur. Our results also show that the influence among

the services is also given by the type of optical fibre being used. While G.652D and G.655 fibres are considerably less susceptible to service interactions, if infrastructure is made up of G.653 fibre, higher service spacing should definitely be considered.

### 3.3 Sensitivity Comparison of an Interferometry and Polarization Methods

This section presents comparative measurement of the polarization based sensing system and the interferometry based sensing system to determine the sensitivity and accuracy of both systems. Each system has its advantages and disadvantages, however the accuracy and sensitivity of the measurements are basic parameters that are important to know.

#### 3.3.1 Experimental Setup

The experimental measurement scheme is shown in Fig. 3.15. The scheme consists of two separate sensing systems in one setup. Using one complex setup for both measurements ensured almost identical conditions for both systems.

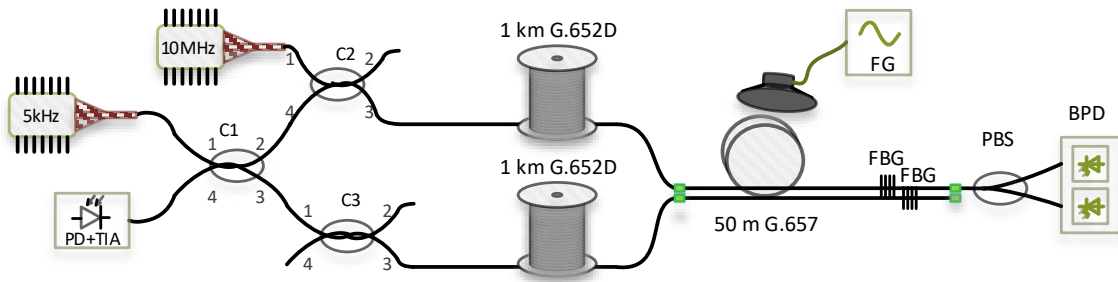


Fig. 3.15: Experimental setup for simultaneous measurement of two sensing systems. FG: Function Generator, PBS: Polarization Beam Splitter, FBG: Fibre Bragg Grating, PD: Photodetector, TIA: Transimpedance Amplifier, LD: Laser Diode.

Ultra-stable and narrow linewidth laser source PureSpectrum™-NLL (less than 5 kHz, corresponding to approximately 19 km coherence length) with a wavelength 1550.92 nm is used for the Michelson interferometer setup. A CW signal is in fused optical coupler C1 (2×2, 50:50 split ratio) divided into sensing arm and reference arm. Both signals then travel through couplers C2 and C3. While coupler C2 is used for launching a signal from the second laser diode into the fibre under test, coupler C3 has only a balancing function of the second arm: phase and insertion loss compensation. As mentioned above, an interferometer requires two arms with similar lengths (more precisely, the difference in the length of the arms must be less than the coherence length of the laser). For the measurement we used two separate 1 km long spools of optical fibre G.652D followed by 50 m long FTTH (Fibre to the Home) cable G.657A (4 coloured fibres in jelly, aramid yarns, PE outer sheath). As a mirrors FBGs with a reflectance about 90% were used. The Bragg wavelength

corresponds to the central wavelength of the narrow linewidth laser source, and the bandwidth is less than 0.1 nm. Signals corresponding to the Bragg wavelength are reflected back to coupler C1, and other signals pass through. The reflected signals from both arms interfere in coupler C1 and final signal is then detected on a photodetector (with an integrated transimpedance amplifier) connected to port 4 of coupler C1. The experimental setup of the Michelson interferometer is shown in Fig. 3.16 and is highlighted in green.

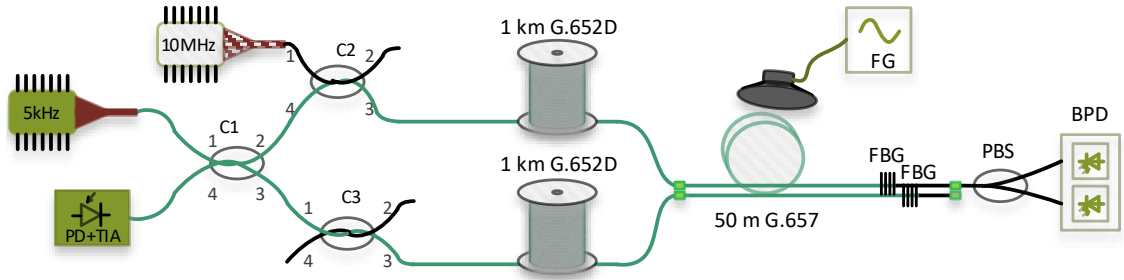


Fig. 3.16: Experimental setup of the Michelson interferometer is highlighted in green.

The polarization-based sensing system scheme is simpler, and only one fibre is needed (see Fig. 3.17). A laser diode with a linewidth of approximately 10 MHz generates the CW signal that is launched through the coupler C2 into the fibre under test. The laser wavelength is 1555 nm, which is different from the Bragg wavelength signal that is not reflected by FBG and passes to the polarization beam splitter that splits a single input into its orthogonal linear polarizations through two fibre outputs. As a receiver, we used a balanced detector. Two optical input signals are subtracted from each other, resulting in common mode noise cancellation. Using a balanced detector allows extraction of small changes in the signal path from the interfering noise floor [5]. Although the most common technique for measurement of acoustic vibrations is based on use of a polarimeter for polarization changes evaluation (as in [87]) we decided to use polarization beam splitter and BPD (Balanced Photodetector). By using a BPD, we can directly evaluate frequency of acoustic vibration instead of angular changes. Moreover, a BPD is a less expensive solution than a polarimeter. More information may be found in Section 4.2.

As a source of vibration, we used a loudspeaker and a signal generator. While both fibre spools were isolated from the source of acoustic vibration as much as possible (they were placed in another part of the room, laid on the foam to insulate the vibration from the floor), the cable was attached directly to the speaker with a tape. In the case of the Michelson interferometer, both arms (sensing and reference) were in the same cable, and the reference arm was therefore not isolated from sources

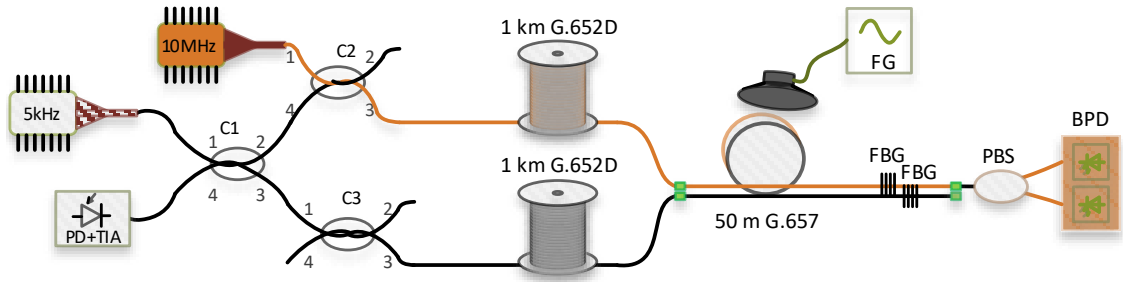


Fig. 3.17: Experimental setup of polarization interferometer is highlighted in orange.

of vibration. Thanks to a slightly different position of both fibres in the cable, each fibre was affected by acoustic waves differently. Signals from both systems propagate within the fibre-created acoustic wave by a loudspeaker, causing refractive index changes, and light travels by a different path. Electrical signals from both detectors are acquired using a 100 kS/s sampling rate for subsequent processing.

### 3.3.2 Results and Discussion

In real networks, fibres are in cables that are in HDPE (High Density Polyethylene) conduits and are  $\approx 70$  cm underground, and HDPE filters out higher frequencies. That is why for our laboratory measurements, we chose frequencies of 1025 Hz, 530 Hz and 130 Hz. A harmonic signal was generated by an AWG (Arbitrary Waveform Generator) and a loudspeaker.

We also tried to evaluate systems sensitivity on mechanical vibrations near the real fibre optic cable however the acoustic vibrations were not precisely defined, thus the results are rather for a demonstration and function test.

#### Sine Wave, Frequency 1030 Hz

The highest test frequency of a harmonic signal was 1030 Hz with an intensity  $10 V_{pp}$  (peak-to-peak voltage). Fig. 3.18 shows time signal and corresponding spectra of the interferometry system and the polarization system.

In a long-term test, the measured frequencies for both systems corresponded exactly to the generated frequency from the generator, as can be seen in Fig. 3.18. From the time domain signal of the interferometry system a modulated acoustic signal can be directly observed and signal intensity is relatively high, peak value is  $\approx -28$  dB. The signal from the polarization system was weak, and in the time domain, it was not possible to evaluate the modulated signal, unlike the interferometric system. The signal peak value was approximately 46 dB lower, with a value of

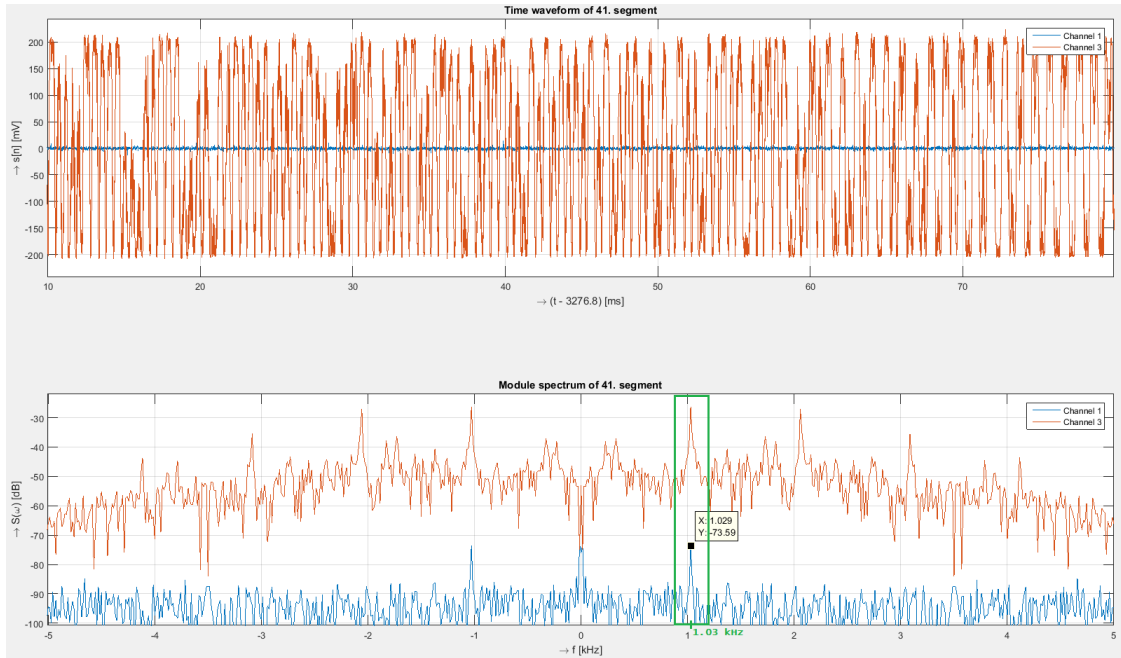


Fig. 3.18: Received signals from both sensing systems (interferometer – red signal, polarization – blue signal) and their spectra (below) for 1030 Hz.

–74 dB. In the interferometry system, sensitivity was much higher; however, sub-harmonic frequencies can be seen in the spectrum of the signal.

Fig 3.19 shows the details of the response from the polarization system. In the time signal, the amplitude fluctuates, making it difficult to recognize the modulated signal, but the spectrum shows a peak at a frequency of  $\approx 1027$  Hz with an intensity of –76 dB. These values correspond to a short time window, so they are slightly different from long-time values, which are more averaged.

### Sine Wave, Frequency 530 Hz

Next, measurements were conducted for a harmonic signal with a frequency 530 Hz and intensity of  $10 V_{pp}$ . Fig. 3.20 shows the time signal and corresponding spectra of the interferometry system and polarization system.

For long-term testing, measured frequency from both systems corresponded to the generated frequency 530 Hz from the generator, as can be seen in Fig. 3.20. The time domain signal of the interferometry system captures the modulated frequency, while the signal from the polarization system is very weak. The peak values of the interferometer were approximately –30 dB, and –72 dB for the polarization system.

In addition to the main frequency at 530 Hz, we can see in the spectrum of the interferometry system its multiple sub-harmonic frequencies with relatively high intensity.

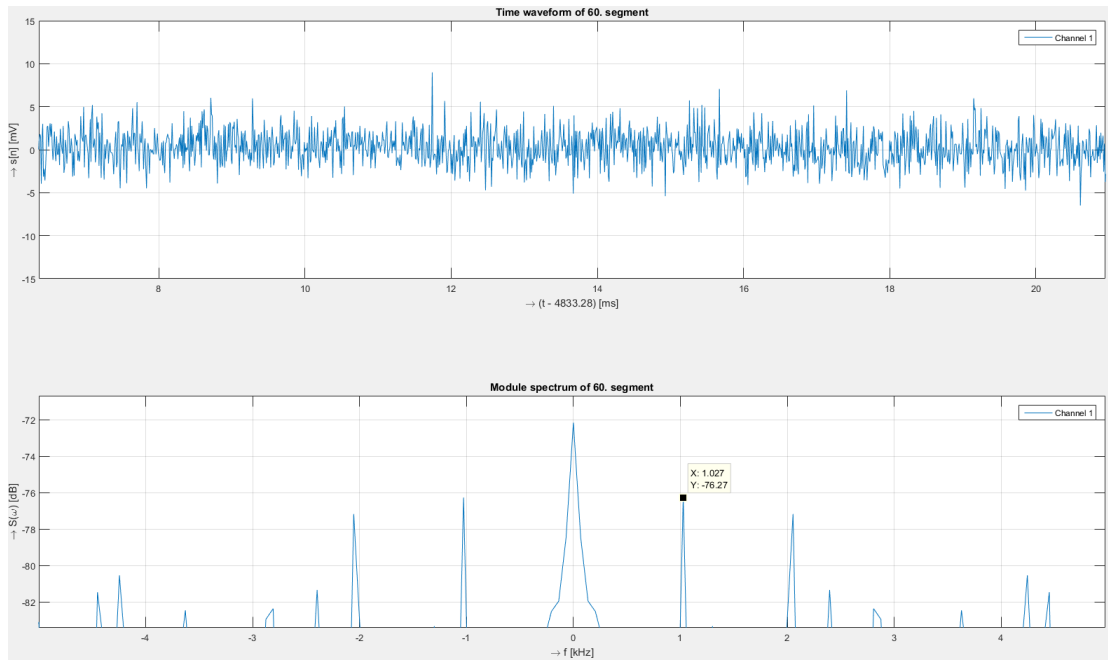


Fig. 3.19: Detail of received signal for polarization measurement and corresponding spectra (below) for 1030 Hz.

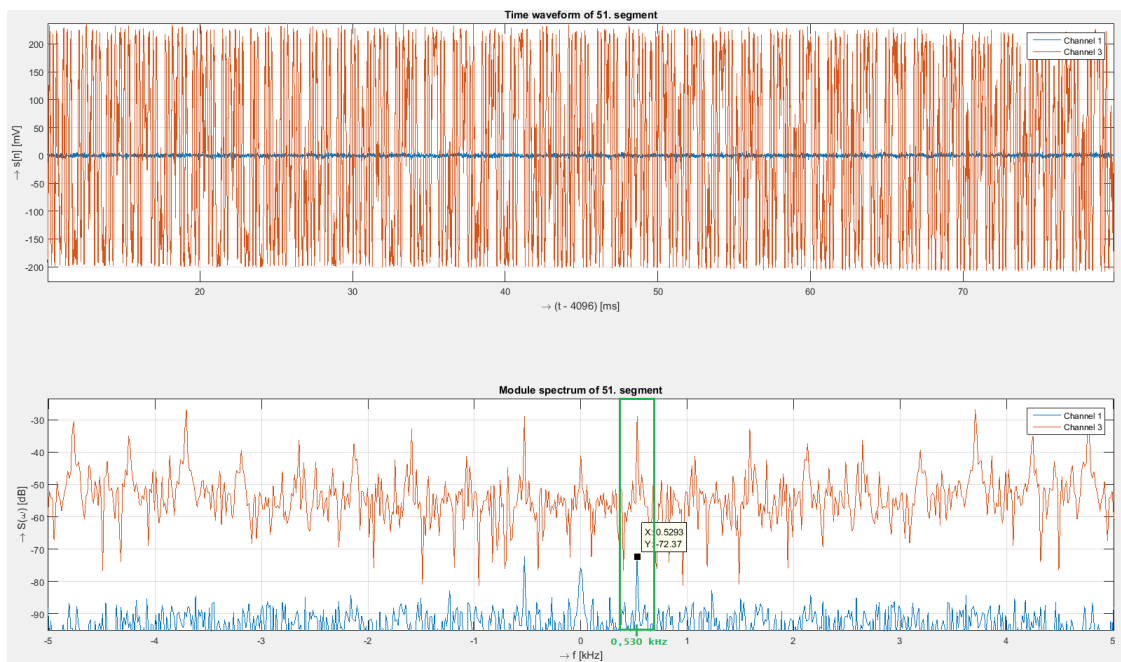


Fig. 3.20: Received signals from both sensing systems (interferometer – red signal, polarization – blue signal) and their spectra (below) for 530 Hz.

### Sine Wave, Frequency 130 Hz

The last measurement under laboratory conditions was performed for a harmonic signal with a frequency of 130 Hz and an amplitude of  $10V_{pp}$ . In Figure 3.21, we

can see the time signal and corresponding spectra of the interferometry system and polarization system.

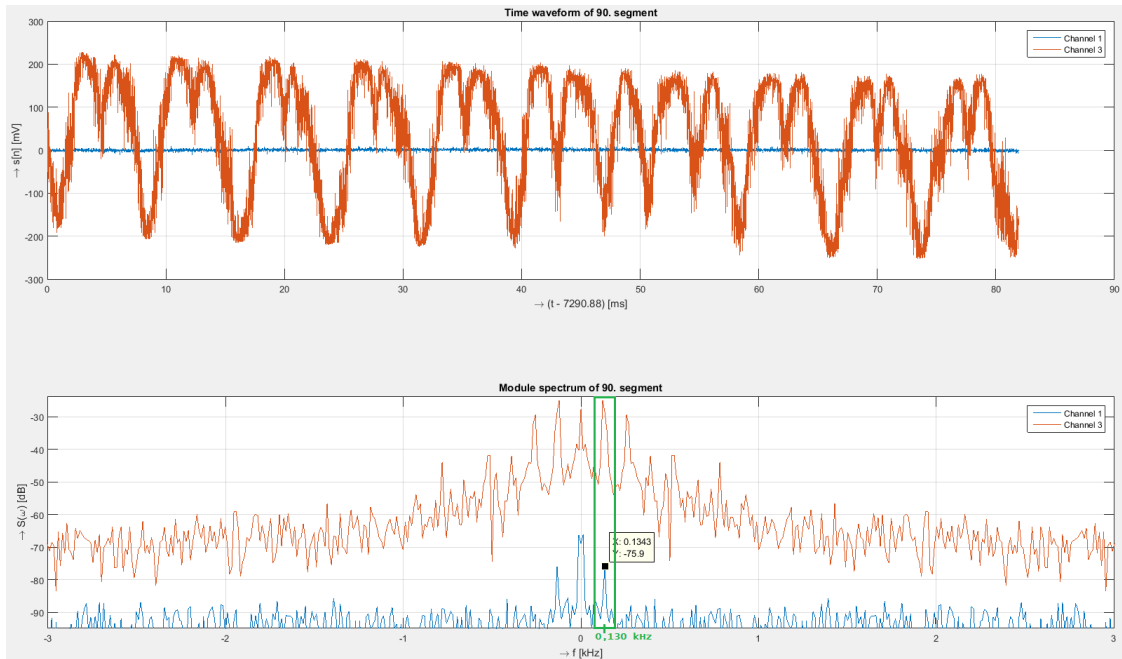


Fig. 3.21: Received signals from both sensing systems (interferometer – red signal, polarization – blue signal) and their spectra (below) for 130 Hz.

As in the previous cases, both systems measured the frequency correctly but with different intensities. While in the case of the interferometer, the signal was relatively strong, with a value of  $-25$  dB, and in the time domain, it was possible to observe the modulated acoustic signal, in the case of the polarization system, the signal was weak, and the peak intensity at 130 Hz was approximately  $-76$  dB. In addition to the main frequency, we can see other sub-harmonic frequencies in the case of interferometry system.

Below, in Fig. 3.22 are depicted calculated 3D spectrograms for all three frequencies measured by the polarization systems. The results show that with increasing frequency, the sensitivity of the system slightly decreases, and the SNR (Signal-to-Noise Ratio) deteriorates.

### Real Network Infrastructure Measurement

In this part, we briefly show the impact of mechanical vibrations on both systems. Compared to laboratory measurements, for polarization analysis, we used a Thorlabs polarimeter to show results on the Poincaré sphere. For this purpose, a 13 km length optical route between BUT (Brno University of Technology) and MU (Masaryk University) in the city of Brno was chosen (see Fig. 3.23).

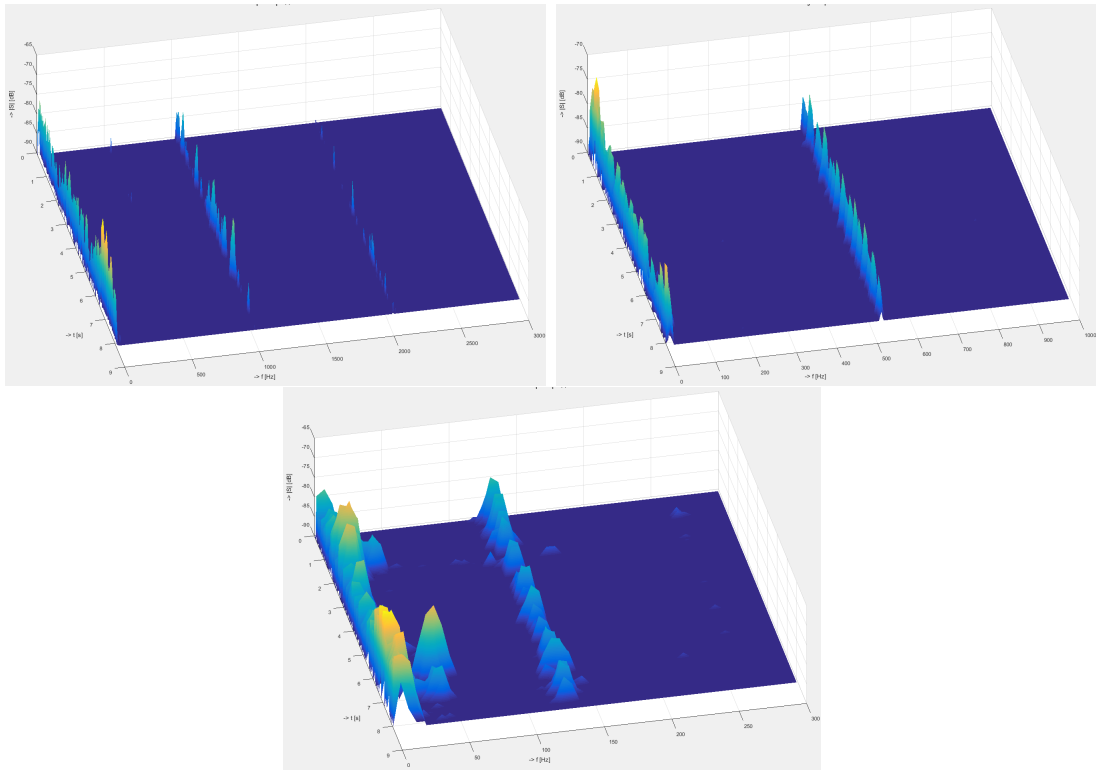


Fig. 3.22: Polarization system. Comparison of calculated 3D spectrogram for all measured frequencies. Top-left: 1030 Hz, top-right 530 Hz, and bottom: 130 Hz.

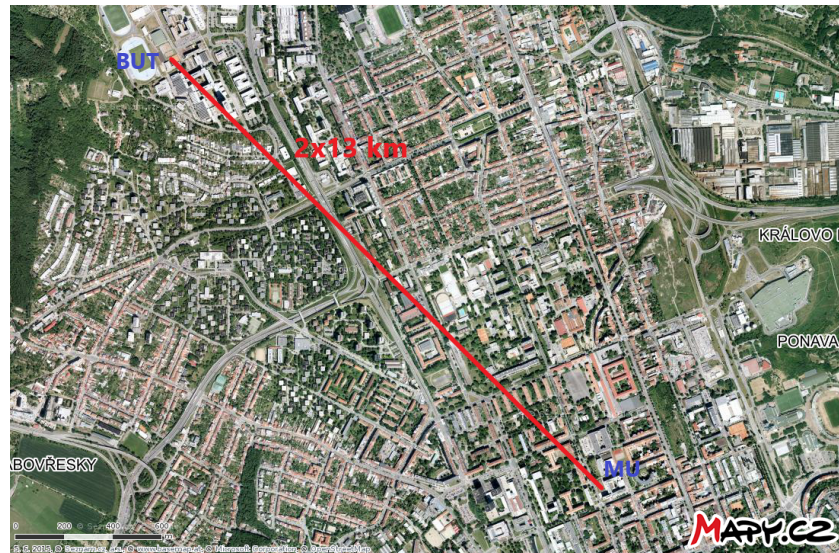


Fig. 3.23: Experimental university network between BUT and MU.

Fig. 3.24 and Fig. 3.25 show the time domain signal and its corresponding spectrum, respectively, for the mechanical vibration caused by knocking on a wall near a rack unit.

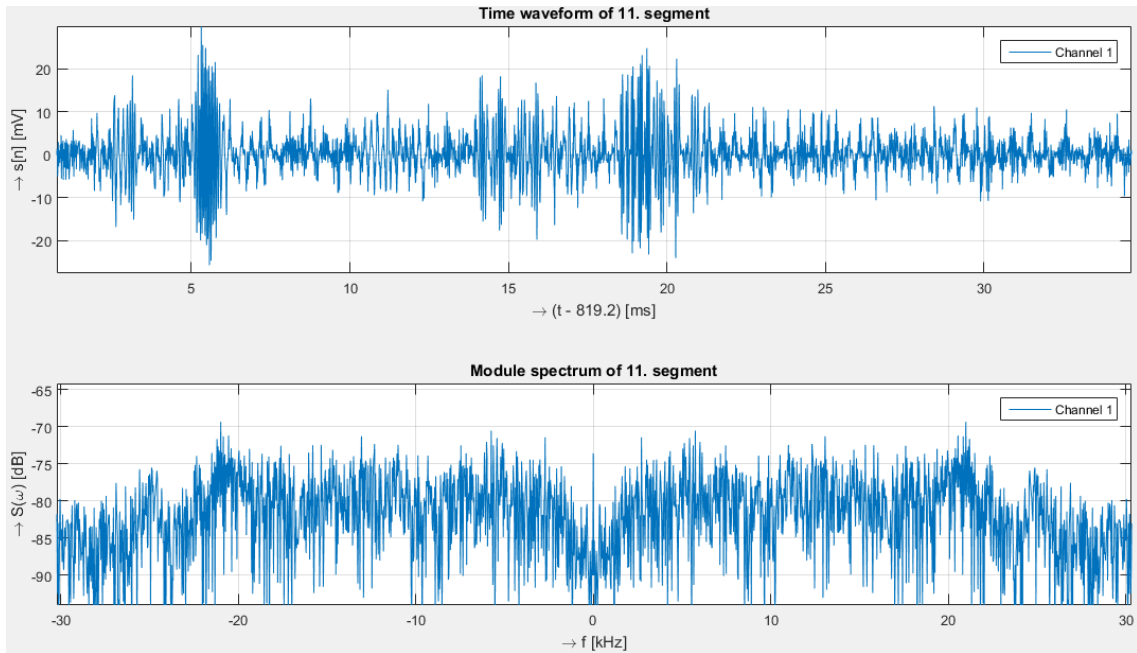


Fig. 3.24: Knocking on a wall near a rack unit close to an optical fibre. Response in time and corresponding spectra (below) measured with the interferometry system.

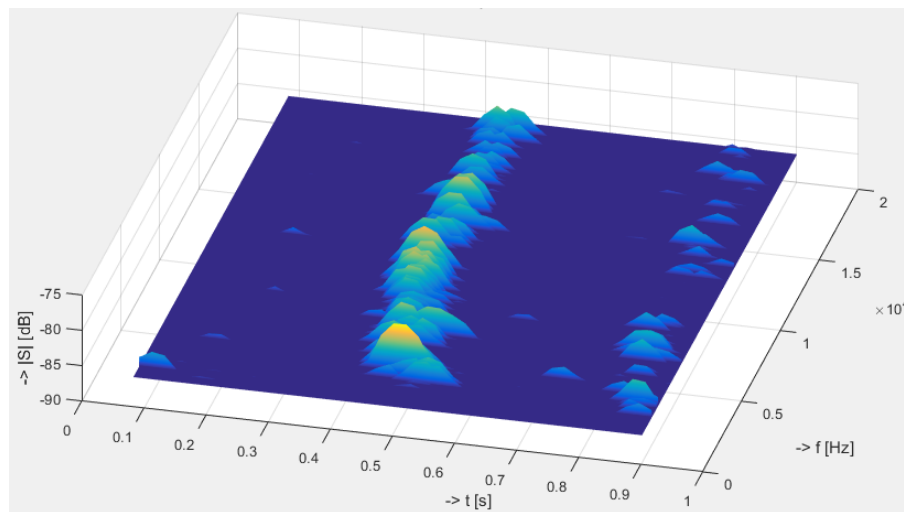


Fig. 3.25: 3D spectrogram. Knocking on a wall near a rack unit close to an optical fibre; measured with the interferometry system.

Compared to laboratory measurements, the signal was noisier. The main reason for noise was that the cable was located in the city of Brno, passing under roads or tram tracks several times. Even though, for example, tram ride passage is a relatively strong source of vibration, it was not possible to analyse these events even after postprocessing. Nevertheless, all these sources caused a certain increased noise level in the interferometric system.

In Fig 3.26 is depicted SOP change caused by mechanical vibrations: knocking near the fibre optic cable. The state of polarization change is plotted on the Poincaré sphere (Fig. 3.26 left) and is also described by Stokes parameters (Figure 3.26 right) that characterize the polarization change.

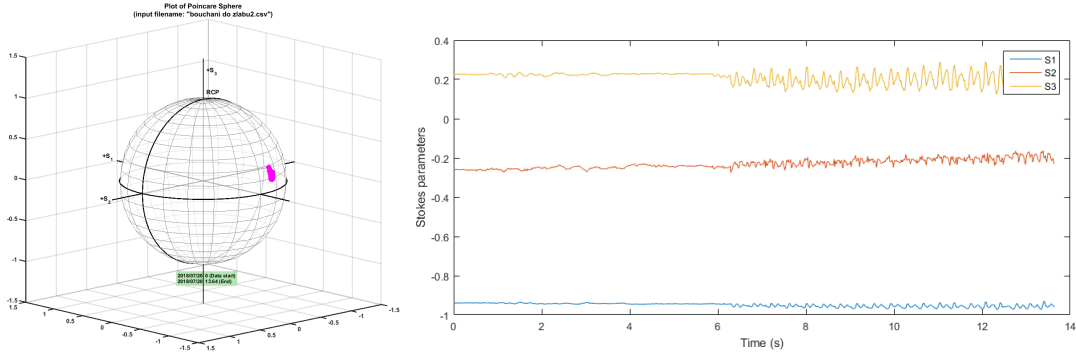


Fig. 3.26: SOP change caused by mechanical vibration near the cable. L: the Poincaré sphere, R: Stokes parameters.

### 3.3.3 Conclusions

In this paper, we briefly introduced two different acoustic vibration detection techniques for critical infrastructure protection, where both systems are capable of parallel operation with data transmission because power levels are relatively low. From our results, it is obvious that the interferometry-based sensing system is much more sensitive to surrounding events than is the polarization based sensing system. Many other sub-harmonic frequencies could be caused by the use of the loudspeaker. The signal intensity from the polarization-based sensing system was low, and without post-processing, it was not possible to evaluate the events. Another very important finding is possibility of using two optical fibres from one cable. Although it is generally stated that the reference arm must be isolated from the source of interference, the measurement confirmed that two fibres that are exposed to the same event can be used.

## 4 Novel Systems Based on Interferometric and Reflectometric Principles for Efficient Distributed Sensing

This chapter presents author's proposals and novel designs of distributed sensing systems for use in critical infrastructure protection. Each proposal focuses on different technology and suggest completely new setup to make it more effective. The main goal of these proposed systems and methods is suitability of putting them into practice.

Proposals are presented in the following sections as follows:

- Section 4.1 presents several possible solutions of amplification of weak signals in reflectometric systems.
- Section 4.2 presents an alternative solution to a polarimeter based on polarization beam splitter and balance photodetector which offers a cheap and compact undemanding solution.
- Section 4.3 presents a proposal of novel design for dual Mach-Zehnder interferometer based on a frequency shift and using only one fibre pair and measurement from one side.

### 4.1 $\Phi$ -OTDR Signal Amplification

Phase-sensitive optical time-domain reflectometry seems to be the most appropriate solution for acoustic vibration along standard optical fibre detection. In general, the sensing system measures phase changes of the received Rayleigh back-scattered signal in the fibre. Since the back-scattered signal intensity is decreased about tens of decibels in comparison to the forward propagating pulse power level, the received signal power level is very low. That is why the main limiting parameter of the system is the power level of the back-scattered signal, which limits maximum achievable distance. For a long reach sensing it is necessary to create high-power optical pulses with a short time-duration. Direct pulse amplification by EDFA is an issue because of the pulses low repetition rate. We have designed and verified a simple method using a holding beam for amplifying of pulses with low repetition rate by standard telecommunication EDFA booster instead of deployment of an expensive optical shutter. A second CW laser with a different wavelength for EDFA stabilization is used in our setup. Because the pulse losses its energy during propagation in the fibre and with longer distances the received signal power is lower. We have performed measurement using distributed amplification by 1<sup>st</sup> order RA (Raman Amplifier).

In telecommunications this amplifier is used to compensate for fibre losses. The last setup uses remote amplification by remotely pumped EDF (Erbium Doped Fibre) placed after a few tens of kilometers of sensing fibre. A pump laser is placed in the transmitter part of the system from where EDF is pumped. In this Section an overview of few techniques for  $\phi$ -ODTR signals amplification and their verification by measurement is presented. For all Sections the pulse power fluctuations were measured and will be discussed.

#### 4.1.1 Pulse Signal Amplification with a Low Repetition Rate by Standard Telecommunication EDFA

In this measurement we have used a standard telecommunication EDFA for the pulse signal amplification. Since the sensor systems uses repetition rates in the order of kHz (see Eq. (2.17)), standard telecommunication EDFAs may have a problem with stabilization of amplified signal (the telecommunication signals repetition rates are from the order of hundreds of MHz up to tens of GHz).

##### Measurement Setup

The setup for this measurement (see Fig. 4.1) was based on basic  $\Phi$ -OTDR setup. As optical source the OEwaves ultra-narrow spectral linewidth stable laser with central wavelength 1 550 nm was used. Since the output power of the laser was 20 mW and based on the knowledge of the received Rayleigh back-scatter optical power (see Eq. (2.14)), using EDFA is necessary.

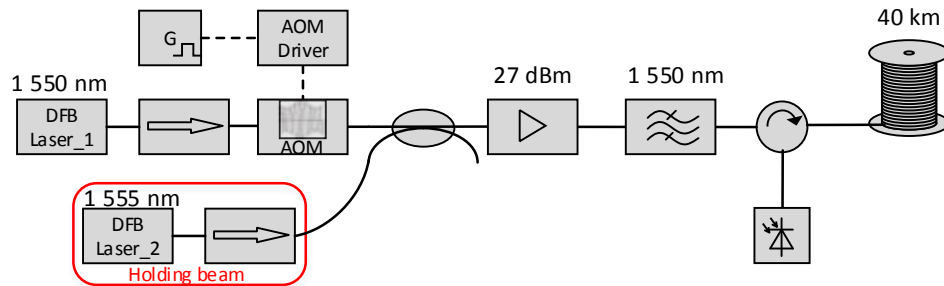


Fig. 4.1: Setup for optical pulse signal amplification using holding beam. Block G: signal generator, AOM: acousto-optic modulator.

AOM maximum input power was 300 mW with insertion loss less than 3 dB. After modulation the signal was amplified by EDFA booster (set to gain mode) with maximum output optical power  $\approx 27$  dBm. Second laser for EDFA stabilization was a common DFB laser CW laser with central wavelength of 1 555 nm. FUT (Fibre

Under Test) was realized by 40 km length optical fibre coil. For detection the PIN photodiode with a 200 MHz bandwidth was used.

## Results and Discussion

The first measurement was without holding beam (second laser was switched off). For pulse repetition rate 100 kHz and pulse duration 1 000 ns the difference between minimum and maximum power of the optical pulse was 102%. With the pulse repetition rate of 100 kHz and pulse duration 500 ns the power fluctuations were 78%. Limit value of pulse duration was 400 ns. Shorter pulse durations caused power fluctuations that were so large that sometimes there were outages. Also lower repetition rates caused large power fluctuations. For 1 000 ns the outages started at 67 kHz and for 500 ns at 75 kHz.

In the second measurement the holding beam laser was switched on. Power fluctuations did not exceed 25% for all repetition rates and all pulse durations. Fig. 4.2 shows results for both measurements – without holding beam and with holding beam. The part of these fluctuations (fluctuations till 10%) are caused by pulse generation in AOM as was reported in [106]. The rest of fluctuations are caused by amplification of low repetition rate pulse signals with holding beam in EDFA. To verify this, we have performed one more measurement, where the setup was quite modified. Optical signal was as first amplified and after that coupled into the AOM. Power fluctuations in this setup did not exceed 10%.

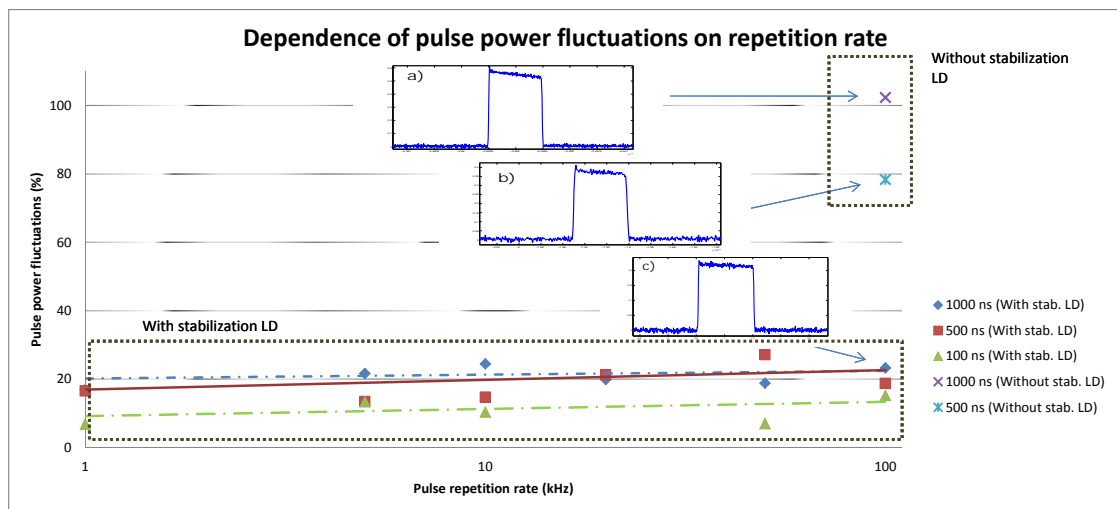


Fig. 4.2: Pulse stability with and without using stabilization LD.

Decreasing values of power fluctuations for shorter pulse durations in Fig. 4.2 can be caused by transfer characteristics of an electrical amplifier at the receiver and

also by electrical amplification characteristic which is part of a sampling acquisition card.

Details in Fig. 4.2 show output pulses degradation. Difference between the height of rising and falling edges was 11 % for pulse duration of 500 ns (Fig. 4.2a) and 15 % for pulse duration of 1 000 ns (Fig. 4.2b) in the setup without holding beam. For pulse duration 1 000 ns in the setup with holding beam the difference was only 6 % (Fig. 4.2c).

#### 4.1.2 Pulse Signal Amplification by Raman Amplifier

RA can be with advantage deployed for enlargement of achieved distance, neglecting partially fibre attenuation. Unfortunately, the pump signal is also attenuated when propagated in the fibre. It poses limits to achievable distance enlargement, especially in standard telecommunication fibres G.652 where the Raman gain coefficient is low and maximal pump power is limited by used optical connectors. Pump power is decreasing in transmission fibre as pump propagates, until it falls under some threshold level. Evolution of pump power is described as [43]:

$$P_p(z) = P_0 \cdot \exp(-\alpha_p \cdot z). \quad (4.1)$$

Where  $P_0$  is the input pump power and  $\alpha_p$  is the fibre attenuation at the pump wavelength. In practical situation when signal power satisfies small signal condition  $P_p \gg P_s$ , we can neglect pump depletion and describe signal evolution by [43]

$$P_s(L) = P_s(0) \cdot \exp(g_r \cdot P_0 \cdot L_{eff} - \alpha_s \cdot L), \quad (4.2)$$

where  $g_r$  is the Raman gain coefficient,  $\alpha_s$  is the fibre attenuation at signal wavelength and  $L_{eff}$  is given by [46]

$$L_{eff} = \alpha_p^{-1} \cdot [1 - \exp(-\alpha_p \cdot L)]. \quad (4.3)$$

By differentiation of Eq. (4.2), we can determine the optimal fibre length  $L_{opt}$ . Signal level increase till this length and after that signal starts to decrease because of attenuation [46].

$$L_{opt} = -\alpha_p^{-1} \cdot \ln(\alpha_s \cdot g_r^{-1} \cdot P_0^{-1}). \quad (4.4)$$

Using Eq. 4.4 and typical values of  $\alpha_p$ ,  $\alpha_s$  and  $g_r$  for SSMF (Standard Single-Mode Fibre) and NZDSF (Non-Zero Dispersion-Shifted Fibre) we can determine suitable lengths as shown in Fig. 4.3.

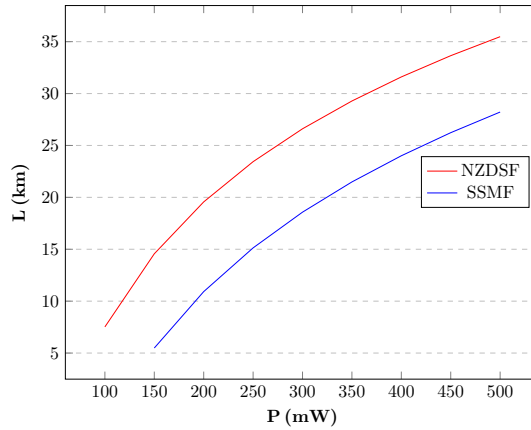


Fig. 4.3: Optimal length of optical fibre link for different pump powers.

### Setup of the measured system

The setup for this measurement was similar to setup used in measurements in Section 4.1.1. Acousto-optic modulator with maximum input power 300 mW was changed to AOM with maximum input optical power 1 W. Due to this change it was possible to amplified the CW optical signal in EDFA booster (set to gain mode) with maximum output optical power 27 dBm and after that modulate the optical signal. The total length of the FUT was again 40 km. Raman amplifier was in case of co-propagating amplification placed in front of the FUT and for counter-propagation amplification was placed at the far end of the FUT.

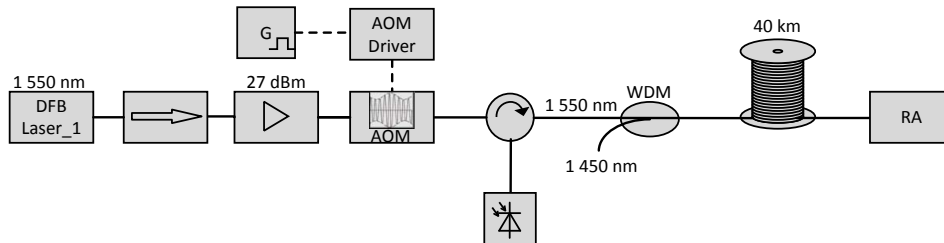


Fig. 4.4: Setup for optical pulse signal amplification by distributed Raman amplification. RA: Raman Amplifier, WDM: Wavelength Division Multiplex coupler.

### Results and Discussion

The first measurement was performed with counter-propagating Raman amplification. In this setup the RA was placed at the end of the optical link. WDM (Wavelength Division Multiplex) coupler enables split Rayleigh back-scatter signal that continue to port 2 of the circulator and Raman pump signal that is led out of the fibre.

Without any output optical power of the RA the end of the FUT was difficult to identify from the Rayleigh back-scatter response (top-left detail in Fig. 4.5). Pulse power fluctuations measured at the end of the FUT were greatest and probably mostly caused by electrical amplification in the receiver part. For output optical power 300 mW of the RA the back-scatter response from the FUT was well balanced (bottom-left detail in Fig. 4.5). Since power fluctuations were also low (compared to e.g. signal without any amplification by RA) it can be said that this setup is optimal for FUT with a length of a 40 km. When the output optical power of the RA was increased the total back-scatter response from the FUT was unbalanced. Response from the end of the fibre was much higher than from the beginning (bottom-right detail in Fig. 4.5). With higher optical power of the RA stability of optical pulses decreased.

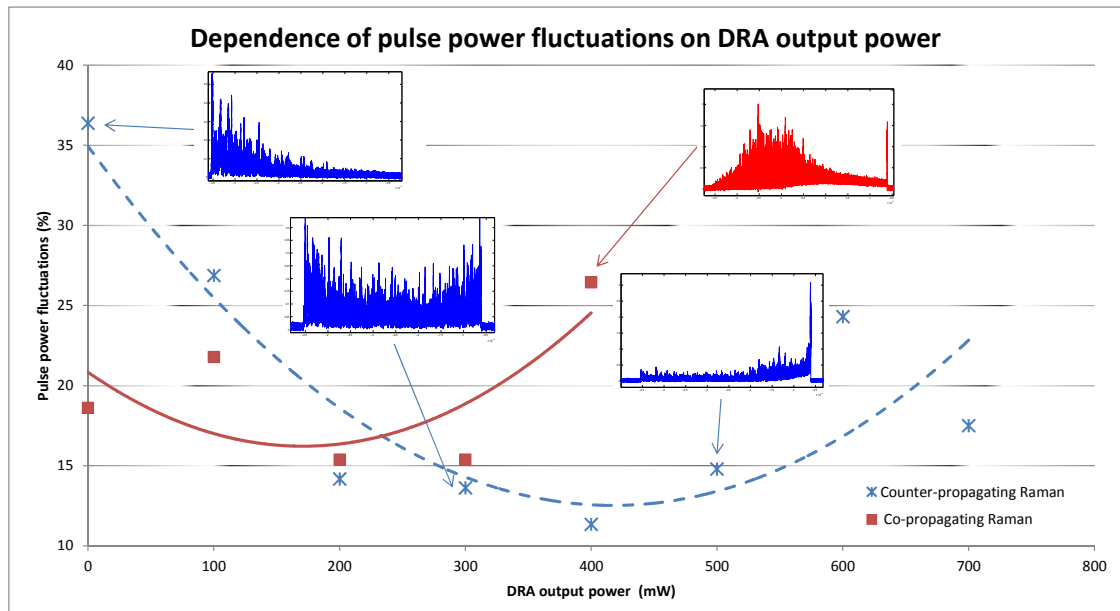


Fig. 4.5: Pulse power stability for different output powers of the co-propagating and counter-propagating Raman amplification.

For the second measurement the RA was placed instead WDM coupler and pump signal was co-propagated with the pulse signal. With increasing pump signal of the RA the Rayleigh back-scatter response from the FUT degraded. However, e.g. for RA output power 300 mW the response seems to be optimal and balanced, but in detail view the response is very noisy and also phase sensitivity is low. This degradation is caused by non-linear phenomena due to high powers of both – optical pulse signal as well as the Raman pump signal. Fig. 4.6 shows the response from the FUT for system with RA output power 300 mW. Detail in the top-right corner in the Fig. 4.6 then shows noise of the back-scatter signal.

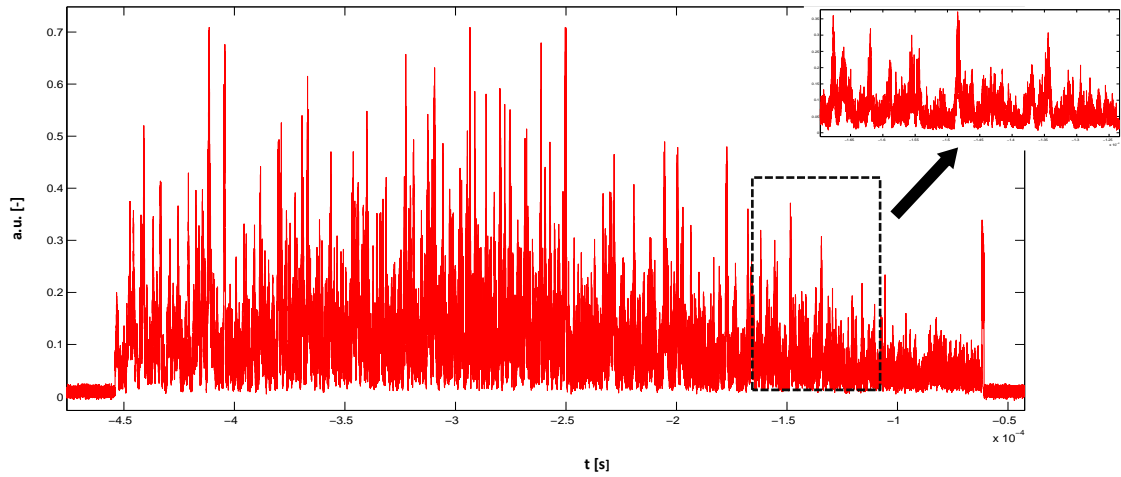


Fig. 4.6: Back-scatter response from the FUT for 300 mW output power of the RA.

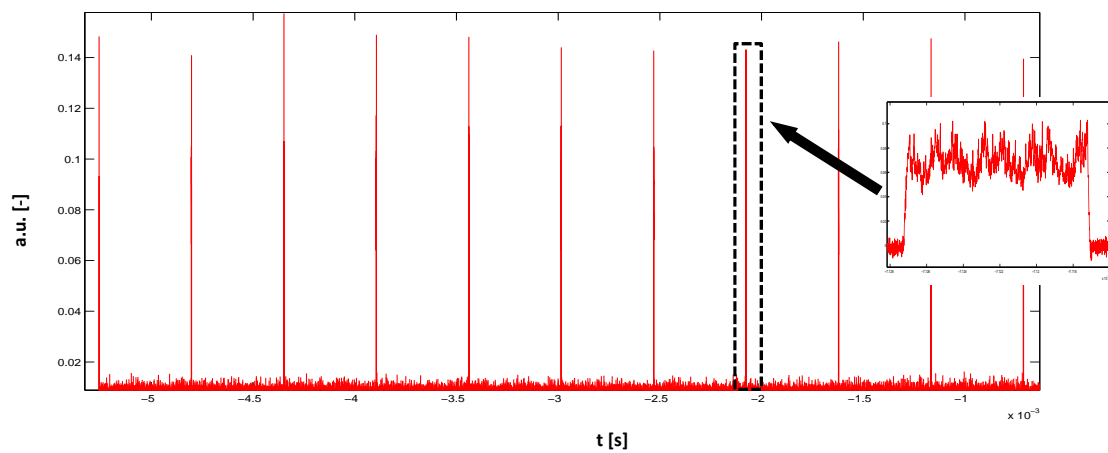


Fig. 4.7: Pulse power fluctuations and its degradation due to non-linear phenomena.

As you can see in Fig.4.5 measurement of pulse power fluctuations were carried out for the RA maximum output power 400 mW. The reason is large power fluctuations of higher RA output optical powers as is shown in Fig. 4.7.

### 4.1.3 Remote Amplification of a Pulse Signal

Erbium doped fibre amplifiers are the most use optical amplifiers in optical networks. Using configuration with pump laser placed in the transmitter part of the sensoric system and erbium doped optical fibre placed after tens of kilometers it is possible to remotely amplify optical signals and compensate the optical fibre attenuation.

When maximum gain of EDFA is lower than 20 dB a spontaneous emission can be neglected. Then by the determination stationary conditions we get [50],

$$N_2 = \frac{I_p/I_{sp}^a + I_s/I_{ss}^a}{I_p/I_{sp}^a + I_p/I_{sp}^e + I_s/I_{ss}^a + I_s/I_{ss}^e + 1} N_1. \quad (4.5)$$

Where  $I_{sp}^a = h\nu_p/\tau\sigma_p^a$ ,  $I_{sp}^e = h\nu_s/\tau\sigma_p^e$ ,  $I_{ss}^a = h\nu_s/\tau\sigma_s^a$ , and  $I_{ss}^e = h\nu_s/\tau\sigma_s^e$ . The frequency of the signal and of the pump are  $\nu_s$  and  $\nu_p$ ,  $h$  is the Planck's constant,  $\tau$  is the spontaneous emission decay lifetime,  $\sigma_s^a$  and  $\sigma_s^e$  are the stimulated absorption and emission cross sections of the signal beam,  $\sigma_p^a$  and  $\sigma_p^e$  represents the stimulated absorption and emission cross sections of the pump beam. Intensity of the optical signal is  $I_s$  and of the pump beam  $I_p$ , the total dopant density distribution is  $N_t(r) = N_1(r) + N_2(r)$ , where  $N_t$ ,  $N_1$  and  $N_2$  are all assumed to be radially symmetric [50].

We can define  $I_s(z, r) = P_s(z) f_s(r)$  and  $I_p(z, r) = P_p(z) f_p(r)$ , where  $P_s(z)$  and  $P_p(z)$  are optical powers of the signal and pump beams, and  $f_s(r)$  and  $f_p(r)$  are the normalized signal and pump transverse intensity profiles.

If  $R = \int_0^\infty N_t(r) f(r) r dr / \int_0^\infty N_t(r) r dr$  the pumping efficiency  $|dP_s/dP_p|$  increases with  $R$  for all  $P_s$  and  $P_p$ . For different lengths of erbium doped fibre it is possible to get equations for both co-propagating and counter-propagating pumping [50],

$$\left[ (P_s^{out} - P_s^{in}) \left( \frac{1}{I_{ss}^e} - \frac{\sigma_p^e}{\sigma_p^a I_{ss}^a} \right) + \ln \left( \frac{P_s^{out}}{P_s^{in}} \right) \frac{1}{R} \right] \frac{\sigma_p^a}{\sigma_s^a} = \quad (4.6)$$

$$= \left[ (P_p^{in} - P_p^{out}) \left( \frac{\sigma_s^e}{\sigma_s^a I_{sp}^a} - \frac{1}{I_{sp}^e} \right) - \ln \left( \frac{P_p^{in}}{P_p^{out}} \right) \frac{1}{R} \right]. \quad (4.7)$$

From Eq. (4.7),  $R$  may be obtained by measurements of  $P_s^{out}$  and  $P_p^{out}$  for given  $P_s^{in}$  and  $P_p^{in}$ . For maximum gain defined as  $G = P_s^{out}/P_s^{in}$  maximum output power of the pump laser is [50],

$$P_{p,op}^{out} = \frac{1}{R \left( \sigma_s^e/\sigma_s^a I_{sp}^a - 1/I_{sp}^e \right)}, \quad (4.8)$$

and

$$\frac{\nu_p}{\nu_s} \frac{P_s^{in}}{P_{p,op}^{out}} (G - 1) + \frac{\sigma_p^a}{\sigma_s^a} \ln(G) = \frac{P_p^{in}}{P_{p,op}^{out}} - 1 - \ln \left( \frac{P_p^{in}}{P_{p,op}^{out}} \right). \quad (4.9)$$

Propagation equation for the optical signal is [50],

$$\frac{dP_s}{dz} = -P_s \left[ \alpha_s + \left( \frac{1}{h\nu_s} \frac{dP_s}{dz} \pm \frac{1}{h\nu_p} \frac{dP_p}{dz} \right) h\nu_s/P_s^{IS} \right]. \quad (4.10)$$

Where  $\alpha_s$  is the absorption constant of the signal beam and is described as  $\alpha_s = 2\pi\sigma_s^a \int_0^\infty N_t(r) f(r) r dr$ . Parameter  $P_s^{IS} = Ah\nu_s/\tau\Gamma(\sigma_s^a + \sigma_s^e)$  is the intrinsic saturation power of the signal beam. By solving of the differential Eq. (4.10) output optical power of the signal at  $z = L$  may be obtained,

$$P_s^{out} = P_s^{in} \cdot \exp(-\alpha_s L) \exp \left[ \left( \frac{P_p^{in} - P_p^{out}}{h\nu_p} + \frac{P_s^{in} - P_s^{out}}{h\nu_s} \right) \frac{h\nu_s}{P_s^{IS}} \right]. \quad (4.11)$$

Without the pump beam  $P_s^{out} \cong P_s^{in} \exp(-\alpha_s L)$  for small input optical power of the signal and then  $\alpha_s = \log(P_s^{in}/P_s^{out})/L$ . When  $P_s^{in}$  approaches to  $P_s^{IS}$ ,  $P_s^{out} \cong P_s^{IS} \exp(1 - \alpha_s L)$ . This means that both the absorption constant and intrinsic saturation power of the signal may be obtained from absorption saturation measurement. Optimal fibre length  $L_{op}$  for maximum gain can be obtained from Eq. 4.11 [75]:

$$L_{op} = -\frac{1}{\alpha_s} \cdot \left\{ \ln(G) + \frac{h\nu_s}{P_s^{IS}} \left[ \frac{P_{p,op}^{out} - P_p^{in}}{h\nu_p} + \frac{P_s^{in}}{h\nu_s} (G - 1) \right] \right\}. \quad (4.12)$$

### Setup of the Measured System

The setup for remote amplification is based on the setup used in measurements in Section 4.1.2. Transmitter part of the system is the same and also all parameters stayed unchanged. Only optical link part has changed. The total length of the FUT with a length of 40 km was increased by 20 km long optical fibre coil. In this measurement two EDFs were tested – a 10 m of a metro EDF, MP980, with absorption of about 6 dB/m and a 4 m of EDF, I-25(980/125), with absorption of about 30 dB/m. The pump laser was coupled to the FUT using WDM coupler and pump signal was co-propagated with the pulse signal. Setup of the measurement system is shown in Fig. 4.8.

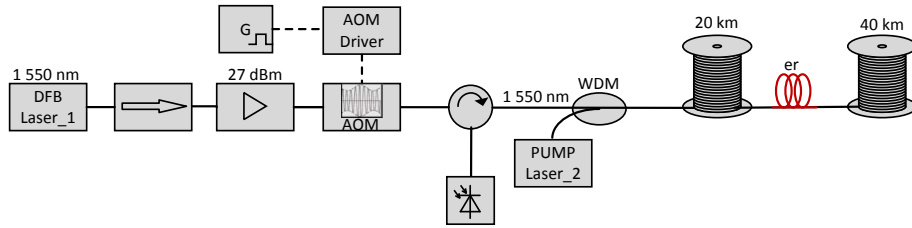


Fig. 4.8: Setup of the measurement system for remote amplification.

### Results and Discussion

When the pump laser was switched off absorption of the EDF totally absorbed optical signal. This situation was almost the same for the pump laser output power until 105 mW. On the first detail from the left in Fig. 4.9 is shown the back-scatter signal for laser pump output power of 105 mW. Back-scatter signal from the FUT was detected only for the first 20 km.

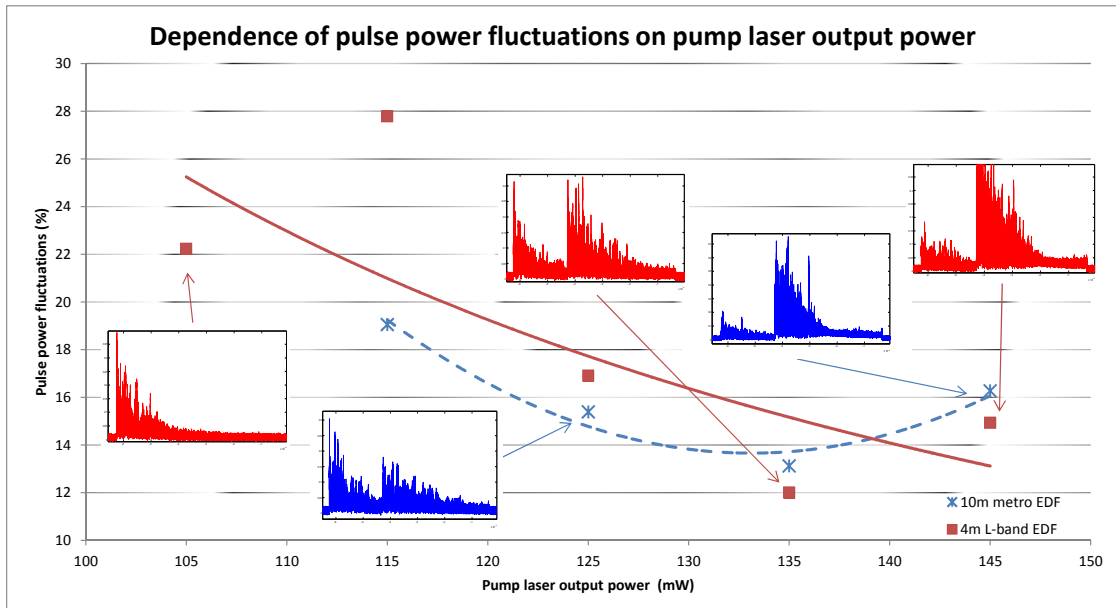


Fig. 4.9: Verification of the remote amplification and its influence on the optical power stability of the optical pulse.

With increasing optical power of the pump laser a stimulated emission exceeded absorption in the EDF and amplification occurred. For a 10m long metro EDF ideal amplification occurred when output power of the pump laser was 125 mW. Ideal amplification for the second EDF, a 4 of L-band EDF, was with pump laser output power of 135 mW. Back-scatter signals for both EDFs can be seen in details in Fig. 4.9. When increasing laser pump output power response from the second fibre coil with a length of 40 km is much higher then from the first fibre coil. This amplification of the second part of the FUT continues until optical power of the laser pump exceed some threshold value and system begins to behave like a laser. In this case the response from the FUT is unstable and fails to reflect the response of the FUT. For the all measured optical output powers of the pump laser the system was relatively stable and well sensitive to phase changes caused by acoustic vibrations.

#### 4.1.4 Conclusion

In this Section we have presented 3 advanced methods for optical signal amplification. First method is focused on a high-power optical pulse amplification by standard telecommunication EDFA. Pulse power fluctuation were below 30 % for all the measurements. Other two methods describes the Raman amplification and remote pumping amplification. For both of them was successfully confirmed their suitability for distributed amplification. In addition, both of them enable keeping optical link passive, because they do not need any active equipment in the link.

## 4.2 Novel Method of Measurement of Polarization Transient Effects Caused by Mechanical Stress on Optical fibre

Sensing in biology, chemistry, engineering and many other scientific and technology areas is more frequently based on optical fibre sensors. The sensing element in optical fibre sensor technology is the optical fibre itself. The physical structure of the optical fibre can be influenced by external perturbations (e.g. temperature, strain, pressure, acoustic wave). As a result, the optical wave, propagating through the fibre, is directly affected by these deteriorating events. By measuring the parameters of the propagating optical wave one can estimate the value of these distractions. The fibre optics sensors are desired mostly for their electromagnetic interference immunity, electrically passive operation, sensitivity and capabilities of multiplexing [47]. Polarization sensors are based on the photoelastic effect where the refractive index of the material is changed according to external perturbations.

Currently, the fibre optics technology used for sensing is almost the same as the technology used in fibre optic communications which gives us great opportunity to carry out simultaneous measurement of different parameters on the communication fibre link. This approach allows monitoring the fibre link in order to provide security and reliability of the critical infrastructures [87]. Together with proactive damage detection algorithm proposed in [9] it is possible to fulfill the highest reliability standards. Long term monitoring of SOP on the real communication link gives information about elastic and inelastic transients [67, 22, 11, 105].

### 4.2.1 Methodology

In order to verify the possibility of sensing the optical fibre route, we build up the experimental laboratory workplace (Fig. 4.10). As a transmitter, low-noise DFB laser LD101 with a wavelength 1550 nm and 5 MHz spectral width was used. The fibre link was emulated by 1 km long G.652D fibre spool. To simulate the external perturbations we used fibre wound piezoelectric stretcher Optiphase PZ3-SMF2-O with 15.2 m of SMF28e+ fibre. The stretcher has ability to stretch the fibre with parameter 1.3  $\mu\text{m}/\text{V}$ . For driving the stretcher arbitrary waveform generator was used.

The polarization monitoring of the fibre route was carried out with the polarization beam splitter and balanced detector Koheron PD100B-AC. The balanced detector performs the difference between the two voltage signals ( $V_1, V_2$ ) from polarization beam splitter which corresponds to the optical power. Thus, it is able

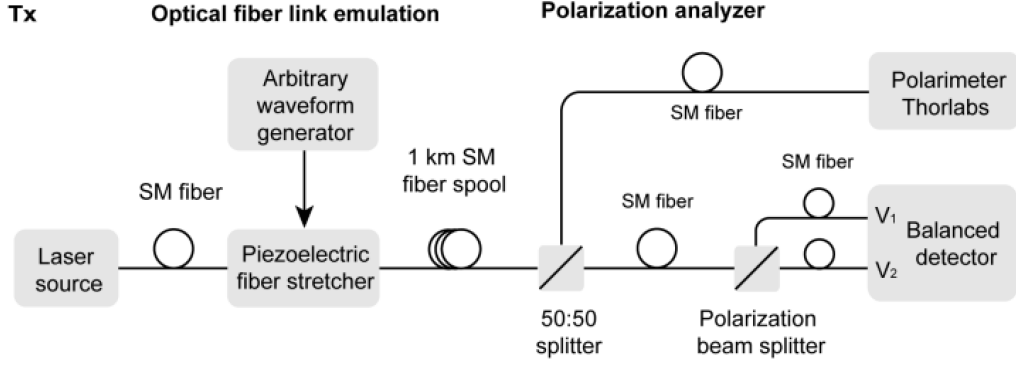


Fig. 4.10: The scheme of the workplace

to detect the polarization rotation of optical wave induced by external perturbations. The difference signal was sampled with frequency a 120 kHz by Redpitaya development platform and samples were sent to PC (Personal Computer) for post-processing. The polarization rotation rate from the sampled difference signal is determined as follows [87]:

$$\Delta\sigma_{Bal} = 2\sin^{-1} \left( \frac{1}{2} \Delta \left[ \left| \frac{V_1 - V_2}{V_1 + V_2} \right| \right] \right) \frac{1}{\Delta t}. \quad (4.13)$$

To compare the results from the balanced detector, half of the optical signal was connected to commercially available polarimeter Thorlabs PAX1000. The maximal sampling frequency of the polarimeter was 400 Hz, however logging of the parameters was able only with frequency 50 Hz. During the measurement, the normalized Stokes parameters from polarimeter were simultaneously recorded. The polarization rotation was determined from central angle difference  $\Delta\sigma$  between two points (specified by Stokes parameters) on Poincaré sphere. Polarization rotation rate equation is:

$$\Delta\sigma_{Pol} = 2\sin^{-1} \left( \frac{\sqrt{(\Delta S_1)^2 + (\Delta S_2)^2 + (\Delta S_3)^2}}{2} \right) \frac{1}{\Delta t}, \quad (4.14)$$

where  $S_1, S_2, S_3$  are the normalized Stokes parameters.

## 4.2.2 Results and Discussion

For the sake of verification, we carried out two measurement campaigns. Within the first measurement, the fibre stretcher was modulated by 10 V pulse with a duration of 10 ms and 0,5 Hz repetition rate. The polarization rotation was measured simultaneously with a balanced detector and polarimeter.

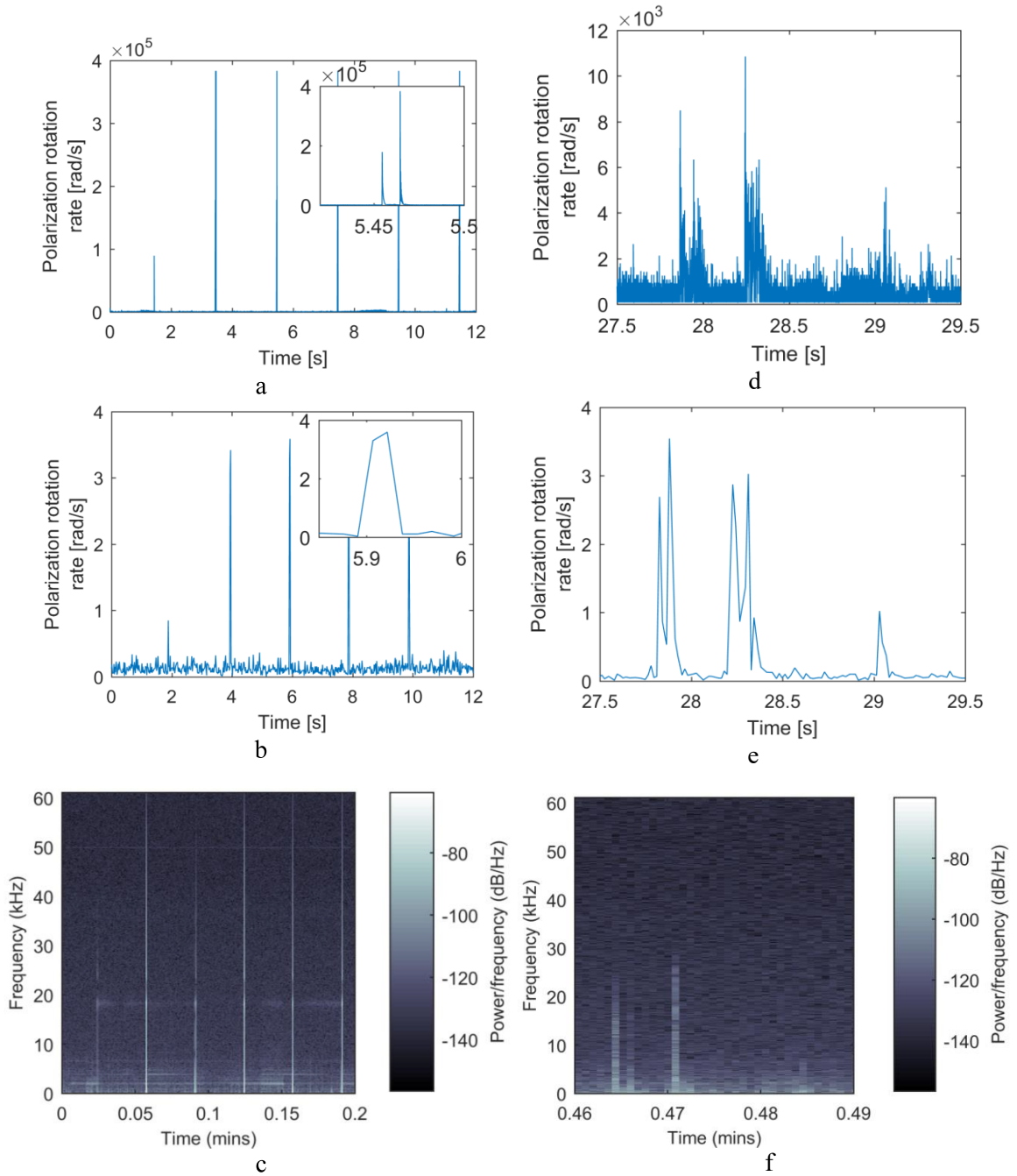


Fig. 4.11: Left: The response of the polarization fibre sensor on 1 ms pulses (a) Output signal from the balanced detector, (b) Polarization rotation rate detected with polarimeter, (c) Spectrogram of the signal from the balanced detector. Right: The response of the polarization fibre sensor on mechanical stress induced by knocking on the fibre (d) Output signal from the balanced detector, (e) Polarization rotation rate detected with polarimeter, (f) Spectrogram of the signal from the balanced detector.

Because of the higher sampling rate, it is clear that polarization rotation rate measurement is more sensitive with the balanced detector (Fig. 4.11a). Zoomed plot shows detail of the pulse. In Fig. 4.11b the measurement based on Stokes parameters from polarimeter is shown. In order to detect the polarization change within the optical fibre route the spectrogram of the difference signal can be used (Fig. 4.11c).

The second measurement was carried out while knocking on the fibre spool for simulation of the real perturbation. The response measured by a balanced detector is depicted in Fig. 4.11d. The change of polarization was also measured by polarimeter, see Fig. 4.11e). In comparison with the previous measurement, the amplitude of the polarization rotation rate is smaller which is given by the slower deteriorating event. The knocking is also visible in spectrogram in the Fig. 4.11f.

The response and sensitivity of the polarimeter based on balanced detector depend mainly on the polarization state before the polarization beam splitter. The system is maximally sensitive when the polarization will be linear with angle  $\pi/4$ . On the other hand, when the light wave will be horizontally or vertically polarized the response of the system will be minimal. The sensitivity is usually improved by placing the properly rotated  $\lambda/2$  waveplate before polarizing beam splitter. In our case, the polarization in long single-mode fibre is changing randomly, so more sophisticated polarization analyzer should be placed in front of the splitter. However, the main idea of this measurement was to keep the measurement system as simple as we can. The polarization state of the optical wave is not fully characterized in comparison with polarimeter measurement. Despite the fact that it is not possible to say nothing about the ellipticity of the polarization, the method is sensitive enough to detect the polarization transient effects on the fibre route. Thanks to high sampling frequency it is possible to detect fast elastic transients in polarization.

### 4.2.3 Conclusion

The Section was focused on verification of the method for state of polarization analysis. The method was based on polarization beam splitter and a balanced detector. In order to provide quick analysis, the signal from the detector was processed by FPGA (Field Programmable Gate Array) platform. The gathered experimental data was compared with data from polarimeter. The proposed method shows satisfactory results for monitoring of the unexpected events near the fibre route.

## 4.3 Distributed Fibre Optic Sensing System Based on Dual Mach-Zehnder Interferometer Using Frequency Shift

The technical solution relates to a distributed fibre optic sensing system based on the dual Mach-Zehnder interferometer principle allowing localization of events using a single pair of optical fibres. The system is used as a distributed acoustic sensor to protect perimeters and also some fibre optic critical infrastructures.

This technical solution is industrially well applicable especially for monitoring acoustic/mechanical vibrations in the vicinity of telecommunication optical cables, on fibres with active data traffic. Due to the use of continuous low-power radiation, there is no interaction with the data traffic in the surrounding channels. Using a remote unit, an opposing propagating signal is frequency-shifted from the laser carrier signal, thereby creating a second interferometer in the same pair of optical fibres, thereby enabling event localization. Compared to the known solutions, the device uses only one pair of fibres. Except a laser of sufficiently long coherence length, it contains no expensive and complex components and is usable at all working wavelengths of the fibres used. The technical solution also includes remote monitoring including monitoring of processed optical signals. Since this novel configuration of dual Mach-Zehnder interferometer is currently in process of patent application (application is under evaluation) only basic scheme and principles are described.

### 4.3.1 Scheme and Principle of the Invention

The principle of the solution is further explained and described in Fig 4.12, which shows a block diagram of the device. In the enclosed drawing, the optical lines are indicated by solid lines and the electrical lines by dashed lines.

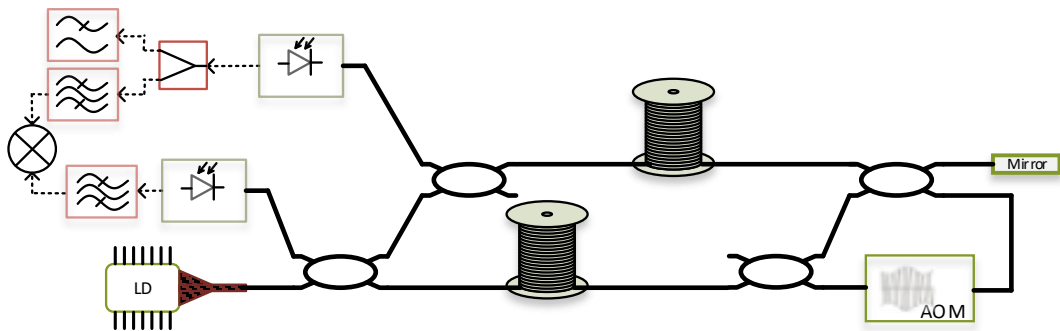


Fig. 4.12: Scheme of the dual Mach-Zehnder interferometer using frequency shift.

As was already mentioned, the main disadvantage of interferometric systems in basic configuration is the inability to locate the event and the need to combine multiple techniques or the need to use three optical fibres if the event localization is required. These deficiencies are solved by distributed optical fibre sensing system based on dual Mach-Zehnder interferometer principle using frequency shift of unmodulated counterclockwise signal. The system consists of a main and remote units. The main device comprises first and second optical couplers (2x2, 50:50), the remote unit comprising also two couplers (third and fourth optical couplers, also 2x2, 50:50). The outputs of the first coupler are coupled to the input ports of the second and third couplers using a reference and a sensing fibres. One input port of the first coupler is connected to the input of one photodetector and the last port of the first coupler is used to connect a highly coherent narrow-linewidth laser source. The second input port of the second coupler is coupled to the second photodetector and one output port (the last port of the second coupler is unconnected) is coupled to the input of the fourth coupler. A reflector (prefer is Faraday rotator mirror which neglects the effect of polarization) is connected to one output of the fourth coupler and reflects the clockwise output of the interferometer back to the main unit. The second output is connected to the output of an acousto-optical modulator, which is driven by an OXCO (Oven Controlled Crystal Oscillator) of the appropriate frequency and shifts the laser frequency by the oscillator frequency. The acousto-optical modulator input is connected to the output port of the third coupler. The benefits of the new solution/invention is that the signal for the counterclockwise interferometer is not transmitted to the far end by a dedicated fibre, but by means of a third coupler a portion of the signal is separated from the clockwise interferometer. This signal is then shifted by a defined frequency using an acousto-optical modulator and via the fourth coupler this new signal is coupled to the reference and sensing fibres. This creates a counterclockwise interferometer. If an event occurs near the fibre optic cable, both clockwise and counterclockwise interferometers detect it. Due to the different direction of propagation of both interferometers, the location of the event can be calculated using the Eq. 2.10. The advantage of the proposed solution is also the placement of outputs from both interferometers in the main unit, thus ensuring correct synchronization of both interferometers outputs. Based on experimental measurements, one pair of optical fibres from the same optical cable can be used.

## 5 Conclusion

This habilitation thesis provided the overview about distributed fibre optic sensing techniques suitable for use in fibre optic networks with active data transmission. The thesis focused on conventional and advanced techniques enabling detection of events near the fibre and thus creating a smart infrastructure for critical infrastructures protection. Further, the thesis investigated the deployment of selected schemes on fibres with active data and non-data transmissions. Finally, the thesis presented advanced techniques for a signal amplification in reflectometry systems and also two author's proposals that are designed for use in current optical networks. Both systems and schemes are designed in order to be suitable for deployment on fibres with active data and non-data transmissions using DWDM technology. The expected contribution is threefold. Pedagogical, i.e., to produce a unified overview about conventional and advanced distributed fibre optic sensing schemes that can be used for critical infrastructures protection and also the description of main parameters related to the solved topic; practical, i.e., to present assessment of the suitability of selected technologies for application to active fibres in terms of possible mutual interference and also in terms of the sensitivity of the sensing systems itself; and scientific, i.e., to produce novel designs with advanced features that which are more efficient, more economical and better applicable to practice. The pedagogical contribution is addressed in Chapter 2 that presents the theoretical background with the description of laser diode wavelength, relation between peak and average power, laser linewidth which is very important for almost all distributed sensing systems, coherence length which is just as important a parameter as linewidth, and polarization of the light. Moreover, the Chapter also introduces description of the main distributed sensing techniques based on optical interferometry, i.e., Mach-Zehnder interferometer, Michelson interferometer, and polarization interferometer, and also description of techniques based on reflectometry principle, i.e., Rayleigh based  $\Phi$ -OTDR and Brillouin based B-OTDR. The practical contribution is addressed in Chapter 3 that evaluates possible interaction of a high-power sensing signals with accurate time/stable frequency transfer, and high-speed data transfer. The chapter discusses the influence of pulse width, repetition rate and output power level of the sensing signal on other services at 100 GHz spacing, which corresponds to DWDM channel grid. These results are used to optimize the settings of partial parameters of the sensory system and at the same time to optimize the transmission paths in order to avoid mutual interference of individual signals in the fibre. The chapter also discusses the sensitivity of two interferometric sensor systems. The sensitivity of the system is very important, as it can significantly affect the quality of the detection – high sensitivity may cause high interference (if used infrastructure is e.g. under

the road), and low sensitivity can cause that some events will not be detected at all. The scientific contribution is addressed in the Chapter 4 that contains two novel proposals of sending systems and also advanced techniques for a signal amplification in reflectometry systems where backscatter signals are low and hence high-power signal must be used. The proposed novel systems and advanced amplification techniques are presented in three sections. Section 4.1 presents advanced techniques of signal amplification. The results of the Section should allow to minimize optical power thanks to the possibility to use for example Raman amplification, holding beam or remote pumping (due to the fact that the remote pumping uses Erbium doped fibre in the route, in this case it is not possible to use existing infrastructure without modification). Section 4.2 presents a novel detection technique for SOP analysis based on polarization beam splitter and balance photodetector which offers a cheap and easy to use solution. This solution is suitable for implementation into current data networks because there are no special requirements for laser source and it is possible to analyze modulated data signal. Section 4.3 presents the solution for distributed sensing based on dual Mach-Zehnder interferometer. The presented system allows to realize a dual interferometer with only pair of fibres. This unique involvement is the subject of patent proceeding and therefore only basic information is presented. The mentioned results and proposals have been published in journals with impact factors and international conferences dedicated to telecommunications/ or sensing.

# Bibliography

- [1] ALTMANNOVÁ, Lada, Michal ALTMANN, Michal HAŽLINSKÝ, et al. Photonic Services: Challenge for Users and for Networkers. *GÉANT Association* [online]. Czech Republic: GÉANT, 2013 [cit. 2019-08-12]. Available at: <https://bit.ly/2ONPe2u>
- [2] ARDANUY, Philip E., Jeffery J. PUSCHELL, Josef VOJTECH, et al. Joint accurate time and stable frequency distribution infrastructure sharing fiber footprint with research network. In: *Proc. SPIE 9977, Remote Sensing System Engineering VI, 99770F* [online]. Proc. SPIE: SPIE, 2016, 2016-9-19, 99770F- [cit. 2019-08-02]. DOI: 10.1117/12.2237205. ISBN 978-1-5106-0345- 5. Available at: <http://proceedings.spiedigitallibrary.org/proceeding.aspx?doi=10.1117/12.2237205>
- [3] AOKI, Y., K. TAJIMA a I. MITO. Input power limits of single-mode optical fibers due to stimulated Brillouin scattering in optical communication systems. *Journal of Lightwave Technology*, 1988 [online]. **6**(5), 710-719 [cit. 2019-08-22]. DOI: 10.1109/50.4057. ISSN 07338724. Available at: <http://ieeexplore.ieee.org/document/4057/>
- [4] BAKER, Matthew j., Caryn S. HUGHES a Katherine A. *Biophotonics: Vibrational Spectroscopic Diagnostics*. Hollywood: Morgan & Claypool Publishers, 2016. ISBN 978-1-6817-4007-2.
- [5] Balanced Amplified Photodetectors with Fast Monitor Output. *THORLABS* [online]. [cit. 2019-09-12]. Available at: [https://www.thorlabs.com/newgrouppage9.cfm?objectgroup\\_id=5201](https://www.thorlabs.com/newgrouppage9.cfm?objectgroup_id=5201)
- [6] BARCIK, Peter, Petr MUNSTER, Petr DEJDAR, Tomas HORVATH a Josef VOJTECH. Measurement of Polarization Transient Effects Caused by Mechanical Stress on Optical Fiber. In: *8th International Conference on Fiber Optics in Access Networks (FOAN)*. Sarajevo: IEEE, 2019, s. 27–29. ISBN 978-1-7281-1563-4.
- [7] BARNOSKI, M. K., M. D. ROURKE, S. M. JENSEN a R. T. MELVILLE. Optical time domain reflectometer. *Applied Optics* [online]. 1977, **16**(9) [cit. 2019-08-22]. DOI: 10.1364/AO.16.002375. ISSN 0003-6935. Available at: <https://www.osapublishing.org/abstract.cfm?URI=ao-16-9-2375>
- [8] BLOOM, B. J., T. L. NICHOLSON, J. R. WILLIAMS, et al. An optical lattice clock with accuracy and stability at the 10<sup>18</sup> level. *Nature*. 2014, **506**(7486), 71-75. DOI: 10.1038/nature12941. ISSN 0028-0836. Available at: <http://www.nature.com/articles/nature12941>
- [9] BOITIER, F., V. LEMAIRE, J. PESIC, L. CHAVARRIA, P. LAYEC, S. BIGO a E. DUTISSEUIL. Proactive Fiber Damage Detection in Real-time Coherent Receiver. In: *2017 European Conference on Optical Communication (ECOC)* [online]. IEEE, 2017, 2017, s. 1-3 [cit. 2019-09-25]. DOI: 10.1109/ECOC.2017.8346077. ISBN 978-1-5386-5624-2. Available at: <https://ieeexplore.ieee.org/document/8346077/>
- [10] BORDÉ, Christian J. Base units of the SI, fundamental constants and modern quantum physics. *Philosophical Transactions of the Royal Society A: Mathematical, Physical and Engineering Sciences*. 2005, **363**(1834), 2177-2201. DOI: 10.1098/rsta.2005.1635. ISSN 1364-503X. Available at: <http://www.royalsocietypublishing.org/doi/10.1098/rsta.2005.1635>

- [11] BORODITSKY, M., M. BRODSKY, N.J. FRIGO, P. MAGILL a H. ROSENFELDT. Polarization dynamics in installed fiberoptic systems. In: *2005 IEEE LEOS Annual Meeting Conference Proceedings* [online]. IEEE, 2005, 2005, s. 414-415 [cit. 2019-09-25]. DOI: 10.1109/LEOS.2005.1548054. ISBN 0-7803-9217-5. Available at: <http://ieeexplore.ieee.org/document/1548054/>
- [12] CALONICO, D., E. K. BERTACCO, C. CALOSSO, et al. Optical frequency transfer with a 1284 km coherent fiber link. In: *2014 European Frequency and Time Forum (EFTF)*. Neuchatel, Switzerland: IEEE, 2014, s. 1-4. DOI: 10.1109/EFTF.2014.7331412. ISBN 978-1-4799-5252-6. Available at: <http://ieeexplore.ieee.org/lpdocs/epic03/wrapper.htm?arnumber=7331412>
- [13] Coherence Length. *RP Photonics Encyclopedia* [online]. RP Photonics Consulting [cit. 2019-09-10]. Available at: [https://www.rp-photonics.com/coherence\\_length.html](https://www.rp-photonics.com/coherence_length.html)
- [14] CORIANT GROOVE G30 NETWORK DISAGGREGATION PLATFORM. *Coriant* [online]. USA: Coriant, 2019 [cit. 2019-01-12]. Available at: <https://www.coriant.com/products/coriant-groove-g30-network-disaggregation-platform>
- [15] COSTA, B., B. SORDO, U. MENAGLIA, L. PICCARI a G. GRASSO. Attenuation measurements performed by backscattering technique. *Electronics Letters* [online]. 1980, **16**(10) [cit. 2019-08-22]. DOI: 10.1049/el:19800251. ISSN 00135194. Available at: [https://digital-library.theiet.org/content/journals/10.1049/el\\_19800251](https://digital-library.theiet.org/content/journals/10.1049/el_19800251)
- [16] CUCKA, Milan, Pavol SALIK, Rastislav ROKA, Petr MUNSTER and Miloslav FILKA. Simulation Models of Pulse Generator for OTDR in Matlab and VPIphotonics. In: *2018 41st International Conference on Telecommunications and Signal Processing (TSP)* [online]. IEEE, 2018, 2018, s. 1-4 [cit. 2019-08-01]. DOI: 10.1109/TSP.2018.8441274. ISBN 978-1-5386-4695-3. Available at: <https://ieeexplore.ieee.org/document/8441274/>
- [17] CUCKA, Milan, Petr MUNSTER, Lukas KOČI, Tomas HORVATH, Miloslav FILKA and Josef VOJTECH. Transmission of High Power Sensor System and DWDM Data System in One Optical Fiber. *Journal of Communications Software and Systems* [online]. 2016, 190-194 [cit. 2019-08-01]. DOI: 10.24138/jcomss.v12i4.77. ISSN 18456421. Available at: <https://jcomss.fesb.unist.hr/index.php/jcomss/article/view/77>
- [18] *Distributed Optical Fibre Sensing: Overview*. University of Southampton, s. 4-53.
- [19] DOSTAL, Jiri a Vladimir SMOTLACHA. Next generation of architecture for precise time measurements. In: *2015 IEEE East-West Design & Test Symposium (EWDTS)*. Batumi, Georgia: IEEE, 2015, s. 1-3. DOI: 10.1109/EWDTS.2015.7493161. ISBN 978-1-4673-7776-8.
- [20] EBENHAG, Sven-Christian, Per Olof HEDEKVIST, Per JARLEMARK a EMARLSON. Measurements and Error Sources in Time Transfer Using Asynchronous Fiber Network. *IEEE Transactions on Instrumentation and Measurement*. 2010, **59**(7), 1918-1924. DOI: 10.1109/TIM.2009.2028214. ISSN 0018-9456. Available at: <http://ieeexplore.ieee.org/document/5280272/>
- [21] ELLIS, Andrew D., Mingming TAN, Md Asif IQBAL, et al. 4 Tb/s Transmission Reach Enhancement Using  $10 \times 400$  Gb/s Super-Channels and Polarization Insensitive Dual Band Optical Phase Conjugation. *Journal of Lightwave Technology*.

- 2016, **34**(8), 1717-1723. DOI: 10.1109/JLT.2016.2521430. ISSN 0733-8724. Available at: <http://ieeexplore.ieee.org/document/7390192/>
- [22] SALAUN, Suzanne, Frederic NEDDAM, Julien POIRRIER, Bruno RAGUENES a Maryse MOIGNARD. Fast SOP variation measurement on WDM systems are the OPMD fast enough?. In: NEDDAM a RAGUENES. *35th European Conference on Optical Communication*. Vienna, Austria: IEEE, 2009, s. 1–2. ISBN 978-1-4244-5096-1.
- [23] *Fiber optic sensors: an introduction for engineers and scientists*. 2nd ed. Editor Eric UDD, editor William B. SPILLMAN. Hoboken: Wiley, c2011. ISBN 978-0-470-12684-4.
- [24] *FOSA Urges "Smart Infrastructure" Technology* [online]. United states: Fiber Optic Sensing Association, 2019 [cit. 2019-09-25]. Available at: <https://www.fiberopticsensing.org/blog/fosa-urges-smart-infrastructure-technology>
- [25] *FTB-700G V2 Series* [online]. EXFO, 2019 [cit. 2019-09-12]. Available at: <https://www.exfo.com/en/discontinued-products/ftb-700g-v2-series/>
- [26] *G.694.1 Spectral grids for WDM applications: DWDM frequency grid*. Geneva: ITU-T, 2012.
- [27] GIORGETTA, Fabrizio R., William C. SWANN, Laura C. SINCLAIR, Esther BAUMANN, Ian CODDINGTON a Nathan R. NEWBURY. Optical two-way time and frequency transfer over free space. *Nature Photonics*. 2013, **7**(6), 434-438. DOI: 10.1038/nphoton.2013.69. ISSN 1749-4885. Available at: <http://www.nature.com/articles/nphoton.2013.69>
- [28] HOLÍK, Tomáš. *Distribúovaný teplotní senzor*. Brno, 2016. Bachelor thesis. Brno university of technology. Vedoucí práce Petr Münster.
- [29] HORVATH, Tomas, Vlastimil CLUPEK, Petr MUNSTER a Vaclav OUJEZSKY. Key Exchange with PUF in NG-PON2 Networks. In: *2019 42nd International Conference on Telecommunications and Signal Processing (TSP)*. Budapest, Hungary: IEEE, 2019, 2019, s. 118-121. DOI: 10.1109/TSP.2019.8769082. ISBN 978-1-7281-1864-2. Available at: <https://ieeexplore.ieee.org/document/8769082/>
- [30] HORVATH, Tomas, Patrik CYMOREK, Petr MUNSTER, Vaclav OUJEZSKY a Josef VOJTECH. Simulations of Grant Allocation in NG-PON2 Networks Using OPNET Modeler. *Journal of Communications Software and Systems*. 2018, **14**(4), 281-289. DOI: 10.24138/jcomss.v14i4.525. ISSN 18456421. Available at: <https://jcomss.fesb.unist.hr/index.php/jcomss/article/view/525>
- [31] HORVATH, Tomas, Lukas MALINA and Petr MUNSTER. On security in gigabit passive optical networks. In: *2015 International Workshop on Fiber Optics in Access Network (FOAN)* [online]. IEEE, 2015, 2015, s. 51-55 [cit. 2019-08-01]. DOI: 10.1109/FOAN.2015.7320479. ISBN 978-1-4673-7625-9. Available at: <http://ieeexplore.ieee.org/document/7320479/>
- [32] HORVATH, Tomas, Petr MUNSTER, Patrik CYMOREK, Vaclav OUJEZSKY a Josef VOJTECH. Implementation of NG-PON2 transmission convergence layer into OPNET modeler. In: *2017 International Workshop on Fiber Optics in Access Network (FOAN)*. Munich, Germany: IEEE, 2017, 2017, s. 1-5. DOI: 10.1109/FOAN.2017.8215254. ISBN 978-1-5386-2413-5. ISSN 2378-8488. Available at: <http://ieeexplore.ieee.org/document/8215254/>

- [33] HORVATH, Tomas, Petr MUNSTER, Vaclav OUJEZSKY a Josef VOJTECH. Activation Process of ONU in EPON/GPON Networks. In: *2018 41st International Conference on Telecommunications and Signal Processing (TSP)*. Athens, Greece: IEEE, 2018, 2018, s. 1-5. DOI: 10.1109/TSP.2018.8441216. ISBN 978-1-5386-4695-3. Available at: <https://ieeexplore.ieee.org/document/8441216/>
- [34] HORVATH, Tomas, Petr MUNSTER, Josef VOJTECH and Vladimir SMOTLACHA. Simultaneous Transmission of Photonic Services over One Fiber with an ITU 100 GHz Grid. *Sensors* [online]. 2019, **19**(7) [cit. 2019-08-01]. DOI: 10.3390/s19071601. ISSN 1424-8220. Available at: <https://www.mdpi.com/1424-8220/19/7/1601>
- [35] HORVATH, Tomas, Petr MUNSTER, Josef VOJTECH, Radek VELC and Vaclav OUJEZSKY. Simultaneous transmission of accurate time, stable frequency, data, and sensor system over one fiber with ITU 100-GHz grid. *Optical Fiber Technology* [online]. 2018, **40**, 139-143 [cit. 2019-08-01]. DOI: 10.1016/j.yofte.2017.11.016. ISSN 10685200. Available at: <https://linkinghub.elsevier.com/retrieve/pii/S1068520017303851>
- [36] HORVATH, Tomas, Petr MUNSTER, Lubos DUBRAVEC and Miloslav FILKA. Novel rogue optical network unit detection algorithm for gigabit passive optical networks. *Optica Applicata* [online]. Poland, 2016, 09.08.2016, **46**(4), 190–210 [cit. 2019-08-01]. Available at: [https://yadda.icm.edu.pl/baztech/element/bwmeta1.element.baztech-506d7542-1e8e-4ff1-81a9-197c8fdbef71/c/9\\_horvath\\_i\\_inni\\_optappl\\_2016\\_3.pdf](https://yadda.icm.edu.pl/baztech/element/bwmeta1.element.baztech-506d7542-1e8e-4ff1-81a9-197c8fdbef71/c/9_horvath_i_inni_optappl_2016_3.pdf)
- [37] HORVÁTH, Tomáš, Petr MÜNSTER, Michal JURČÍK, Lukáš KOČÍ and Miloslav FILKA. Timing measurement and simulation of activation process in GPON networks. *Optica Applicata* [online]. 4. Poland, 2015, 22.12.2015, **45**(4), 459–470 [cit. 2019-08-01]. ISSN 0078-5466. Available at: [https://yadda.icm.edu.pl/baztech/element/bwmeta1.element.baztech-46675f14-7a95-4d8e-a502-c0becf87f620/c/optappl\\_4504p459.pdf](https://yadda.icm.edu.pl/baztech/element/bwmeta1.element.baztech-46675f14-7a95-4d8e-a502-c0becf87f620/c/optappl_4504p459.pdf)
- [38] HORVATH, Tomas, Petr MUNSTER, Michal JURCIK a Miloslav FILKA. Novel Algorithm in Activation Process of GPON Networks. *Journal of Communications Software and Systems*. 2017, **11**(4), 204-209. DOI: 10.24138/jcomss.v11i4.99. ISSN 1846-6079. Available at: <https://jcomss.fesb.unist.hr/index.php/jcomss/article/view/99>
- [39] HORVATH, Tomas, Petr MUNSTER and Miloslav FILKA. Security Issues in NGA networks. In: *OK2015 - 27th Conference and Exhibition on OPTICAL COMMUNICATIONS 2015*. Prague: Agentura Action M, Vršovická 68, 101 00 Praha 10, Czech Republic, 2015, s. 37–38. ISBN 978-80-86742-41- 0.
- [40] HORVATH, Tomas, Petr MUNSTER, Vaclav OUJEZSKY and Josef VOJTECH. Activation Process of ONU in EPON/GPON/XG-PON/NG-PON2 Networks. *Applied Sciences* [online]. 2018, **8**(10), 1–18 [cit. 2019-08-01]. DOI: 10.3390/app8101934. ISSN 2076-3417. Available at: <http://www.mdpi.com/2076-3417/8/10/1934>
- [41] HORVATH, Tomas, Petr MUNSTER, Josef VOJTECH, Ondrej HAVLIS a Martin GALLO. Transmission Convergence Layer of NG-PON2 in VPIphotonics Tool. *Journal of Communications Software and Systems*. 2017, **13**(3), 141-147. DOI: 10.24138/jcomss.v13i3.359. ISSN 18456421. Available at: <https://jcomss.fesb.unist.hr/index.php/jcomss/article/view/359>

- [42] CHOU, C. W., D. B. HUME, T. ROSENBAND a D. J. WINELAND. Optical Clocks and Relativity. *Science*. 2010, **329**(5999), 1630-1633. DOI: 10.1126/science.1192720. ISSN 0036-8075. Available at: <http://www.sciencemag.org/cgi/doi/10.1126/science.1192720>
- [43] ISLAM, Mohammed N. *Raman amplifiers for telecommunications*. New York: Springer, c2004. ISBN 0387007512.
- [44] JAKOUBEK, Petr a Radim ŠIFTA. *Využití polarizačního multiplexu v optických přístupových sítích*. Brno, 2015. Bachelor thesis. Brno university of technology.
- [45] JIANG, Zhiheng, Shinn-Yan LIN a Wen-Hung TSENG. Fully and optimally use the redundancy in a TWSTFT network for accurate time transfer. In: *2017 Joint Conference of the European Frequency and Time Forum and IEEE International Frequency Control Symposium (EFTF/IFC)*. Besancon, France: IEEE, 2017, 2017, s. 676-680. DOI: 10.1109/FCS.2017.8088998. ISBN 978-1-5386-2916-1. ISSN 2327-1949. Available at: <http://ieeexplore.ieee.org/document/8088998/>
- [46] KARASEK, M., J. VOJTECH a J. RADIL. Channel addition-removal response in a cascade of three distributed Raman fiber amplifiers transmitting 10×10 GE channels: experimentation and modeling. *Journal of Optical Networking* [online]. 2008, **7**(1) [cit. 2019-09-25]. DOI: 10.1364/JON.7.000015. ISSN 1536-5379. Available at: <https://www.osapublishing.org/jon/abstract.cfm?uri=jon-7-1-15>
- [47] KERSEY, A.D., M.A. DAVIS, H.J. PATRICK, M. LEBLANC, K.P. KOO, C.G. ASKINS, M.A. PUTNAM a E.J. FRIEBELE. Fiber grating sensors. *Journal of Lightwave Technology* [online]. **15**(8), 1442-1463 [cit. 2019-09-25]. DOI: 10.1109/50.618377. ISSN 07338724. Available at: <http://ieeexplore.ieee.org/document/618377/>
- [48] KOČI, Lukas, Tomas HORVATH, Petr MUNSTER, Michal JURCIK and Miloslav FILKA. Transmission convergence layer in XG-PON. In: *2015 38th International Conference on Telecommunications and Signal Processing (TSP)* [online]. Prague: IEEE, 2015, 2015, s. 104-108 [cit. 2019-08-01]. DOI: 10.1109/TSP.2015.7296232. ISBN 978-1-4799-8498-5. Available at: <http://ieeexplore.ieee.org/document/7296232/>
- [49] KOČI, Lukas, Petr MUNSTER, Tomas HORVATH, Milan CUČKA a Miloslav FILKA. The Influence of Digital Modulations on 320 Gbit/s Optical Time Division Multiplexing. *Journal of Communications Software and Systems*. 2017, **11**(4), 187-191. DOI: 10.24138/jcomss.v11i4.96. ISSN 1846-6079. Available at: <https://jcomss.fesb.unist.hr/index.php/jcomss/article/view/96>
- [50] LIN, M.-C. a S. CHI. The gain and optimal length in the erbium-doped fiber amplifiers with 1480 nm pumping. *IEEE Photonics Technology Letters* [online]. 1992, **4**(4), 354-356 [cit. 2019-09-25]. DOI: 10.1109/68.127211. ISSN 1041-1135. Available at: <http://ieeexplore.ieee.org/document/127211/>
- [51] LOPEZ, Olivier, Adil HABOUCCHA, Bruno CHANTEAU, Christian CHARDONNET, Anne AMY-KLEIN a Giorgio SANTARELLI. Ultra-stable long distance optical frequency distribution using the Internet fiber network. *Optics Express*. 2012, **20**(21), 23518-23526. DOI: 10.1364/OE.20.023518. ISSN 1094-4087. Available at: <https://www.osapublishing.org/oe/abstract.cfm?uri=oe-20-21-23518>

- [52] LOPEZ, O, B CHANTEAU, A BERCY, et al. Ultra-stable long distance optical frequency distribution using the Internet fiber network and application to high-precision molecular spectroscopy. *Journal of Physics: Conference Series*. 2013, **467**(1), 1-6. DOI: 10.1088/1742-6596/467/1/012002. ISSN 1742-6588. Available at: <http://stacks.iop.org/1742-6596/467/i=1/a=012002?key=crossref.95c79eb1e58d21c076612d01ff3ffb42>
- [53] LOPEZ, Olivier, Christian CHARDONNET, Anne AMY-KLEIN, Amale KANJ, Paul-Eric POTTIE, Daniele ROVERA, Joseph ACHKAR a Giorgio SANTARELLI. Simultaneous remote transfer of accurate timing and optical frequency over a public fiber network. In: *2013 Joint European Frequency and Time Forum & International Frequency Control Symposium (EFTF/IFC)*. Prague, Czech Republic: IEEE, 2013, s. 474-476. DOI: 10.1109/EFTF-IFC.2013.6702214. ISBN 978-1-4799-0342-9.
- [54] LUCKI, Michal. Nové trendy v elektronických komunikacích: Optické systémy a sítě. In: *Impresum* [online]. Praha: CVUT v Praze, s. 6 [cit. 2019-08-21]. Available at: <https://publi.cz/books/241/06.html>
- [55] LUDLOW, Andrew D., Martin M. BOYD, Jun YE, Ekkehard PEIK a Piet O. SCHMIDT. Optical Atomic Clocks. *ArXiv.org* [online]. USA: Cornell University, 2014 [cit. 2019-01-14]. Available at: <https://arxiv.org/pdf/1407.3493.pdf>
- [56] MALINA, Lukas, Petr MUNSTER, Jan HAJNY and Tomas HORVATH. Towards Secure Gigabit Passive Optical Networks - Signal Propagation based Key Establishment. In: *Proceedings of the 12th International Conference on Security and Cryptography* [online]. SCITEPRESS - Science and Technology Publications, 2015, 2015, p. 349-354 [cit. 2019-08-02]. DOI: 10.5220/0005559903490354. ISBN 978-989-758-117-5. Available at: <http://www.scitepress.org/DigitalLibrary/Link.aspx?doi=10.5220/0005559903490354>
- [57] MALINA, Lukas, Tomas HORVATH, Petr MUNSTER and Jan HAJNY. Security solution with signal propagation measurement for Gigabit Passive Optical Networks. *Optik* [online]. 2016, **127**(16), 6715-6725 [cit. 2019-08-01]. DOI: 10.1016/j.ijleo.2016.04.069. ISSN 00304026. Available at: <https://linkinghub.elsevier.com/retrieve/pii/S0030402616303448>
- [58] MINARDO, A., R. BERNINI a L. ZENI. Accurate distributed temperature measurements by Brillouin scattering fiber-optic sensor. In: *Proceedings of IEEE Sensors 2003 (IEEE Cat. No.03CH37498)* [online]. IEEE, 2003, s. 348-352 [cit. 2019-08-22]. DOI: 10.1109/ICSENS.2003.1278956. ISBN 0-7803-8133-5. Available at: <http://ieeexplore.ieee.org/document/1278956/>
- [59] MOTUZ, Rastislav, Petr MUNSTER a Miloslav FILKA. PMD Study & Measurement – Fixed Analyzer Method. *Journal of Communications Software and Systems*. 2017, **11**(4), 199-203. DOI: 10.24138/jcomss.v11i4.98. ISSN 1846-6079. Available at: <https://jcomss.fesb.unist.hr/index.php/jcomss/article/view/98>
- [60] MUNSTER, Petr, Tomas HORVATH, Ondrej HAVLIS, Josef VOJTECH, Josef RADIL, Radek VELC a Edvin SKALJO. Simultaneous transmission of standard data, precise time, stable frequency and sensing signals and their possible interaction. In: *SPIE Optics + Optoelectronics*. Prague, Czech Republic: SPIE, 2017, 2017-5-16, 102312A-7. DOI: 10.1117/12.2266240. ISSN 0277-786X. Available at: <http://proceedings.spiedigitallibrary.org/proceeding.aspx?doi=10.1117/12.2266240>

- [61] MUNSTER, Petr, Jan RADIL, Josef VOJTECH, et al. Simultaneous transmission of the high-power phase sensitive OTDR, 100Gbps dual polarisation QPSK, accurate time/frequency, and their mutual interferences. In: *SPIE Commercial + Scientific Sensing and Imaging 2017*. Anaheim, California, United States: SPIE, 2017, 2017-4-27, 102080D-7. DOI: 10.1117/12.2267259. Available at: <http://proceedings.spiedigitallibrary.org/proceeding.aspx?doi=10.1117/12.2267259>
- [62] MUNSTER, Petr, Josef VOJTECH, Petr SYSEL, Radim SIFTA, Vit NOVOTNY, Tomas HORVATH, Stanislav SIMA and Miloslav FILKA.  $\phi$ -OTDR signal amplification [online]. In: . 2015-5-5, s. 950606- [cit. 2019-08-01]. DOI: 10.1117/12.2179026. Available at: <http://proceedings.spiedigitallibrary.org/proceeding.aspx?doi=10.1117/12.2179026>
- [63] MUNSTER, Petr, Josef VOJTECH, Tomas HORVATH, Ondrej HAVLIS, Pavel HANAK, Milan CUCKA and Miloslav FILKA. Simultaneous transmission of distributed sensors and data signals. In: *2016 39th International Conference on Telecommunications and Signal Processing (TSP)* [online]. IEEE, 2016, 2016, s. 761-764 [cit. 2019-08-01]. DOI: 10.1109/TSP.2016.7760987. ISBN 978-1-5090-1288-6. Available at: <http://ieeexplore.ieee.org/document/7760987/>
- [64] MUNSTER, Petr, Tomas HORVATH and Josef VOJTECH. Distributed Sensing Based on Interferometry and Polarization Methods for Use in Fibre Infrastructure Protection. *Sensors* [online]. 2019, **19**(8) [cit. 2019-08-01]. DOI: 10.3390/s19081810. ISSN 1424-8220. Available at: <https://www.mdpi.com/1424-8220/19/8/1810>
- [65] MUNSTER, Petr, Tomas HORVATH, Josef VOJTECH, et al. Interference of Data Transmission in Access and Backbone Networks by High-Power Sensor System. *Fiber and Integrated Optics* [online]. 2017, **36**(3), 144-156 [cit. 2019-08-01]. DOI: 10.1080/01468030.2017.1327624. ISSN 0146-8030. Available at: <https://www.tandfonline.com/doi/full/10.1080/01468030.2017.1327624>
- [66] MUNSTER, Petr, Tomas HORVATH, Petr SYSEL, Josef VOJTECH and Radek VELC. Comparison of interferometry based and polarization based sensing systems for use in fiber infrastructure protection. In: *2017 International Workshop on Fiber Optics in Access Network (FOAN)* [online]. IEEE, 2017, 2017, s. 1-3 [cit. 2019-08-01]. DOI: 10.1109/FOAN.2017.8215255. ISBN 978-1-5386-2413-5. Available at: <http://ieeexplore.ieee.org/document/8215255/>
- [67] NELSON, Lynn E., Martin BIRK, Sheryl L. WOODWARD a Peter MAGILL. Field measurements of polarization transients on a long-haul terrestrial link. In: *IEEE Photonic Society 24th Annual Meeting* [online]. IEEE, 2011, 2011, s. 833-834 [cit. 2019-09-25]. DOI: 10.1109/PHO.2011.6110816. ISBN 978-1-4244-8939-8. Available at: <http://ieeexplore.ieee.org/document/6110816/>
- [68] NEWBURY, Nathan R. Frequency and Timing Distribution using Optical Methods. In: *CLEO: 2015*. San Jose, California United States: OSA, 2015, 2015, STh3N.5. DOI: 10.1364/CLEO\_SI.2015.STh3N.5. ISBN 978-1-55752-968-8. Available at: [https://www.osapublishing.org/abstract.cfm?URI=CLEO\\_SI-2015-STh3N.5](https://www.osapublishing.org/abstract.cfm?URI=CLEO_SI-2015-STh3N.5)

- [69] NOVOTNÝ, Vít, Petr SYSEL, Radko KRKOŠ, Petr MÜNSTER, Radim ŠIFTA, Jiří ŠTEFL, Pavel POSPÍCHAL and Zdeněk MALÝ. The Opto-Fiber Sensory System is used for Intrusion Detection Monitored Areas and to Prevent Damage. *Czech Defence Industry Review* [online]. Vykáň, 289 15 Kounice: MS Line, 2015, 21.01.2015, **22**(1), 22–23. Available at z: <http://www.msline.cz/index.php?page=cdis-review&cislo=cdis-review-1-2015>
- [70] OHNO, Hiroshige, Hiroshi NARUSE, Mitsuru KIHARA a Akiyoshi SHIMADA. Industrial Applications of the BOTDR Optical Fiber Strain Sensor. *Optical Fiber Technology* [online]. 2001, **7**(1), 45–64 [cit. 2019-08-22]. DOI: 10.1006/ofte.2000.0344. ISSN 10685200. Available at: <https://linkinghub.elsevier.com/retrieve/pii/S1068520000903444>
- [71] *Optical Fibres, Cables and Systems* [online]. Geneva, Switzerland: International Telecommunication Union, 2010 [cit. 2019-09-26]. ISBN 9789261190613. Dostupné z: [https://www.itu.int/dms\\_pub/itu-t/opb/hdb/T-HDB-OUT.10-2009-1-PDF-E.pdf](https://www.itu.int/dms_pub/itu-t/opb/hdb/T-HDB-OUT.10-2009-1-PDF-E.pdf)
- [72] *Optics in our time*. New York, NY: Springer Berlin Heidelberg, 2016. ISBN 9783319319025.
- [73] OUJEZSKY, Vaclav, Tomas HORVATH a Petr MUNSTER. Application for Determining whether IP Addresses belong to a Map by Coordinates. In: *2019 42nd International Conference on Telecommunications and Signal Processing (TSP)*. Budapest, Hungary: IEEE, 2019, 2019, s. 14–18. DOI: 10.1109/TSP.2019.8769100. ISBN 978-1-7281-1864-2. Available at: <https://ieeexplore.ieee.org/document/8769100/>
- [74] OUJEZSKY, Vaclav, David CHAPCAK, Tomas HORVATH a Petr MUNSTER. Security Testing Of Active Optical Network Devices. In: *2019 42nd International Conference on Telecommunications and Signal Processing (TSP)*. Budapest, Hungary: IEEE, 2019, 2019, s. 9–13. DOI: 10.1109/TSP.2019.8768811. ISBN 978-1-7281-1864-2. Available at: <https://ieeexplore.ieee.org/document/8768811/>
- [75] POBORIL, Radek, Petr SISKA, Jan LATAL, Martin SMRZ, Jakub CUBIK, Stanislav KEPAK a Vladimir VASINEK. Measuring Optimal Length of the Amplifying Fiber in Different Working Conditions of the Amplifier. *Advances in Electrical and Electronic Engineering* [online]. 2015, **12**(6), 557 - 566 [cit. 2019-09-25]. DOI: 10.15598/aeec.v12i6.939. ISSN 1804-3119. Available at: <http://advances.utc.sk/index.php/AEEE/article/view/939>
- [76] PROHAZKA, Ivan a Fumin YANG. Photon counting module for laser time transfer via Earth orbiting satellite. *Journal of Modern Optics*. 2009, **56**(2-3), 253–260. DOI: 10.1080/09500340802155396. ISSN 0950-0340. Available at: <http://www.tandfonline.com/doi/abs/10.1080/09500340802155396>
- [77] RADIL, Jan, Petr MUNSTER, Tomas HORVATH, Ondrej HAVLIS, Pavel SKODA and Josef VOJTECH. Sensoric and data applications in national research and educational networks. In: *2017 Conference on Lasers and Electro-Optics Pacific Rim (CLEO-PR)* [online]. IEEE, 2017, 2017, s. 1–3 [cit. 2019-08-01]. DOI: 10.1109/CLEOPR.2017.8118855. ISBN 978-1-5090-6290-4. Available at: <http://ieeexplore.ieee.org/document/8118855/>
- [78] RADIL, Jan, Tomas HORVATH, Petr MUNSTER, Ondrej HAVLIS, Pavel SKODA, Vladimir SMOTLACHA and Josef VOJTECH. Photonic applications and their coexistence with standard data transmissions. In: *Instrumentation Engineering in the XXI Century. Integration*

- of Science, Education and Production* [online]. 2017, 2018-12-07, s. 37-42 [cit. 2019-08-01]. DOI: 10.22213/2658-3658-2017-37-42. Available at: <http://ieet.istu.ru/papers.php/?p=4>
- [79] REZA, Ali, Sara TOFIGHI, Marzieh BATHAEE a Farnaz FARM. Optical Fiber Interferometers and Their Applications. PADRON, Ivan, ed. *Interferometry - Research and Applications in Science and Technology* [online]. InTech, 2012, 2012-03-21 [cit. 2019-08-20]. DOI: 10.5772/34346. ISBN 978-953-51-0403-2. Available at: <http://www.intechopen.com/books/interferometry-research-and-applications-in-science-and-technology/optical-fiber-interferometer-and-their-applications>
- [80] ROSEN BAND, T., D. B. HUME, P. O. SCHMIDT, et al. Frequency Ratio of Al<sup>+</sup> and Hg<sup>+</sup> Single-Ion Optical Clocks; Metrology at the 17th Decimal Place. *Science*. 2008, **319**(5871), 1808-1812. DOI: 10.1126/science.1154622. ISSN 0036-8075. Available at: <http://www.sciencemag.org/cgi/doi/10.1126/science.1154622>
- [81] ROST, M, D PIESTER, W YANG, T FELDMANN, T WÜBBENA a A BAUCH. Time transfer through optical fibres over a distance of 73 km with an uncertainty below 100 ps. *Metrologia*. 2012, **49**(6), 772-778. DOI: 10.1088/0026-1394/49/6/772. ISSN 0026-1394. Available at: <http://stacks.iop.org/0026-1394/49/i=6/a=772?key=crossref.0cd3b0aaaf513cb716b6ebc6b8244894>
- [82] SALEH, Bahaa E. A. a Malvin Carl TEICH. *Fundamentals of photonics*. 2nd ed. Hoboken, N.J.: Wiley Interscience, 2007. ISBN 978-0-471-35832-9.
- [83] SIFTA, Radim, Filip KOVAC, Miloslav FILKA and Petr MUNSTER. Temperature Dependence of Polarization Mode Dispersion. In: *DGaO- Proceedings. DGaO- PROCEEDINGS* [online]. Erlangen: DGaO-PROCEEDINGS, 2015, 27.08.2015, s. 1 [cit. 2019-08-02]. ISSN 1614- 8436. Available at: [https://www.dgao-proceedings.de/download/116/116\\_p38.pdf](https://www.dgao-proceedings.de/download/116/116_p38.pdf)
- [84] SIFTA, Radim, Petr MUNSTER, Petr SYSEL, Tomas HORVATH, Vit NOVOTNY, Ondrej KRAJSA a Miloslav FILKA. Distributed Fiber-Optic Sensor for Detection and Localization of Acoustic Vibrations. *Metrology and Measurement Systems* [online]. 2015, **22**(1), 111-118 [cit. 2019-08-01]. DOI: 10.1515/mms-2015-0009. ISSN 2300-1941. Available at: <http://journals.pan.pl/dlibra/publication/104302/edition/90306/content>
- [85] SIFTA, Radim, Petr MUNSTER, Ondrej KRAJSA, Vit NOVOTNY a Jaroslav KOTON. Distributed fiber sensor for acoustic vibrations. In: *Fourth Forum of Young Researchers. In the framework of International Forum Education Quality — 2014*. Izhevsk: Publishing House, 2014, s. 368–371. ISBN 978-5-7526-0649- 6.
- [86] SIKORA, Pavel, Tomas HORVATH, Petr MUNSTER and Vaclav OUJEZSKY. Efficiency Tests of DBA Algorithms in XG-PON. *Electronics* [online]. 2019, **8**(7), 1–17 [cit. 2019-08-01]. DOI: 10.3390/electronics8070762. ISSN 2079-9292. Available at: <https://www.mdpi.com/2079-9292/8/7/762>
- [87] SIMSARIAN, Jesse E. a Peter J. WINZER. Shake Before Break: Per-Span Fiber Sensing with In-Line Polarization Monitoring. In: *Optical Fiber Communication Conference* [online]. Washington, D.C: OSA, 2017, 2017, M2E.6- [cit. 2019-09-12]. DOI: 10.1364/OFC.2017.M2E.6. ISBN 978-1-943580-23-1. Available at: <https://www.osapublishing.org/abstract.cfm?URI=OFC-2017-M2E.6>

- [88] SLAPAK, Martin, Josef VOJTECH a Petr MUNSTER. Polarization Changes as Early Warning System in Optical Fiber Networks. In: *2019 42nd International Conference on Telecommunications and Signal Processing (TSP)*. Budapest, Hungary: IEEE, 2019, 2019, s. 597-600. DOI: 10.1109/TSP.2019.8768862. ISBN 978-1-7281-1864-2. Available at: <https://ieeexplore.ieee.org/document/8768862/>
- [89] SLIW CZYNSKI, Ł., P. KREHLIK, Ł. BUCZEK a M. LIPINSKI. Frequency Transfer in Electronically Stabilized Fiber Optic Link Exploiting Bidirectional Optical Amplifiers. *IEEE Transactions on Instrumentation and Measurement*. 2012, **61**(9), 2573-2580. DOI: 10.1109/TIM.2012.2188663. ISSN 0018-9456. Available at: <http://ieeexplore.ieee.org/document/6166467/>
- [90] SMOTLACHA, Vladimír a Josef VOJTECH. Accurate time distribution using optical fiber. In: *2015 International Association of Institutes of Navigation World Congress (IAIN)*. Prague, Czech Republic: IEEE, 2015, 2015, s. 1-5. DOI: 10.1109/IAIN.2015.7352265. ISBN 978-1-4673-7634-1. Available at: <http://ieeexplore.ieee.org/document/7352265/>
- [91] STILES, Jim. *DB, dBm, dBw* [online]. The Univ. of Kansas, 2005 [cit. 2019-09-10]. Available at: <http://www.ittc.ku.edu/jstiles/622/handouts/dB.pdf>
- [92] *Success at SPIE Photonics Europe 2018* [online]. Prague: CESNET, 2018 [cit. 2019-09-11]. Available at: <https://www.cesnet.cz/cesnet/reports/press-releases/success-at-spie-photonics-europe-2018/?lang=en>
- [93] *The Corning Fiber Advantage* [online]. United States: Corning [cit. 2019-09-25]. Available at: <https://www.corning.com/worldwide/en/contact-us.html#corp-comm>
- [94] VOJTECH, Josef, Ondrej HAVLIS, Martin SLAPAK, et al. Joint stable optical frequency and precise time transfer over 406 km of shared fiber lines - Study. In: *2017 40th International Conference on Telecommunications and Signal Processing (TSP)*. Barcelona, Spain: IEEE, 2017, 2017, s. 694-697. DOI: 10.1109/TSP.2017.8076076. ISBN 978-1-5090-3982-1. Available at: <http://ieeexplore.ieee.org/document/8076076/>
- [95] VOJTECH, Josef, Jan RADIL, Ondrej HAVLIS, Vladimír SMOTLACHA, Pavel SKODA and Petr MUNSTER. Effects of reflections in present optical networks with bidirectional transmissions. In: *Conference and Exhibition on OPTICAL COMMUNICATIONS 2016* [online]. Praha: Action M Agency, 2016, s. 25-26 [cit. 2019-08-02]. ISBN 978-80-86742-45- 8.
- [96] VOJTECH, Josef, Martin SLAPAK, Pavel SKODA, et al. Joint accurate time and stable frequency distribution infrastructure sharing fiber footprint with research network. *Optical Engineering* [online]. 2017, **56**(2), 6715-6725 [cit. 2019-08-01]. DOI: 10.1117/1.OE.56.2.027101. ISSN 0091-3286. Available at: <http://opticalengineering.spiedigitallibrary.org/article.aspx?doi=10.1117/1.OE.56.2.027101>
- [97] VOJTECH, Josef, Martin SLAPAK, Pavel SKODA, et al. Precise time transfer on the IPE - VUGKT line – a detailed analysis. In: *2016 39th International Conference on Telecommunications and Signal Processing (TSP)* [online]. IEEE, 2016, 2016, s. 757-760 [cit. 2019-08-02]. DOI: 10.1109/TSP.2016.7760986. ISBN 978-1-5090-1288-6. Available at: <http://ieeexplore.ieee.org/document/7760986/>

- [98] VOJTĚCH, Josef, Vladimír SMOTLACHA a Jan RADIL. All optical two-way time transfer in strongly heterogeneous networks. In: *Proceedings Volume 9202, Photonics Applications for Aviation, Aerospace, Commercial, and Harsh Environments V*. San Diego, California, United States: SPIE, 2014, 2014-9-5, 92020S-. DOI: 10.1117/12.2061346. ISBN 9781628412291. ISSN 0277-786X. Available at: <http://proceedings.spiedigitallibrary.org/proceeding.aspx?doi=10.1117/12.2061346>
- [99] VOJTECH, Josef, Vladimír SMOTLACHA a Pavel SKODA. Simultaneous transmission of accurate time in parallel with stable optical frequency in real fibre network over 612 km. In: *2015 Optoelectronics Global Conference (OGC)*. Shenzhen, China: IEEE, 2015, 2015, s. 1-3. DOI: 10.1109/OGC.2015.7336835. ISBN 978-1-4673-7731-7. Available at: <http://ieeexplore.ieee.org/document/7336835/>
- [100] VOJTECH, Josef, Vladimír SMOTLACHA, Pavel SKODA, et al. Photonic services, their enablers and applications. In: *SPIE Optical Engineering + Applications*. USA: SPIE, 2012, 2012-10-23, 85160H. DOI: 10.1117/12.929908. ISBN 9780819492333. ISSN 0277-786X. Available at: <http://proceedings.spiedigitallibrary.org/proceeding.aspx?doi=10.1117/12.929908>
- [101] VOJTECH, Josef, Vladimír SMOTLACHA, Pavel SKODA, et al. Optical stabilization for time transfer infrastructure. In: *Applied Optical Metrology II*. SPIE, 2017, 2017-8-23, s. 1-6. DOI: 10.1117/12.2274815. ISBN 9781510612037. Available at: <https://www.spiedigitallibrary.org/conference-proceedings-of-spie/10373/2274815/Optical-stabilization-for-time-transfer-infrastructure/10.1117/12.2274815>
- [102] VOJTECH, Josef, Martin SLAPAK, Tomas HORVATH, et al. Transmission Delay Stabilization Using Commercial Pluggable Small Form Factor Transceiver Based on V-Cavity Laser. In: *2018 41st International Conference on Telecommunications and Signal Processing (TSP)*. Athens, Greece: IEEE, 2018, 2018, s. 1-5. DOI: 10.1109/TSP.2018.8441487. ISBN 978-1-5386-4695-3. Available at: <https://ieeexplore.ieee.org/document/8441487/>
- [103] WANG, B., C. GAO, W. L. CHEN, et al. Precise and Continuous Time and Frequency Synchronisation at the  $5 \times 10^{-19}$  Accuracy Level. *Scientific Reports*. 2012, **2**(1), 1-5. DOI: 10.1038/srep00556. ISSN 2045-2322. Available at: <http://www.nature.com/articles/srep00556>
- [104] WEISS, Marc. Getting accurate time from GNSS receivers: Considerations to approach nanosecond time. In: *2017 IEEE International Symposium on Precision Clock Synchronization for Measurement, Control, and Communication (ISPCS)*. Monterey, CA, USA: IEEE, 2017, 2017, s. 1-5. DOI: 10.1109/ISPCS.2017.8056746. ISBN 978-1-5090-5718-4. ISSN 1949-0313. Available at: <http://ieeexplore.ieee.org/document/8056746/>
- [105] WOODWARD, Sheryl L., Lynn E. NELSON, Charles R. SCHNEIDER, Laurie A. KNOX, Maurice O'SULLIVAN, Charles LAPERLE, Michael MOYER a Sik FOO. Long-Term Observation of PMD and SOP on Installed Fiber Routes. *IEEE Photonics Technology Letters* [online]. 2014, **26**(3), 213-216 [cit. 2019-09-25]. DOI: 10.1109/LPT.2013.2290473. ISSN 1041-1135. Available at: <http://ieeexplore.ieee.org/document/6663615/>

- [106] YUELAN LU, TAO ZHU, LIANG CHEN a XIAOYI BAO. Distributed Vibration Sensor Based on Coherent Detection of Phase-OTDR. *Journal of Lightwave Technology* [online]. 2010 [cit. 2019-09-25]. DOI: 10.1109/JLT.2010.2078798. ISSN 0733-8724. Available at: <http://ieeexplore.ieee.org/document/5585644/>
- [107] ZHANG, Hao, Guiling WU, Liang HU, Xinwan LI a Jianping CHEN. High-Precision Time Transfer Over 2000-km Fiber Link. *IEEE Photonics Journal*. 2015, **7**(6), 1-9. DOI: 10.1109/JPHOT.2015.2499541. ISSN 1943-0655. Available at: <http://ieeexplore.ieee.org/document/7323786/>